A Water Quality Model for Shallow River-Lake Systems and its Application in River Basin Management

David Kneis

A dissertation submitted to the Faculty of Mathematics and Natural Sciences at the University of Potsdam, Germany
for the degree of Doctor of Natural Sciences (Dr. rer. nat.) in Geoecology

Submitted	23 April 2007
Defended	19 June 2007
Published	July 2007

Referees

Prof. Axel Bronstert	University of Potsdam, Institute of Geoecology
PD Dr. Dietrich Borchardt	Kassel University, Center for Environmental Systems Research
Prof. Jesús Carrera	Institute of Earth Sciences 'Jaume Almera', Barcelona

Elektronisch veröffentlicht auf dem
Publikationsserver der Universität Potsdam:
http://opus.kobv.de/ubp/volltexte/2007/1464/
urn:nbn:de:kobv:517-opus-14647
[http://nbn-resolving.de/urn:nbn:de:kobv:517-opus-14647]

Contents

Abstract

This work documents the development and application of a new model for simulating mass transport and turnover in rivers and shallow lakes. The simulation tool called 'TRAM' is intended to complement mesoscale eco-hydrological catchment models in studies on river basin management. TRAM aims at describing the water quality of individual water bodies, using problem- and scale-adequate approaches for representing their hydrological and ecological characteristics. The need for such flexible water quality analysis and prediction tools is expected to further increase during the implementation of the European Water Framework Directive (WFD) as well as in the context of climate change research.

The developed simulation tool consists of a transport and a reaction module with the latter being highly flexible with respect to the description of turnover processes in the aquatic environment. Therefore, simulation approaches of different complexity can easily be tested and model formulations can be chosen in consideration of the problem at hand, knowledge of process functioning, and data availability. Consequently, TRAM is suitable for both heavily simplified engineering applications as well as scientific ecosystem studies involving a large number of state variables, interactions, and boundary conditions.

TRAM can easily be linked to catchment models off-line and it requires the use of external hydrodynamic simulation software. Parametrization of the model and visualization of simulation results are facilitated by the use of geographical information systems as well as specific pre- and post-processors.

TRAM has been developed within the research project 'Management Options for the Havel River Basin' funded by the German Ministry of Education and Research. The project focused on the analysis of different options for reducing the nutrient load of surface waters. It was intended to support the implementation of the WFD in the lowland catchment of the Havel River located in North-East Germany.

Within the above-mentioned study TRAM was applied with two goals in mind. In a first step, the model was used for identifying the magnitude as well as spatial and temporal patterns of nitrogen retention and sediment phosphorus release in a 100 km stretch of the highly eutrophic Lower Havel River. From the system analysis, strongly simplified conceptual approaches for modeling N-retention and P-remobilization in the studied river-lake system were obtained.

In a second step, the impact of reduced external nutrient loading on the nitrogen and phosphorus concentrations of the Havel River was simulated (scenario analysis) taking into account internal retention/release. The boundary conditions for the scenario analysis such as runoff and nutrient emissions from river basins were computed by project partners using the catchment models SWIM and ArcEGMO-Urban. Based on the output of TRAM, the considered options of emission control could finally be evaluated using a site-specific assessment scale which is compatible with the requirements of the WFD. Uncertainties in the model predictions were also examined.

According to simulation results, the target of the WFD – with respect to total phosphorus concentrations in the Lower Havel River – could be achieved in the medium-term, if the full potential for reducing point and non-point emissions was tapped. Furthermore, model results suggest that internal phosphorus loading will ease off noticeably until 2015 due to a declining pool of sedimentary mobile phosphate. Mass balance calculations revealed that the lakes of the Lower Havel River are an important nitrogen sink. This natural retention effect contributes significantly to the efforts aimed at reducing the river's nitrogen load.

If a sustainable improvement of the river system's water quality is to be achieved, enhanced measures to further reduce the immissions of both phosphorus and nitrogen are required.

Kurzfassung

Die vorliegende Arbeit dokumentiert Konzept und Anwendung eines Modells zur Simulation von Stofftransport und -umsatz in Flüssen und Flachseen. Das Simulationswerkzeug TRAM wurde als Ergänzung zu mesoskaligen Wasser- und Stoffhaushaltsmodellen konzipiert, um die Beschaffenheit einzelner Wasserkörper auf dieser räumlichen Skala in adequater Weise abbilden zu können. Dieser Aufgabenstellung kommt im Zuge der Umsetzung der EU-Wasserrahmenrichtlinie (WRRL) besondere Bedeutung zu.

Das entwickelte Simulationsmodell TRAM setzt sich aus einem Transport- und einem Reaktionsmodell zusammen. Letzteres zeichnet sich durch eine hohe Flexibilität hinsichtlich der Beschreibung gewässerinterner Stoffumsatzprozesse aus. Es können mit geringem Aufwand unterschiedlich komplexe Ansätze der Prozessbeschreibung getestet und die – je nach Problemstellung, Systemverständnis und Datenverfügbarkeit – angemessene Modellformulierung gewählt werden. TRAM eignet sich somit gleichermaßen für stark vereinfachende Ingenieur-Anwendungen wie für wissenschaftliche Analysen, die komplexe aquatische Ökosystemmodelle mit einer Vielzahl an Zustandsvariablen, Interaktionen und Randbedingungen erfordern.

Weitere Charakteristika von TRAM sind die Koppelbarkeit mit öko-hydrologischen Einzugsgebietsmodellen sowie einem hydrodynamischen Modell, die Unterstützung von Modellparametrisierung und Visualisierungen durch Geografische Informationssysteme (GIS) und ein klar strukturiertes Daten-Management.

TRAM wurde im Rahmen des BMBF-geförderten Forschungsprojekts 'Bewirtschaftungsmöglichkeiten im Einzugsgebiet der Havel' entwickelt. Gegenstand dieses Projektes war die Analyse von Handlungsoptionen zur Verminderung von Nährstoffeinträgen in die Oberflächengewässer des Havel-Einzugsgebiets als Beitrag zur Erreichung der Ziele der WRRL.

Mit dem Einsatz von TRAM wurden zwei Zielstellungen verfolgt: In einem ersten Schritt wurden Bedeutung und Muster der gewässerinternen Stickstoff-Retention sowie der Phosphor-Freisetzung aus See-Sedimenten quantifiziert (Systemanalyse). Auf dieser Basis konnten vereinfachte, konzeptionelle Ansätze zur Beschreibung von N-Retention und P-Remobilisierung abgeleitet werden. In einem zweiten Schritt wurden, unter Nutzung dieser Ansätze, die Auswirkungen verringerter externer Nährstoffeinträge auf gewässerinterne N- und P-Konzentrationen simuliert (Szenario-Analysen) und die Unsicherheiten der Modellrechnungen untersucht. Als Randbedingungen für die Szenario-Analysen dienten Simulationsergebnisse der öko-hydrologischen Einzugsgebietsmodelle SWIM und ArcEGMO, welche durch Projektpartner zur Verfügung gestellt wurden. Die mittels TRAM berechneten Nährstoffkonzentrationen bildeten schließlich die Grundlage für eine Evaluierung der Handlungsoptionen anhand einer gewässertypspezifischen, WRRL-konformen Bewertungsskala.

Die Simulationsergebnisse zeigen, dass die Zielvorgabe der WRRL bezüglich Gesamt-Phosphor im Falle der Unteren Havel mittelfristig erreicht werden kann, wenn das Potential zur Senkung der Einträge aus punktförmigen und diffusen Quellen voll ausgeschöpft wird. Weiterhin kann im Zeitraum bis 2015 bereits mit einem merklichen Nachlassen der internen Phosphat-Freisetzung aufgrund einer Aushagerung der Sedimente gerechnet werden. Mit Hilfe von Massenbilanzierungen ließ sich zeigen, dass die Havelseen eine bedeutende Stickstoff-Senke darstellen. Dieser natürliche Retentionseffekt unterstützt wesentlich die Bemühungen zur Verminderung der Stickstoff-Belastung.

Im Sinne einer nachhaltigen Verbesserung der Wassergüte der Unteren Havel erscheinen verstärkte Anstrengungen zur weiteren Reduzierung sowohl der Phosphor- als auch der Stickstoff-Emissionen geboten.

Chapter 1

Introduction

1.1 Context of the study

The study presented here was undertaken in 2003–2006 as a contribution to the joint research project 'Management options for the Havel River Basin'. As indicated by the project's name, the spatial focus was on the catchment of the Havel River which is located in the lowlands of North-East Germany and comprises a total area of about 24000 km^2.

The project was funded by the German Federal Ministry for Education and Research (BMBF) in order to support the implementation of the European Water Framework Directive (WFD). The WFD became the legal basis of water management in the European Union in 2000 and its fundamental aim is to achieve a good ecological status in all major rivers, lakes, aquifers, and coastal waters by 2015 (European Commission, 2000) with lower targets being set for heavily modified water bodies.

When putting the WFD into practice, there are a number of aspects where scientific research is required, starting with the definition of the 'good status' for specific types of surface waters and parameters. Scientific approaches are also necessary for localizing and analyzing current deficits and threats. Finally, the search for possible management strategies and their assessment involves methods of quantitative system analysis.

With respect to the Havel River Basin, it is likely that the quality targets of the WFD will not be met by 2015 in many rivers and lakes due to structural deficits and pollution by the nutrients nitrogen and phosphorus (LUA, 2005b). The project 'Management options for the Havel River Basin' addressed both problems but the clear emphasis was on the eutrophication issue.

The focal points of this research project are summarized below:

- Target nutrient levels for rivers and lakes of different morphological and ecological types were derived (LUA, 2005a).
- Management scenarios were designed which include alternative options for reducing the input of nitrogen (N) and phosphorus (P) into surface waters (Jacobs & Jessel, 2003).
- The impacts of the scenarios on water budgets, nutrient export rates, and in-river/lake concentrations of N and P were analyzed quantitatively using eco-hydrological catchment and water quality models (Biegel et al., 2005; Habeck, 2006; Kneis et al., 2006; Krause, 2005).
- Finally, the scenarios and the included management options were assessed with respect to effectiveness and efficiency in the light of the previously identified water quality targets.

The project's results were intended to assist in the selection of management options by decision makers. A full outline of the project's aims, research guidelines, and major results can be found in the publications by Bronstert et al. (2005) and Bronstert & Itzerott (2006).

1.2 Focus of this thesis

In the quantitative analysis and comparison of management strategies, eco-hydrological catchment models are frequently used for simulating a river basin's water budget and processes of mass transport (e.g. Kronvang et al., 1999; Schreiber et al., 2005). Since these models aim at simulating meso- to large-scale catchments, their spatial discretization is usually coarse, typically with a grid size of 1×1 km. Such a coarse spatial resolution is chosen for the sake of computational efficiency. Furthermore, the acquisition of detailed geographical information for whole catchments is often impractical and strongly generalized data must be used.

As a consequence, the representation of individual water bodies in meso- or large-scale catchment models is mostly poor. The Water Framework Directive, however, focuses just on the ecological status of individual lakes and river sections.

From this point of view, water quality simulation tools are required which can easily be linked to (or integrated into) existing catchment models (e.g. Van Griensven & Bauwens, 2003). The scope of such 'extensions' must be a better representation of individual water bodies with respect to their hydraulic features and their source or sink functions in mass transport. In order to facilitate the coupling of models, adjustable interfaces are an important requisite. Furthermore, a flexible spatial and temporal discretization of the water quality simulation tools is important for making coupled models applicable on different scales.

The development of a simple and flexible transport and water quality model is addressed in the first part of this thesis. The model aims at bridging the identified gap between the requirements of the WFD on the one hand and the capabilities of present hydrological catchment models on the other hand. The model called TRAM[1] is intended to serve as an extension to hydrological catchment models being used in studies on river basin management. TRAM was designed to allow for a refined and scale-adequate representation of transport and water quality processes in lowland rivers and shallow lakes.

The second part of this thesis covers the application of TRAM within the project 'Management options for the Havel River Basin'. In this study, the focus of modeling was on the simulation of total phosphorus and nitrogen concentrations in a large river-lake system under different management scenarios.

From the analysis of field data and studies on similar systems it was known that internal turnover processes such as nitrogen retention and phosphorus release affect the ambient nutrient concentrations in the studied river and river-lake systems in general (Behrendt & Opitz, 2000; Kneis, 2002; Schettler, 1995). Consequently, adequate modeling approaches had to be implemented in TRAM which take into account the turnover effects referred to earlier. Considering the complexity of the natural system on the one hand and the amount of available data on the other hand, the development and calibration of these approaches was a major crux.

For analyzing the impact of altered river basin management, TRAM was coupled to the catchment models SWIM (Krysanova et al., 2000) and ArcEGMO-Urban (Biegel et al., 2005). Thus, TRAM's boundary conditions, i.e. flow rates and nutrient loads in the system's inflows, were simulated by project partners for different management scenarios. The output from the coupled models finally provided the basis for assessing the effectiveness of possible management options with respect to the requirements of the WFD.

In summary, the two major aspects covered by this thesis are the design concepts of the newly developed transport and water quality simulation tool TRAM as well as the model's first practical application in the context of river basin management.

[1] TRAM simply stands for transport model

1.3 Outline of the chapters

The subsequent text is sectioned into four major chapters:

The introductory **Chapter 2** provides an overview of the basic approaches to water quality modeling with respect to the simulated type of water body, the description of turnover processes as well as the representation of space and time.

Sect. 2.3 presents the intentions behind the development of a new water quality model TRAM. The major objectives of model design are derived from deficits of existing models and the requirements of river basin management.

Chapter 3 provides a comprehensive outline of the basic concepts of TRAM. It is described how river networks can be approximated by a set of coupled reactors and the dependence on a hydrodynamic model is addressed (Sect. 3.1 & Sect. 3.2). Furthermore, the chapter describes how TRAM allows for the implementation of user-defined turnover submodels and which algorithms are used for solving the equations of reactive transport (Sect. 3.3–Sect. 3.5). A substantial part of Chapter 3 covers the description of TRAM's input data and methods of preprocessing (Sect. 3.6). It is pointed out which kinds of information are required for a successful application of the model. However, the chapter is not intended to replace a user's manual. In the final sections, some aspects of the model's source code and possible objectives for further development are discussed.

Chapter 4 describes the use of TRAM for simulating the dynamics of nitrogen and phosphorus in the Lower Havel River. In Sect. 4.1, the objectives of water quality simulation within the project 'Management options for the Havel River Basin' are explained in detail. Subsequently, an introduction to the study site is given which provides basic information on hydrological conditions as well as the river's major water quality problem which is eutrophication.

A major part of Chapter 4 is dedicated to the presentation of the hydrodynamic submodel for the Havel River and the approaches for simulating nutrient turnover in the studied river-lake system (Sect. 4.3–Sect. 4.4). An outline of aquatic nutrient cycles is included in the description of the turnover submodel, giving an idea of the system's complexity. This basic knowledge is believed to be essential for understanding both the need for strong simplifications in the model as well as their consequences.

After dealing with parameter estimation, Sect. 4.5 illustrates which quantitative information on nutrient dynamics can be attained from the calibrated model.

The last part of the chapter (Sect. 4.6) deals with the simulation of management scenarios focusing on a reduction of nutrient emissions. In this context, the coupling of TRAM to other models and the nature of the scenarios are addressed. In Sect. 4.6.4, the impact of altered nitrogen and phosphorus loading on in-river nutrient levels as predicted by TRAM is presented. The subsequent Sect. 4.6.5 attempts to uncover the uncertainty associated with the simulation results.

In the final **Chapter 5**, major results from the modeling study are summarized and conclusions are drawn. Suggestions for future research are made, based on the experiences described in Chapter 4.

Chapter 2

State of the art and intentions for model development

2.1 The scope of water quality modeling

In general, a water quality model is a simplified mathematical representation of an aquatic system. Water quality models aim at describing the dynamics or steady state of the system's major physical, chemical, and biological state variables. In order to do so, the models take into account transport phenomena as well as biogeochemical turnover processes.

Water quality models are primarily used in research on complex aquatic ecosystems. Simulation tools provide a means to integrate the present understanding of the system's functioning and to compare model predictions with observations. The deviation between simulated and observed data indicates how incomplete our understanding of the system actually is. From analyses of the simulation errors, the impact of those processes which are not explicitly considered in the model can be figured out. Furthermore, the interpretation of residuals stimulates the formulation of new hypotheses on the system's functioning.

Models which have proven their value for a certain problem are also used in water resources management. For example, water quality control is one of the main issues of the European Water Framework Directive. In the implementation process of the WFD four basic steps can be distinguished (adapted from Von Keitz & Schmalholz, 2002):

1. the identification of significant threats to waters,
2. the definition of appropriate and site-specific quality targets,
3. the evaluation of potential management actions,
4. the implementation of measures which are proven to be most efficient.

In step 2–4, quantitative methods of system analysis can be helpful. By using appropriate water quality simulation tools it becomes possible:

- to evaluate the contribution of different sources of pollution (pressures and impacts analysis),
- to identify reasonable quality targets, e.g. concentrations for nutrients, toxins, etc.,
- to assess the impact of management actions on water quality before actual measures are taken (scenario analyses). By identifying efficient and inefficient measures costs can be saved and management can be optimized.

The demands for water quality modeling rise constantly. Although new simulation tools are developed and existing ones are improved, the currently

available simulation models often cannot yet fully satisfy the requirements of the practice.

2.2 A short overview on water quality modeling approaches

Numerous water quality models have been developed in recent decades and new approaches for special applications are frequently published. A tabular overview of established, full-fledged river water quality modeling systems can be found in Reichert et al. (2001) and Borchardt (1998).

Instead of discussing selected models in detail, the following sections give a more general overview on the different approaches to water quality simulation. The focus is placed on (1) the type of water body, (2) the implementation of turnover processes, (3) the spatial dimensionality, and (4) the time scale.

2.2.1 Type of water body

First of all, a distinction between river water quality models (RWQM) and lake models (LWQM) is necessary.

Rivers are characterized by a continuous, mostly unidirectional, movement of water. The depth is usually small (in the order of several cm to a few meters) and turbulences resulting from shear stress at the river bed prevent vertical stratification. In a typical lake, the through-flow rate Q is small compared to the total volume of the water body V. Thus, the theoretical residence time of the water in a lake V/Q is large compared to a channel section of equal length. Mixing of the lake water is usually controlled by wind action and – in deep lakes of the temperate zone – thermal stratification occurs.

Obviously, different approaches are required for describing the hydrodynamics in running and standing waters. Due to the great differences in water residence time, turbulence, and depth, the dominating turnover processes may be different as well. Therefore, RWQM and LWQM do not necessarily focus on the same state variables and interactions.

The classical objective of RWQM was to simulate the effect of organic pollution on a river's oxygen level because of its significance for aquatic life and its variability in space and time. The pioneering Streeter-Phelps model, describing the balance between O_2 consumption and reaeration, is presented in all relevant textbooks (e.g. Chapra, 1997). Another important field of RWQM is the simulation of the transport and decay of toxic substances such as organic chemicals or heavy metals which are harmful to river biota and humans. For example, the Rhine Alarm Model or the 'TOXI' module of the WASP model package (Ambrose et al., 2001) are specialized on problems like these. In recent decades, the focus of RWQM has shifted towards a more complete description of the river ecosystem, often considering nutrient cycling and the growth of both heterotrophic and autotrophic organisms. QUAL2K (Chapra et al., 2006) which is an enhanced version of the famous QUAL-2E (Brown & Barnwell, 1987), the 'EUTRO' module of WASP (Ambrose et al., 2001), QSIM (Kirchesch & Schöl, 1999), or the ATV model (Müller, 2002) are examples of more complex RWQM.

The typical scope of LWQM is to analyze how in-lake nutrient concentrations are related to nutrient loading from the catchment. For a long time, statistical-empirical models were used (e.g. Vollenweider, 1979; Vollenweider & Kerekes, 1982). As in RWQM, state of the art dynamic simulation models include a detailed description of nutrient cycling and primary production. Often, organisms of different trophic levels (phytoplankton, bacteria, zooplankton, sometimes even fish) are considered as state variables. Examples of sophisticated process-oriented lake ecosystem models are PCLake (Van Puijenbroek et al., 2004) or SALMO (Petzoldt et al., 2005).

Although a separate development of RWQM and LWQM is reasonable on the one hand, both types of models need to be consistently linked for many applications, because lakes usually receive

their water through tributaries and some rivers exhibit lake-like expansion zones.

A rather new simulation software which is capable of handling stratified as well as vertically mixed systems while solving the complete hydrodynamic equations is CE-QUAL-W2 (Cole & Wells, 2006).

Another approach is taken by multi-compartment water quality models (MWQM) like AQUASIM (Reichert, 1998). This model allows multiple types of 'reactors' to be simulated that differ with respect to hydrodynamics and the dominant transport processes. By linking advective, dispersive, or advective-dispersive reactors, it becomes possible to approximate river-lake systems as well.

For a proper simulation of river and lake water quality, the inclusion of sediment-water interactions is often essential. In many water quality models, benthic fluxes can be taken into account as boundary conditions only. However, advanced MWQM such as AQUASIM also allow for the simulation of transport phenomena in porous bed sediments.

While a number of water quality models include routines to calculate the hydrodynamics, others only (or optionally) provide an interface for importing hydrographs of stage, flow, and other hydraulic variables computed by external software.

2.2.2 Implementation of turnover processes

Although the turnover processes[1] of interest are often similar for a certain type of water body, different environmental conditions may require adaptations. For example, primary production is of minor importance in small creeks but it may significantly influence the water quality of large rivers. And, whereas bicarbonate (HCO_3^-) can be assumed to be always available in most lakes for assimilation by algae, it may be a limiting factor in heavily acidic waters such as mining ponds. In this light, existing water quality models can be distinguished by their flexibility with respect to the description of turnover processes.

Models which are specially designed for a well defined problem usually have a fixed set of state variables. Also fixed is the description of their interaction and only parameter values may be adjusted to fit the model to the river or lake of interest. While the development time for such models may be (relatively) short, they suffer from a lack of flexibility. If, for example, a new process or variable turns out to be relevant but has not been considered in the original code, changes to the model's core are required. The same is true if simplifications to the process description become necessary because data for a certain variable of parameter are unavailable – which is often the case.

Different approaches have been taken in the past to tackle this problem. For example the WASP package (Ambrose et al., 2001) was split into the modules EUTRO and TOXI. While the first handles oxygen dynamics and nutrient cycles, the second module is designed for simulating the transport of organic chemicals, heavy metals, and sediment. Furthermore, the EUTRO module may be run in different levels of complexity.

Flexibility is taken one step further in open-structure water quality models. In these models it is the user, not the developer, who decides on the number and kind of state variables, boundary conditions, and the nature of their interactions. The AQUASIM tool (Reichert, 1998) and the Biogeochemical Reactions Network Simulator BRNS (Regnier et al., 2002; Thullner et al., 2005) are examples for such open-structure models. The simulation tools 'ECO Lab' (DHI, 2006) and DUFLOW follow a similar approach. The open-structure model WEST (World Wide Engine for Simulation, Training and Automation), which is mainly applied to simulations of wastewater treatment plants, was also used for river water quality modeling (Dekissa et al., 2004).

[1] The terms *turnover* and *conversion* process/model are used synonymously throughout this text.

Open-structure water quality models have the great advantage of being applicable to systems of any complexity with respect to the number of simulated variables and interactions. They support empirical, conceptual as well as process-oriented system descriptions. They also allow for deterministic as well as stochastic simulations. The open structure provides the basis for adapting the model to the present knowledge of process functioning and the available amount of information (initial values, boundary conditions, parameters).

While a model with a fixed set of processes and variables 'only' needs to be supplied with data, open-structure models require the model itself to be formulated first. If no template is available for the specific problem this may cost additional time. However, the investment pays out: Once a template is created, it can easily be changed and extended for new applications. Secondly, the modeler is forced to develop a deeper understanding of the simulated processes and their simplified representation. A modeler with this insight is probably able to assess the simulation results and their reliability more realistically. In the author's opinion, an open model structure is, in most situations, preferable.

2.2.3 Spatial dimensionality

Water quality models may be zero-, one-, two-, or three-dimensional with respect to the spatial representation of the model domain. The proper choice depends on the occurrence of spatial gradients in the state variables. For example, a volume of water which is laterally and vertically fully mixed can be handled with a zero dimensional model as there are no spatial concentration gradients at all. Each of the simulated state variables is a time dependent scalar. Shallow ponds and lakes can often be treated in this way. Also river sections have been approximated by a series of interlinked, fully mixed water bodies which is known as the tanks-in-series approach (Jokiel, 1995; Dekissa et al., 2004).

A one-dimensional representation is often suitable for rivers where turbulence guarantees fast lateral and vertical mixing. Then, concentration gradients are mainly oriented parallel to the stream lines. However, a 1D approximation is insufficient if one is interested in near-field phenomena (e.g. the concentrations just downstream of an effluent or tributary) where lateral and vertical homogeneity is not yet achieved. 1D vertical models are employed in the simulation of deep lakes because stratification often causes sharp vertical concentration gradients.

A two-dimensional representation of the model domain may be suitable for simulating wide but shallow channels, channel junctions and estuaries (2D horizontal) or deep, narrow reservoirs with a single major inflow (2D vertical).

The application of three-dimensional models is only necessary if spatial gradients of the state variables occur with respect to all three spatial axes. This might be the case if hydrodynamics are really complex as in deep reservoirs with multiple tributaries or in the ocean. In many surface water applications a restriction in the dimensionality is possible and, if so, should be adopted.

2.2.4 Simulation time scale

Water quality models are applied on all time scales. For example, the simulation of an accidental spill of toxic substances into a river may be limited to a time period of several hours or days, depending on the initial concentration, decay characteristics, dilution rates, and the river length. In contrast, the simulation of eutrophication or restoration of a large lake with a long residence time may require a simulation over many decades. In order to limit computation times to a reasonable level, the degree of simplification and generalization usually increases with the length of the simulation period. A long-term water quality model focusing on the estimation of monthly average concentrations rather than on instantaneous values was developed by Schlaeger (2003).

In some applications one is less interested in the dynamics of a system but in the steady state resulting from certain boundary conditions (e.g. long-term lake nutrient balances). Then, a dynamic simulation may be completely unnecessary. However, for highly non-linear systems, steady state conditions can often be obtained most conveniently as the result of a very long-term simulation with steady input.

2.3 Objectives of model development

2.3.1 Expert recommendations

In 2002, the German Federal Water Institute published a list of recommendations for future research and development in the field of water quality modeling (BfG, 2002). Those recommendations which were considered in the development of TRAM include the following:

- First of all, water quality modeling should be regarded as an optimization problem which aims at balancing the level of model complexity with the reliability of model predictions and the effort for data acquisition. Against this background, the development and use of modular simulation tools which can be run in different levels of complexity is proposed.

- According to BfG (2002), a better representation of sediment-water interactions in water quality simulations should be given special attention. In spite of many decades of research on this topic, a need for combined field studies and model development is diagnosed.

- The use of state-of-the-art hydrodynamic approaches is recommended in order to make water quality models applicable to river networks of complex geometry, including looped systems. It is pointed out that the hydrodynamic submodels must be able to consider all relevant features of river regulation and water resources management.

- As water quality simulation models produce large amounts of data, the development of improved methods of pre- and postprocessing as well as data visualization is proposed. The fact that many programs do not support batch imports of large data sets (e.g. boundary condition time series or geometry data) is identified as a major hindrance for efficient model application.

- It is suggested that newly developed models should be platform independent and well documented to make them useful for others. It is considered a serious waste of resources that many existing models of general interest lack sufficient documentation or cannot be ported from one platform to another.

2.3.2 Specific targets

The subsequent paragraphs summarize the fundamental objectives which guided the development of the TRAM model presented in Chapter 3. These specific targets were derived from the requirements of river basin management in the context of the Water Framework Directive (see Sect. 1.2), the above recommendations by BfG (2002), as well as personal modeling experience.

Open-structure turnover model

The required complexity of a turnover model depends on the nature of the problem, the knowledge about the relevant processes, and the availability of data for model calibration and verification. Furthermore, in different applications, the focus of modeling may be on different state variables and interactions. Consequently, TRAM's conversion model was intended to be of the open-structure type (see Sect. 2.2.2) so as to offer maximum flexibility. In particular, TRAM should support the use of simple empirical as well as more advanced, process-based model formulations. Also, the pos-

sible number of state variables or boundary conditions should not be restricted in any way.

For many biogeochemical processes, model concepts were already published decades ago. With its open structure, TRAM was intended to allow for a convenient re-implementation of such existing concepts in an up-to-date simulation framework.

Hydrodynamic submodel

The poor representation of the hydrodynamics in hydrological catchment models was identified as a severe deficit in Sect. 1.2. In order to overcome this, TRAM was intended to make use of detailed cross-section data for representing the geometry of rivers and lakes. Furthermore, the simulation of control structures such as weirs, gates, and flow diversions was considered to be essential because of its influence on turnover processes.

Since well established hydrodynamic simulation models exist, it was planned to link TRAM with such external software. However, depending on the nature of the river system, the availability of geometry data, and the required accuracy, different approaches for simulating the hydrodynamics may be preferred. Therefore, instead of being tightly coupled to a specific software, TRAM was designed to read stage and flow hydrographs from input files. Such files can easily be created from the output of whatever hydrodynamic or hydrological model.

Linkage to geographic information systems

The linkage of TRAM to a geographical information system (GIS) was considered to be essential for several reasons. First of all, model parametrization can be sped up significantly if all data on model geometry (river network plan, cross-section data, lake bathymetry, etc.) are preprocessed using GIS facilities. Furthermore, a full spatial reference of all simulated water bodies is helpful when TRAM is coupled to a hydrodynamic or catchment model because the locations of boundary conditions can easily be identified. Finally, simulation results may be transfered back into GIS or other postprocessing software for visualization and the creation of maps[2].

In order to guarantee maximum flexibility, a tight coupling of TRAM to any specific software was to be avoided. Instead, the model should support the import and export of data in simple standard formats which can easily be created and read by any GIS with little conversion effort. In most of the existing water quality models, a GIS interface is still lacking.

Handling of data

As pointed out in BfG (2002) the usefulness of a model strongly depends on how efficient data input and output is. Some guidelines for efficient and safe data transfer which have been considered in the development of TRAM are listed below.

- The model's input files conform to existing standards and they can easily be created by preprocessing software or by data base queries.
- The model's output files are directly loadable by software for plotting, statistical evaluation, or data storage.
- Different types of information are stored in separate files. All data items are identified by keywords or described by comments.
- The model can be run in batch mode without any user interaction.

Execution speed

If a water quality model is to be used for long-term simulations over several years or decades, execution speed matters. Speed becomes even more relevant if automatic calibration procedures are applied and if sensitivity or uncertainty analyses are to be carried out. Thus, TRAM had to be implemented in a computer language which, in the first place, allows for the creation of fast and platform independent code.

[2]Water quality maps are an essential part of status reports and management plans according to the WFD.

Availability of software and source code

Among the existing water quality models some are free software but others require the payment of license fees and the source code is unavailable. While proprietary water quality models seem appropriate for commercial use, free modeling software is needed in research and education. This is not only a matter of cost. The availability of the source code guarantees that the model can be adapted to a certain scientific application and last but not least it may promote further development. Consequently, it was planned to make TRAM available to the public at an adequate state of development and documentation.

When the work on this thesis began in 2003, none of the freely available water quality models fulfilled the requirements addressed above. The development of the TRAM model introduced in Chapter 3 was a logical consequence.

Chapter 3

The water quality simulation tool TRAM

3.1 Representation of the river network

3.1.1 The reactor concept

In TRAM, the natural river system is represented by a network of interlinked reactors. Two basic types of reactors are currently available: stirred tanks (STR) and plug-flow reactors (PFR). Both concepts are widely used in water quality modeling (e.g. Chapra, 1997; James, 1993; Reichert, 1998).

Stirred tank reactors
The fundamental property of a STR is complete mixing of the contained water which implies an instantaneous spreading of incoming dissolved or suspended matter all over the water body. Thus, a STR is characterized by spatial homogeneity and any mass transport through a STR is due to dispersive processes only. Advection-bound transport is assumed to be negligible. The stirred tank concept allows for a reasonable approximation of mass transport in shallow, polymictic (i.e. non-stratified) lakes.

Plug-flow reactors
In contrast to STR, the transport of dissolved or suspended matter in plug-flow reactors is due to advection only. The flow is assumed to be unidirectional and mass transport can be imagined as a sequence of separate control volumes (CV) entering and leaving the reactor in tight succession. The exchange of matter between neighboring CV, whether due to molecular diffusion or turbulence, is assumed to be negligible. However, within a control volume itself, spatial homogeneity of the concentrations is assumed. Any CV entering a PFR at its upstream end is released at its downstream boundary with a time lag controlled by the flow velocity. The PFR concept is used for representing river and channel sections where advective transport dominates over dispersive processes.

The disregard of dispersion effects in PFR is quite a significant simplification compared to natural conditions. If longitudinal mixing in river or channel sections cannot be neglected[1], one must use an array of coupled PFR and STR in order to approximate advective-dispersive transport. Several authors (e.g. Jokiel, 1995; Dekissa et al., 2004) used tanks-in-series models instead for representing advective-dispersive transport in river sections. In this approach, the magnitude of dispersion at a given flow rate is controlled by the spatial discretization of the model, i.e. the number of STR per reach length (Jokiel, 1995).

There are cases where it is justifiable to neglect mixing in river or channel sections, for instance if the model is driven by boundary conditions with a coarse time resolution. Since input loads and flow rates are averages over the length of a model time step the input is 'already mixed'. Another exam-

[1] Dispersion cannot be neglected if large spatial concentration gradients occur, e.g. due to highly time-variable boundary conditions. The magnitude of dispersion is largely controlled by the occurrence and relative size of dead zones.

ple is river-lake systems where mixing primarily occurs in the lakes. Concentration hydrographs at a lake's outlet are always smooth, i.e. dc/dt is low. Consequently, spatial concentration gradients (dc/dx) in river sections downstream of lakes are low too, and thus dispersion is of minor importance.

Further compartments

Many turnover processes in surface waters are bound to interfaces between the liquid and solid phases due to sorption effects and the role of attached biofilms. Often, the interstitial of the bottom sediments and the surfaces of aquatic vegetation or rock are of special relevance and must therefore be considered as additional model compartments (e.g. Borchardt & Reichert, 2001; Reichert et al., 2001). Although TRAM does not provide a special type of reactor for representing such compartments, turnover processes at non-mobile surfaces can already be simulated for STR (see Sect. 3.3).

3.1.2 Discretization rules

The application of the above concept to a natural river network requires the latter to be subdivided into reactors. Clearly, a subdivision is always necessary where advection-dominated river sections (represented as PFR) interface with mixed water bodies (modeled as STR).

Apart from this, a further discretization of river reaches into a sequence of separate PFR may be advisable if hydraulic features change significantly along the reach. This is necessary because TRAM makes use of reach-averaged values of basic hydraulic variables in turnover computations instead of accounting for the situation at every single cross-section (see Table 3.3 in 3.3.3 and Eq. 3.17–3.20 in Sect. 3.6.4 for details). Consequently, river or channel sections with significant morphological irregularities (flow depth, wet perimeter, etc.) should not be modeled as a single PFR but by a sequence of shorter plug-flow reactors. The same

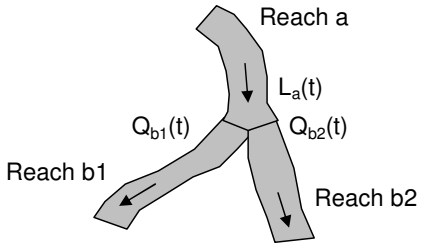

Figure 3.1: *Three reaches forming a split flow junction. $L_a(t)$: Export load hydrographs of reach a, $Q_{b1}(t)$ & $Q_{b2}(t)$: Inflows of the downstream reaches.*

is true when TRAM is applied to impounded channels or free-flowing rivers with significant changes in bed slope. This is because TRAM assumes that the slope of the water surface (dW/dx) within a plug-flow reactor is constant, i.e. $dW/dx \neq f(x)$. In the application to the Lower Havel River (Chapter 4), accuracy requirements allowed for the use of plug-flow reactors with a length of several hundred meters to about 2 km because the slope of the water surface does not exceed a few cm/km.

A special case emerges if river networks with split flow junctions (looped networks) as shown in Fig. 3.1 are simulated. In the example, the import load hydrographs for the reaches b_1 and b_2 downstream of the junction are computed from their inflow hydrographs $Q_{b1}(t)$ and $Q_{b2}(t)$ and the export load hydrograph of the upstream reactor $L_a(t)$ according to the following equations:

$$L_{b1}(t) = L_a(t) \cdot \frac{Q_{b1}(t)}{Q_{b1}(t) + Q_{b2}(t)} \tag{3.1}$$

$$L_{b2}(t) = L_a(t) \cdot \frac{Q_{b2}(t)}{Q_{b1}(t) + Q_{b2}(t)} \tag{3.2}$$

For Eq. 3.1 and 3.2 to be correct, the inflow rates $Q_{b1}(t)$ and $Q_{b2}(t)$ must not contain contributions of any additional lateral inflow to the reactors b_1 and b_2. Thus, a subdivision of plug-flow reactors might be required if lateral inflow just downstream of a split flow junction is to be simulated.

Finally, plug-flow reactors might need to be subdivided into multiple PFR in order to simulate dif-

fuse pollution. Since the current version of TRAM does not allow for a uniform distribution of load boundary conditions over the length of the reach, the use of a couple of short PFR, each receiving a fraction of the total diffuse load, is necessary.

3.1.3 Network topology

The routing of matter through a system of interconnected PFR and STR requires information on the network topology or hierarchy. Each reactor must 'know' its upstream neighbor(s) which supply the flow and load boundary conditions. In the case of flow diversions, a reactor must also know its 'parallel' reactors which share the same boundary conditions (see Eq. 3.1 & Eq. 3.2).

Essentially, stream orders must be assigned to all reactors in order to reflect the upstream-downstream relations. The stream order takes a value of 1 for the most upstream section(s) of the network and the numbers increase in flow direction. The highest stream order is always attached to the reactor located furthest downstream, i.e. the system's outlet.

A utility program was developed for automatic stream order assignment which is also capable of handling looped river networks. Input to this program are two files: The first file defines the shape and spatial position of the plug-flow reactors' stream lines, the second optional file provides the corresponding information for STR (as polygon outlines).

The preprocessing yields a table listing the following information for each reactor:

1. the user-defined reactor name,
2. the assigned stream order,
3. a list of the reactor(s) that supply the upper boundary conditions,
4. a list of reactors that share the same upstream load boundary condition (only non-empty for reactors downstream of split flow junctions).

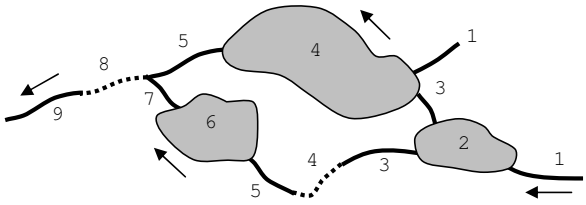

Figure 3.2: *A sample network of plug-flow and stirred tank reactors with stream orders increasing in flow direction.*

Fig. 3.2 shows an example of a simple network of reactors with assigned stream orders.

3.2 Hydrodynamics

If the transport of dissolved or suspended matter in surface waters is to be modeled, a simulation of the hydrodynamics is a prerequisite. For example, information on the flow and the storage volume of a reach is required in order to determine the traveltime of control volumes in a plug-flow reactor. Similarly, information on the stage-dependent reactor volume and flow rates are required for computing the residence time of water and mass in a STR. If the simulated components undergo reactions (e.g. degradation or settling), it is the travel- or residence time which regulates the concentrations in the reactor's outflow.

Because the simulation of hydrodynamics is not included in the TRAM program external software must be used. In a study on the Havel River (Chapter 4), the unsteady 1D hydrodynamic model HEC-RAS (USACE, 2002) was applied. The use of an external program has a number of pros and cons. On the one hand, the separation of hydrodynamics and water quality simulations is advantageous as the user can choose a flow computation approach of the desired complexity, e.g. a hydrodynamic model or a simple hydrologic routing procedure.

On the other hand, the use of separate models is a disadvantage because feedbacks between water quality and hydrodynamic processes cannot be

taken into account without costly iterative simulations[2]. An example where the consideration of such feedbacks might be necessary is the growth of macrophytes in streams. Due to increased flow resistance (higher Manning values), flow velocities can drop significantly and the flow depth increases accordingly. This again, may have an influence on further water quality parameters, such as the retention of phosphorus (Schulz, 2004).

For the sake of computational efficiency, TRAM does not read raw stage[3] and flow hydrographs as output by a hydrodynamic model. Instead, the time series of hydrological variables need to be preprocessed as described in Sect. 3.6.4.

3.3 Turnover processes

3.3.1 Terminology

Basic terms

Prior to describing how turnover processes can be simulated with TRAM, it is worth defining some basic terms.

Element: A class of atoms listed in the Periodic Table. Elements are easily referenced by their unique symbols (C: Carbon, O: Oxygen, ...).

Compound: A compound is a substance with a fixed ratio of elements determining its composition. E.g. all organic substances and water itself are compounds.

Component: A component can be either a compound or even a lumped group of compounds. A component's concentration is often expressed with reference to an element of interest (e.g. dissolved inorganic nitrogen or organic carbon). According to Molins et al. (2004), the term component should be used for a linear combination of species that is not affected by aqueous equilibrium reactions.

Species: If an element of interest occurs in a number of different compounds, the latter are often called *species* with respect to this element. For example, the component dissolved inorganic nitrogen incorporates the three species NO_3^-, NO_2^-, and NH_4^+.

In most instances, the universal term *component* will be used throughout this text. Often, a basic distinction into *organic* and *inorganic* as well as *dissolved* and *suspended* (i.e. *particulate*) components is useful.

Only a few components which can be found in natural waters are *conservative* or *inert*. Instead, most components in the aquatic environment are not only subject to transport but they also undergo *conversion* or *turnover*. The two synonymous terms *turnover* and *conversion* are quite unspecific and may cover processes like:

- the sorption of ions
- settling of suspended matter
- precipitation of insoluble compounds
- decay of organic compounds
- takeup by organisms
- ...

Obviously, some of these turnover or conversion processes are true chemical reactions (e.g. precipitation). In other cases, some fraction of a component may be converted into another one without reactions taking place. Settling for example is actually a transport phenomenon, not a reaction, but it converts the suspended fraction of a component into the corresponding sediment bound fraction. In TRAM, all turnover processes are represented in the same way, no matter whether these are true chemical reactions or not.

In the study of mass balances, the term *retention* is often used for those turnover processes which cause a decrease in a component's concentration

[2] Alternatively, the hydrodynamic and water quality model could be coupled on-line with data exchange in every time step.

[3] The terms *stage* and *water surface elevation* are used synonymously throughout this text.

during its passage through a lake or river section. Retention usually means that some fraction of the load is either retained in the sediment, or it is transformed (such as degradable organic compounds) or it is released to the atmosphere.

Mobile and immobile components

Often, sediment-water interactions such as settling, storage, and remobilization significantly affect the quality of the overlying *water column* or *pelagic zone*. In many water quality models, these interactions are considered by source and sink terms only. If mass balances are to be closed, elemental concentrations in the sediment or attached (*sessile*) biomass must be considered as variables in the model. Consequently, TRAM distinguishes *mobile* and *immobile* components.

Mobile components are generally transported with the flow, i.e. they are either dissolved or suspended in the water column. Their concentration is typically specified in g m^{-3} which is equivalent to mg l^{-1} or ppm. Only loads of mobile components may be exchanged between adjacent reactors.

Immobile components are somehow attached to the bottom of a river or lake. Typically, immobile components exist in the sediment and the corresponding unit is either g m^{-3}, if the thickness of the considered sediment layer is specified, or g m^{-2} (areal concentration). In the first case, total concentrations (mass per volume of sediment) and pore water concentrations (mass per volume of pore water) need to be distinguished.

At present, immobile components can be simulated in STR only, because the implementation for plug-flow reactors is still incomplete (see Sect. 3.8).

Kinetic vs. equilibrium processes

In general, the conversion processes taking place in a control volume of water will tend to an equilibrium. After external perturbations, e.g. due to the input of mass, equilibrium conditions will reestablish within a characteristic time T_p.

For some conversion processes, equilibrium conditions may be reached almost instantaneously. For example, the sorption of ions to mineral surfaces or the dissociation of acids may take place in a period of milliseconds. In such cases, T_p is much shorter than the residence time of the water in the considered control volume T_r, unless flow velocities are extraordinarily large or the control volume is very small. When reactions take place on a very short time scale compared to the time scale of transport processes, i.e. $T_p \ll T_r$, local equilibrium can be assumed (Saaltink et al., 2004). Consequently, the term *equilibrium reactions* or *equilibrium processes* is used (Stumm & Morgan, 1996).

In contrast to that, conversion processes which are controlled by the activity of organisms are often rather slow. For example, the half life of most organic matter compounds in sewage treatment may be in the order of some minutes to days while other organic compounds may be degradated within decades only. In those cases where T_p is greater than T_r equilibrium cannot be assumed and one speaks of *kinetic processes*.

The distinction between kinetic and equilibrium processes has special importance: While the simulation of kinetic processes generally requires *ordinary differential equations* (ODE) to be integrated over time, the concentrations of components which are in equilibrium can often be computed more easily using *algebraic equations* (Reichert, 1998; Thullner et al., 2005).

Process order

Kinetic processes are often characterized by their *reaction order*. The order of a reaction reflects the dependence of the reaction rate on the concentration of the reactants. Most elementary reactions are first- or second-order as they involve either one or two reactants (Stumm & Morgan, 1996). For example, the elementary reaction $A \rightarrow X$ is of first order as the corresponding rate expression is

$$\frac{dC_A}{dt} = -k_1 \cdot C_A \tag{3.3}$$

where C_A is the concentration of A and k_1 is a rate constant (t^{-1}). Examples of complex first order processes are the decay of a degradable substance by microbes but also the growth of a population in its initial phase.

The reaction $A + A \rightarrow X$ is second order because the corresponding rate expression is

$$\frac{dC_A}{dt} = -k_2 \cdot {C_A}^2 \tag{3.4}$$

where the unit of the constant k_2 is $([C] \cdot t)^{-1}$.

The rate law of a third reaction $A + B \rightarrow X$ is shown in Eq. 3.5 with C_B being the concentration of reactant B. As in Eq. 3.4, the unit of k_2 is $([C] \cdot t)^{-1}$.

$$\frac{dC_A}{dt} = -k_2 \cdot C_A \cdot C_B \tag{3.5}$$

In this case, the reaction is said to be first order in A and first order in B, but the *total* reaction order is two. Thus, the total order of a reaction/process is equal to the sum of the exponents associated with each species appearing in the rate expression.

3.3.2 Use of the process matrix for model presentation

For comprehensively presenting a multi-component water quality model the use of a so called 'process matrix' has been proposed (Reichert, 1998; Reichert et al., 2001). The basic layout of such a matrix is shown in Table 3.1.

If the process matrix is read by columns, one can see which processes (row headers) have an influence on the concentration of a specific component (column header). If the stoichiometry coefficient $Q_{i,j}$ is zero, the process corresponding to row j does not affect the component in column i. If $Q_{i,j} > 0$, the concentration of component i rises, if $Q_{i,j} < 0$, the concentration of component i declines due to the action of the j-th process.

The process matrix also reflects mass balances if proper units are chosen for the simulated components (i.e. all components with a common base element X are expressed in g X m^{-3}). If the sum of the stoichiometry coefficients in one row is zero, the mass balance with respect to the process listed in the row header is closed. If different units are used for the components (e.g. mass/volume and mass/area) unit conversion factors must be taken into account in mass balance checks.

The change in the concentration of component i due to process j is calculated by multiplying the stoichiometry coefficients in column i and row j ($Q_{i,j}$) with the corresponding process rate R_j. R_j expresses the velocity of the conversion process. The full differential equation reflecting the impact of all m conversion processes is obtained by summing up the products $Q_{i,j} \cdot R_j$ for all rows of the matrix (Eq. 3.6).

$$\frac{dC_i}{dt} = \sum_{j=1}^{m} Q_{i,j} \cdot R_j \tag{3.6}$$

The mass of a component within a control volume is not exclusively affected by conversion processes but also by the exchange of mass with neighboring control volumes, i.e. by *transport* phenomena. The corresponding *transport terms* are usually not presented in the process matrix.

Fig. 3.3 shows a simplified detail of a water quality model for algal growth in a stirred tank which is suitable for demonstrating the use of the process matrix. In this example, phytoplankton growth is only limited by the availability of a dissolved nutrient X_{dis} and temperature whereas the effect of light intensity is neglected. A simple Michalis-Menten type formulation is used for describing nutrient limitation. Furthermore, settling is the only loss process considered. It is represented by a first order approach as suggested by Scheffer (1998). Due to settling, algal carbon (C_{alg}) is transferred to the sediment together with the organic bound nutrient X. At the sediment's

Table 3.1: *Basic layout of a process matrix for presenting a multi-component water quality model. The process names (1...m) appear as row headers while the names of the simulated components (1...n) form the column headers. The stoichiometry coefficients $Q_{i,j}$ fill the center of the matrix (so-called stoichiometry matrix). The process rates which describe the velocity of the conversion processes are listed in the rightmost column. Usually these are lengthy mathematical expressions presented as a separate list.*

Processes	Component 1	Component 2	...	Component n	Process rates
Process 1	$Q_{1,1}$	$Q_{2,1}$	...	$Q_{n,1}$	Rate expr. 1
Process 2	$Q_{1,2}$	$Q_{2,2}$	...	$Q_{n,2}$	Rate expr. 2
...	...	...	...	...	...
Process m	$Q_{1,m}$	$Q_{2,m}$	...	$Q_{n,m}$	Rate expr. m

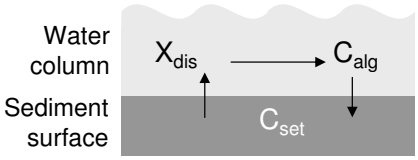

Figure 3.3: *Simplified detail of a water quality model for demonstrating the use of the process matrix. See Table 3.2 for the declaration of symbols.*

surface, the settled organic material (expressed as carbon; C_{set}) is recycled by microbial activity and the released nutrient X is returned to the water column.

The process matrix corresponding to Fig. 3.3 is presented in Table 3.2. Note that only the mass balance for the nutrient X is closed in this example, while the carbon balance is not. In order to close the balance for C too, dissolved inorganic carbon (DIC) had to be introduced as an additional variable. In practice this is unnecessary since DIC is always present in excess unless the pH is very low.

It should be noted that the process matrix shown in Table 3.2 could be simplified. The simplification could be achieved by expressing the concentration of the phytoplankton and the settled organic matter as nutrient equivalent, not as carbon. Then, the nutrient to carbon ratio Q_{XC} would be canceled from the matrix of stoichiometry coefficients. In the rate expressions, C_{alg} and C_{set} would be substituted by X_{alg} and X_{set}, respectively.

3.3.3 User-defined turnover processes in TRAM

3.3.3.1 Potential and limitations

When TRAM was designed, a main objective was to guarantee maximum flexibility with respect to the description of turnover processes. At the current state of development the number of components whose fate can be simulated simultaneously with TRAM is virtually unlimited; the number of turnover processes considered is also chosen by the user.

With respect to the kinds of reactions which can be simulated there is one important restriction: All conversion processes are treated by TRAM as kinetic processes, i.e. the evolution of concentrations is exclusively described by differential equations. Thus, if fast equilibrium processes are to be modeled, these must also be described by ODE using large values for the rate constants. This is possible in principle (Reichert, 1998; Reichert et al., 2001) if appropriate methods of integration are used. However, it is pointed out that there are more elegant strategies for coping with equilibrium reactions involving solvers for mixed algebraic-differential equation systems (e.g. Reichert, 1998; Thullner et al., 2005) and strategies for decoupling components (Molins et al., 2004). Advanced solution algorithms for equilibrium processes are applied in reactive transport models for porous media (Saaltink et al., 1998).

Table 3.2: *Example of a process matrix. The three components are (1) a dissolved nutrient X_{dis}, (2) phytoplankton carbon C_{alg}, and (3) settled phytoplankton material C_{set}. The three considered processes are (1) nutrient-limited phytoplankton growth, (2) settling of phytoplankton, and (3) recycling of the nutrient from settled phytoplankton material due to microbial decay. This example refers to a stirred tank reactor.*

Processes	X_{dis} (g X m^{-3})	C_{alg} (g C m^{-3})	C_{set} (g C m^{-2})	Process rates
Growth	$-Q_{XC}$	1	0	$g(T) \cdot \frac{X_{dis}}{X_{dis} + H_X} \cdot C_{alg}$
Settling	0	-1	V/A	$\frac{u}{D} \cdot C_{alg}$
Recycling	$Q_{XC} \cdot A/V$	0	-1	$k \cdot C_{set}$

X_{dis}: dissolved nutrient in the water column (g X m^{-3})
C_{alg}: phytoplankton carbon in the water column (g C m^{-3})
C_{set}: settled phytoplankton carbon at the sediment surface (g C m^{-2})

g : potential phytoplankton growth rate (s^{-1})
H_X : half-saturation constant for growth limitation due to shortage in X (g X m^{-3})
Q_{XC}: fixed stoichiometric ratio of X and carbon in phytoplankton (g X (g C)$^{-1}$)
u : settling velocity of phytoplankton in turbulent environment (m s^{-1})
k : rate constant of mineralization (s^{-1})
T : water temperature (°C)
V : volume of the stirred tank reactor (m^3)
A : sediment surface area (m^2)
D : mean water depth (m)

It should be acknowledged that biologically driven processes are often the focus of surface water quality simulation, e.g. in eutrophication or BOD models. Here, kinetic formulations are clearly appropriate.

TRAM's flexibility with respect to turnover modeling is due to the fact that the declaration of the $i = 1 \ldots n$ simulated components, the process rate expressions R_j ($j = 1 \ldots m$) for all m processes, and the values of the stoichiometry coefficients $Q_{i,j}$ are not static parts of the source code. Instead, the components' names, the expressions R_j, and the values of $Q_{i,j,}$ are user-defined. Hereby, all information contained in the process matrix can be adapted to the specific problem at hand.

3.3.3.2 Implementation of the open structure

While the components' names are just strings and the stoichiometry coefficients $Q_{i,j}$ are numbers, the process rates R_j are mathematical expressions which may be rather complex. In principle there are two technical alternatives for evaluating user-supplied expressions: the use of an *interpreter* or the generation of *dynamic code*.

Interpreter method

Using an interpreter means that the mathematical expressions R_j ($j = 1 \ldots m$) which are supplied by the user as a string are disassembled into tokens (numbers, variable names, function names, operators and parenthesis) at the very start of a model run. The order of tokens is then converted from the native infix- to so-called postfix-order which allows for the evaluation of the expressions by a series of simple stack operations. When the expressions are evaluated in each time step, only the values of variables need to be updated and the stack operations must be performed. The actual parsing of the expressions needs to be done only once.

If the interpreter method is used, different turnover models can be implemented without the need to make any changes to TRAM's source code. This is very convenient as the abstract source code is entirely hidden from the user and no compilation is necessary. In fact, the idea is quite attractive and it was used by an earlier version of TRAM. But its main deficiency is execution speed. Although, the parsing of expressions is done only once, the interpreted code turned out to run significantly slower than plain compiled FORTRAN code. This was expected in advance, but the difference in execution speed by a factor of 20, even for simple turnover models, demanded alternative solutions (see below).

Dynamic code generation

This method primarily aims at transferring the user-supplied expressions for the process rates R_j into native FORTRAN code. Obviously, this results in a multi-step procedure:

In a first step, the user supplied expressions are parsed and translated into standard FORTRAN code by a preprocessor program TRAMPCODEGEN. In this procedure, the names of variables and constants are substituted by references to the elements of dynamically allocated arrays which hold the respective values at runtime. Basically, two source files are generated in this first step. The first file is a module declaring the names of constants and variables. The second generated source file contains a function to return the derivatives of the components' concentrations using instantaneous values of all involved variables and constants as arguments.

In a second step, the generated *dynamic* parts of the code must be compiled and linked with TRAM's core sources. The built executable is then 'tuned' for the specific application. Because free compilers for modern FORTRAN became available recently (e.g. www.g95.org, 2006), the necessary rebuild of the code no longer conflicts with the objective of making TRAM freely available at a later stage of development.

The major advantage of the dynamic code approach is execution speed. Apart from that, it has the advantage that a large number of mathematical functions and language constructs is available in

FORTRAN as a standard while each of these items would need specific support by the interpreter.

Automatically generated FORTRAN code is also used by the Biogeochemical Reaction Network Simulator (BRNS) developed at Utrecht University, The Netherlands (Regnier et al., 2002). The BRNS uses a MAPLE preprocessor for code generation from user-specified information.

3.3.3.3 Items in user-supplied expressions

The format used for writing user-supplied expressions is discussed in Sect. 3.6.5 along with the description of the model input files. At this point however, the nature of the process rate expressions R_j needs to be examined in more detail. Different types of variables and constants can be used in the formulation of process rates:

Component concentrations
In many cases, the change in a components' concentration is somehow related to its current value. For example, in first order decay of an organic pollutant X, the change in the concentration is given by $dC_X/dt = k \cdot C_X$ with k being a temperature dependent rate constant. Thus, the concentration C_X appears in the process rate.

Hydrologic variables
Often, changes in the concentrations are affected by hydrological variables. For instance, the rate of settling in the turbulent environment of a STR (s^{-1}) was expressed by the quotient of the settling velocity u (m s^{-1}) and the average water depth D (m) in Table 3.2. D can be derived from the reactor volume V and the water surface area A ($D = V/A$). Another example is the exchange of oxygen between river water and the atmosphere. In many models, the essential reaeration coefficient is estimated by empirical relationships from the hydrological parameters stream depth and flow velocity (McCutcheon, 1989). The number and types of available hydrologic variables are different for plug-flow and stirred tank reactors as shown in Table 3.3.

Table 3.3: *Hydrologic variables in stirred tanks (STR) and plug-flow reactors (PFR) which can be referenced in the formulation of process rates. Variables with a + sign are available for the corresponding type of reactor while those marked with – are unimplemented. Note that only reach-averaged values are available for plug-flow reactors (see Sect. 3.6.4).*

Variable	Short name	STR	PFR
average depth	ADEPTH	+	+
storage volume	VOLUME	+	–
surface area	SFAREA	+	–
avg. flow velocity	AVELOC	–	+
wet perimeter	WETPRM	–	+
top width	TWIDTH	–	+

Boundary condition variables
Boundary condition variables are user-declared variables whose dynamics are prescribed rather than being simulated by TRAM. For example, time series of water temperature may be supplied by the user and the values can then be referenced to adjust temperature-dependent rate constants in each time step.

Constants
Along with component concentrations, hydrologic variables and boundary condition variables, the process rates probably always contain fixed parameter values (constants). Typical examples are potential growth and decay constants at a certain reference temperature.

Time
Diurnal and seasonal variations in boundary conditions (e.g. light intensity) may conveniently be modeled as functions of the Julian day or the daytime. In order to support this, the simulation time may be referenced in user-defined expressions.

In order to facilitate the writing of process rates, TRAM automatically considers the transport terms which account for the import and export of mass via the reactor's in- and outflow. These terms, which contain the time-variable import load of mo-

bile components as a fifth type of variable, must not be included in the user-supplied process rate expressions. The names of the auxiliary variables are generated from the user-declared component names by adding the prefix 'impload'. Since the transport terms for immobile components are zero, TRAM omits them automatically.

3.4 Handling of time series

Because the computations described in the subsequent sections include a lot of time series handling, some general remarks need to be made. In TRAM, a time series is considered as a function where the time t is the depended variable (the argument) and $x(t)$ is the independent variable. As the model deals with discretized time series, values for $x(t)$ are available only at intervals Δt which are not necessarily regular. TRAM generally relies on the assumption that the value $x(t)$ is constant within the interval Δt. Thus, time series are handled like step functions with the values of $x(t)$ changing abruptly at the boundaries of time intervals. If for example a time series has the two arguments 01.01.2000 00:00:00 and 01.02.2000 00:00:00 and the corresponding values are 1.0 and 2.0, a constant value of 1.0 is assumed for all days in January. This representation significantly facilitates time series processing but it sets severe restrictions on the resolution Δt in case of highly variable data. A more accurate alternative may be implemented in a future version of TRAM.

The terms *hydrograph* and *time series* are used synonymously throughout this text.

3.5 Computation algorithms

3.5.1 Objectives of computations

TRAM's basic task is to compute the load hydrographs for all simulated components at the outlets of the simulated reactors. Together with the corresponding flow rates, these load hydrographs can be used for calculating the desired information on concentrations. Also, the output load time series serve as boundary conditions in the simulation of downstream reactors. Within a complete model run, the computation is carried out for each single reactor and the procedure advances from the upstream end(s) of the river network to the downstream model boundary.

The algorithms for computing the transport of mobile components in PFR and STR (Sect. 3.5.3, Sect. 3.5.2) were designed with two basic objectives in mind: They should be efficient with respect to execution speed and memory consumption and they should make the implementation of turnover submodels easy.

3.5.2 Reactive transport in stirred tank reactors

Mass balance equation

The computation of reactive transport in a stirred tank reactor is based on a numerical solution of the mass balance equation (Eq. 3.7).

$$\frac{d(V\,C_i)}{dt} = C_{i,in}\,Q_{in} - C_i\,Q_{out} + Z_i \qquad (3.7)$$

In this equation, V (m^3) is the reactor volume and C_i (g m^{-3}) is the concentration of the i-th mobile component in the reactor. Furthermore, $C_{i,in}$ is the concentration in the inflow, and Q_{in} and Q_{out} are the rates of in- and outflow (m^3 s^{-1}), respectively (see Fig. 3.4). The term Z_i (g s^{-1}) accounts for all conversion processes in the reactor which affect the concentration of component i.

By rewriting the left hand side of Eq. 3.7 as in Eq. 3.8 (chain rule),

$$\frac{d(V\,C_i)}{dt} = C_i\,\frac{dV}{dt} + V\,\frac{dC_i}{dt} \qquad (3.8)$$

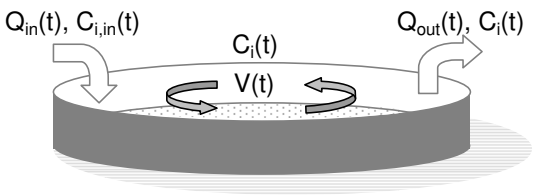

Figure 3.4: *Stirred tank reactor with inflow and outflow of water (Q) and mass of a component i. Input and output loads (L) are given by $L_{i,in} = Q_{in} \cdot C_{i,in}$ and $L_{i,out} = Q_{out} \cdot C_i$ where $C_{i,in}$ is the concentration in the inflow and C_i is the spatially homogeneous concentration in the reactor of volume V.*

and taking into account Eq. 3.9 which reflects the reactor's water balance,

$$\frac{dV}{dt} = Q_{in} - Q_{out} \tag{3.9}$$

Eq. 3.7 can be rearranged to yield Eq. 3.10. A comparison with Eq. 3.7 reveals that the reactor's outflow rate Q_{out} was eliminated.

$$V \frac{d(C_i)}{dt} = Q_{in}(C_{i,in} - C_i) + Z_i \tag{3.10}$$

From Sect. 3.3.2 (Eq. 3.6) it should be known that the term Z_i is equal to product of the stoichiometry coefficients $Q_{i,j}$ and the process rates R_j ($j = 1 \ldots m$) summed up for all m conversion processes after multiplication with the reactor volume V. Thus, the complete derivative of the i-th component's concentration with respect to time is given by Eq. 3.11. It should be realized that the input load ($C_{i,in} \cdot Q_{in}$) can actually be a sum, if the modeled STR has multiple inflows. A term for direct input of mass (e.g. by atmospheric deposition) was not included in Eq. 3.11 since this can be taken into account by adding an appropriate row to the process matrix.

$$\frac{d(C_i)}{dt} = \frac{Q_{in}}{V}(C_{i,in} - C_i) + \sum_{j=1}^{m} Q_{i,j} R_j \tag{3.11}$$

The current version of TRAM also allows for the simulation of immobile components. In contrast to mobile components, no import into the STR via the inflow occurs for immobile components nor is there any export with the reactor's outflow. Consequently, the governing differential equation for immobile components is simplified in that the term $Q_{in}/V \cdot (C_{i,in} - C_i)$ disappears from Eq. 3.11.

If the fate of m components is simulated, a system of m ordinary differential equations like Eq. 3.11 has to be solved. Usually, these are coupled equations as the concentration of a component may appear in multiple process rate expressions. This is illustrated by the example presented in Table 3.2. None of the three components can be simulated individually. For instance, the differential equation for the concentration of the nutrient X_{dis} cannot be integrated without taking into account the simultaneous change in the concentration of the phytoplankton C_{alg}.

Numerical solution

Several algorithms are available for solving systems of coupled ODE. The current version of TRAM offers two alternatives, both adapted from Press et al. (2002). As a standard solver, an adaptive stepsize 5-th order Runge-Kutta scheme was implemented which has the advantage of being robust and quite fast. In some applications, however, a stiff ODE system may be encountered where Runge-Kutta methods fail[4]. This is the case if some processes cause the simulated concentrations to change in the time scale of hours or days (e.g. due to a biological growth process) while other processes result in almost instantaneous changes (e.g. equilibrium reactions). TRAM allows for the integration of stiff ODE systems using a Rosenbrock-Algorithm. By nature,

[4] A stiff system of ODE is one in which some components of the solution are slowly varying while other components are rapidly decaying. Unfortunately, it is necessary to follow the variation in the solution on the shortest length scale (time scale) to maintain stability of the integration, even though accuracy requirements would allow a much larger step size to be used (Press et al., 2002).

this algorithm is somewhat slower than a simple Runge-Kutta method as it involves the evaluation of the Jacobian matrix by numerical differentiation and its subsequent inversion[5]. The Jacobian matrix holds the partial derivatives of the ODE right hand sides with respect to the components' concentrations. For example, in a problem with two components X1 and X2 and two processes P1 and P2, the ODE system to be solved is

$$\begin{aligned} dC_{X1}/dt &= Q_{X1,P1}\, R_{P1} + Q_{X1,P2}\, R_{P2} \\ dC_{X2}/dt &= Q_{X2,P1}\, R_{P1} + Q_{X2,P2}\, R_{P2} \end{aligned}$$

with the stoichiometry coefficients Q and the process rates R (transport terms were neglected). The corresponding Jacobian matrix is shown below.

$$\begin{matrix} \dfrac{\partial(dC_{X1}/dt)}{\partial C_{X1}} & \dfrac{\partial(dC_{X1}/dt)}{\partial C_{X2}} \\ \dfrac{\partial(dC_{X2}/dt)}{\partial C_{X1}} & \dfrac{\partial(dC_{X2}/dt)}{\partial C_{X2}} \end{matrix}$$

The reason why the Jacobian matrix is evaluated numerically is this: As described in Sect. 3.3.3 the TRAM user must supply the right hand sides of the differential equations describing the evolution of the simulated concentrations in time. If the Jacobian matrix was to be calculated analytically, the user had to supply the partial derivatives of these expressions too. In principle this is possible but it is rather inconvenient in case of complex turnover models.

In TRAM, numerical estimates of the partial derivatives are calculated by the so-called 'central derivatives approach'. In this approach, derivatives are determined as the slope of a quadratic spline locally fitted to the function to be derived. Since only the slope of the spline is of interest, not the spline coefficients, the method requires not three but only two evaluations of the ODE right hand sides: one to the left and another one to the right of the location of interest. The increment of the variable with respect to which derivatives are computed is successively reduced by a factor of 0.5 until the largest relative change in a partial derivative falls below a termination threshold.

[5]The matrix inverse is computed by LU decomposition.

Step size control

Apart from the automatic step size adaptation in the Runge-Kutta and the Rosenbrock integrators, TRAM generally adjusts the computational time step in order to satisfy the Courant criterion. The maximum possible step size Δt is given by Eq. 3.12.

$$\Delta t \leq \frac{V}{Q} \tag{3.12}$$

The quotient of the stirred tank reactor's volume V and the flow rate Q is equivalent to the residence time of the water. In TRAM, the actual size of a time step is chosen to be always smaller than half the maximum possible Δt.

Calculation of average loads

Except for the most upstream reactor(s) of the simulated network, the input load of a reactor within a time step Δt is equivalent to the output load from its upstream neighbor(s) within the same Δt. For conservation of mass, the load hydrographs passed from one reactor to another must comprise average loads for each time step, not instantaneous values. However, the numerical solution of the mass balance equations for a STR (Eq. 3.11) yields instantaneous concentration values and some post-processing is necessary in order to obtain the desired 'average-load hydrographs'.

In general, the average load $\overline{L}$ over the period Δt is defined by Eq. 3.13, where Q is the flow rate and C is the concentration.

$$\overline{L} = \frac{1}{\Delta t} \int_{t_0}^{t_0+\Delta t} C(t) \cdot Q(t)\, dt \tag{3.13}$$

Due to the condition of constant flow within Δt (see Sect. 3.4) Eq. 3.13 simplifies to Eq. 3.14, with $\overline{Q}$ being the average flow rate.

$$\overline{L} = \frac{\overline{Q}}{\Delta t} \int_{t_0}^{t_0+\Delta t} C(t)\, dt \tag{3.14}$$

The integral in Eq. 3.14 has to be evaluated using concentrations at discrete times. In the current version of TRAM the trapezoid rule is used for the sake of runtime efficiency. Thus, the average load over a time step is computed as $\overline{L} = \overline{Q} \cdot 1/2 \cdot (C(t_0) + C(t_0 + \Delta t))$. Advanced integration methods, e.g. using cubic splines, could be implemented if critical mass balance errors need to be cured.

3.5.3 Reactive transport in plug-flow reactors

Transport algorithm

In reality, there is a continuous input of water and mass into a river reach as described by the inflow hydrograph and the corresponding concentration time series (chemographs). In TRAM, these input time series are discretized into time steps of duration Δt. Within a single time step, a certain volume of water (forming a control volume) and a corresponding mass of each component enter the plug-flow reactor. The volume V is given by $V = Q \cdot \Delta t$ and the contained mass M_i of component i is given by $M_i = C_i \cdot V$ if the flow Q and the concentration C_i is constant within Δt (see Sect. 3.4). Alternatively, M_i can be expressed as $L_i \cdot \Delta t$ with L_i being the load. Thus, the input into a plug-flow reactor resembles a sequence of control volumes, each containing a certain amount of water and mass of the n simulated components (Fig. 3.5).

For each time step, the PFR's outflow rate Q_{out} can be computed from the inflow rate Q_{in} and the change in the reactor's storage volume V using the water balance equation (Eq. 3.15). The information on Q_{in} as well as V is provided by the hydrodynamic model (see Sect. 3.6.4).

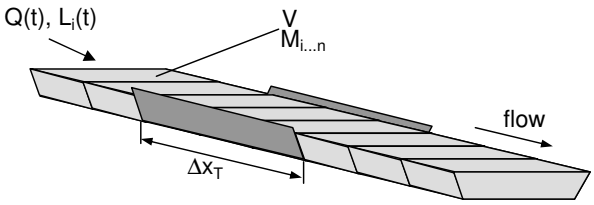

Figure 3.5: *Approximation of the movement of water and mass through a plug-flow reactor of the total length Δx_T by a sequence of control volumes. Each of the control volumes is characterized by its water volume V and the contained masses M_i of the n simulated mobile components. The concentration of the i-th component is defined as M_i/V. The upstream flow and load boundary conditions are denoted $Q(t)$ and $L_i(t)$, respectively.*

$$Q_{out} = Q_{in} - \frac{dV}{dt} \tag{3.15}$$

As a plug-flow reactor is a purely advective system by definition, the *first in – first out* principle applies. In other words: In each time step, the 'oldest' water is exported from the reactor.

In practice, the traveltime of a control volume is hardly an exact multiple of the simulation time step because a plug-flow reactor can be of arbitrary length and flow rates are variable. Therefore, multiple control volumes may contribute to the amount of water and mass leaving the reactor within a simulation time step. Averaging the loads from several control volumes must result in a kind of numerical dispersion. However, the dispersion effect is restricted to the moment when the control volumes pass the reactor's outlet. In some other numerical solutions of the advection equation, which are based on a static space and time discretization, numerical dispersion affects each control volume in every single time step.

Turnover processes

Because the exchange of water between adjacent

control volumes is neglected and spatial homogeneity[6] within each control volume is assumed, the mathematical description of conversion processes is equal to that used for stirred tanks (see Sect. 3.5.2). The only difference is that the terms which describe the mass flux due to in- and outflow are omitted. Also, the amount of water contained in the control volume remains constant during the passage of the plug-flow reactor.

The time available for any turnover to take place in a control volume is given by its traveltime T. However, T may be different for the front and the back end of a control volume (T_{front}, T_{back}) if the flow is unsteady. Because the time-dependence of concentrations is usually nonlinear (e.g. exponential law for first-order reactions), the arithmetic average $1/2 \cdot (T_{front} + T_{back})$ is not a representative estimate of the control volume's mean traveltime. A representative mean traveltime can be derived analytically for special cases only. For the sake of general applicability, TRAM computes the change in the components' concentrations twice, first using T_{front} and another time using T_{back}. The mean of the resulting concentrations is then taken as an estimate of the homogeneous average concentration in the control volume after passage of the PFR. An even more exact solution could be obtained if the component's concentrations C_i were also evaluated at locations x in the middle of the control volume with length Δx: Spline polynomials $C_i(x)$ could then be fitted to describe the spatial concentration gradient in the control volume and the average concentrations could be calculated by solving $\int C_i(x)\, dx/\Delta x$.

It should be noted that the values of all boundary condition variables appearing in the description of turnover processes are considered as reach-averages. This means that user-specified data (e.g. water temperatures) but also the values of hydrologic variables (such as flow velocities or the hydraulic depth; see Sect. 3.6.4) are assumed to be valid for the entire plug-flow reactor within a time step. It is therefore wise to subdivide river sections with highly irregular geometry into several PFR (see Sect. 3.1.2).

As mentioned earlier, TRAM currently does not support the simulation of immobile components in plug-flow reactors.

3.5.4 Routing algorithm

In contrast to many spatially distributed models, TRAM does not update the simulated variables after each simulation time step in the entire model domain. Instead, transport and turnover in a single reactor are always calculated over the full simulation period before the computation proceeds with another reactor of equal or higher stream order. In terms of programing, this means that TRAM's time loop is nested within the loop over the reactors (spatial loop).

Because there is no need to store instantaneous values of all simulated variables in all spatial units of the model domain, this method is efficient with respect to memory consumption. Only the variables which are involved in the simulation of a single reactor need to be allocated. In fact, memory consumption would be a minor problem if only STR were simulated as these do not exhibit spatial variability in concentrations. However, instantaneous concentrations in every single control volume of all PFR would need to be kept in memory if TRAM was solving for the state variables in the entire model domain in every time step.

Another advantage of the method is that it facilitates a stepwise model calibration. Once the parameters for all reactors with a stream order $\leq k$ have been determined, TRAM can be forced to start the computation with reactors of stream order $k + 1$. The required output from the upstream reactors with stream orders $\leq k$ is available from the previous model run(s). Thus, only those sections of the network which were not already calibrated need to be simulated again.

Of course, advantages have their price. It is an obvious drawback of this algorithm that flow re-

[6] vertically and horizontally

versal cannot be handled within a model run as the upstream-downstream relations (i.e. the reactor's stream orders) would change. Although flow reversal is not too common in natural rivers, it may sometimes occur in lowland rivers due to significant withdrawal of water or input of wastewater[7] or due to backwater effects during flood events[8]. Also, flow directions may be variable in shortcut channels between two reaches which have their confluence downstream of the shortcut (there are several examples in the Havel River; see Fig. 4.5). Fortunately, the amount of water and mass transported against the usual flow direction is mostly small. Thus, substituting negative flow rates by very small positive values is often a tolerable makeshift. Certainly, the current version of TRAM is not at all suitable for studying tidal rivers where flow-reversal occurs regularly.

3.6 TRAM's input data

The following sections give an overview of the data and control parameters which are required for running a TRAM simulation. In many cases, parts of input files will be presented in order to illustrate which kinds of data must be provided to TRAM and its preprocessing tools.

3.6.1 General remarks on data input

TRAM intentionally does not have a graphical user interface and all data are read from plain ASCII text files or they are passed as command line arguments. This might seem old-fashioned but, apart from the saving in development time and platform independence, there is a number of great advantages. For example, TRAM can be run in batch jobs which integrate all modeling steps: preprocessing, simulation, and postprocessing. Also, TRAM's input files can easily be generated by utility software, such as scripts that query a SQL data base. Moreover, well structured text files provide an automatic documentation of each model run. If the need for a graphical user interface ever arises, it could be easily implemented as a separate application which prepares the simulation input files and then starts TRAM as a batch job or calls it as a DLL routine.

In order to make data input convenient and safe, TRAM uses a standard format for most of its input files: the so-called '.ini'-format. This standard is used by many WINDOWS applications that do not access the registry for storing configuration data. The '.ini'-format requires that each data value or array is preceded by a descriptive keyword (e.g. key= value). Keyword-value pairs again can be grouped by context into separate 'sections' whose names appear in square brackets. The use of this (or a XML-based) structuring convention is believed to be essential for serious model applications. All input data are instantaneously human-readable without additional comments and the chance of data confusion is very low. Finally, the use of unique keywords for data identification facilitates automatic editing of TRAM's input files by utility software (see e.g. Sect. 4.4.4.1). Apart from keywords, values, and data section headers, an '.ini'-file (short: ini-file) can contain comments. The standard comment character is the semicolon and the double cross (#) is a non-standard alternative. An example of an ini-file is given in Fig. 3.6.

3.6.2 Model units

In principle, the units for expressing quantities of length, area, volume, and mass can be freely chosen as long as all input data are consistent. It is however recommended to keep to the convention that all lengths are given in meters, areas in m^2, and volumes in m^3. The suggested base unit of mass is gram (g). This avoids confusion and possible unit conversion errors.

[7] As happened in 2003 in the Spree River, Berlin.

[8] Flow reversal occurred at the mouth of the Havel River in August 2002 when the sluice gate at Neuwerben was opened to divert up to 700 $m^3\ s^{-1}$ of water from the Elbe River into the Havel floodplain and polder system.

The basic time unit in TRAM is the second which is also the highest possible resolution for time-variable in- and output. The internal time step in numerical computations may be even less than a second but such small increments often indicate errors in the input data or the user-supplied equations of the turnover model.

3.6.3 Network description

The 'network description file' declares the number[9] and names of the simulated reactors and provides information on the network's topology (see Sect. 3.1.3). Details of a sample file are shown in Fig. 3.6, which also demonstrates the ini-format introduced in Sect. 3.6.1. Most of the items shown in Fig. 3.6 are sufficiently commented upon but the last three keywords need some further explanation. After the key *'upstream_sections'* the names of the reactor(s) located directly upstream of the current reactor (given in the section header in brackets) must be listed. During simulation, the output loads of the referenced reactors are summed for each component and the resulting load hydrographs are used as boundary conditions for the current reactor.

The key *'parallel_sections'* is followed by a list of those reactors which receive input loads from the same upstream reactor(s) as the current reactor (given in the section header). This list is non-empty only if the current reactor is located downstream of a split flow junction. During simulation, the load from the upstream reactors is distributed over the receiving reactors weighted by their individual inflow rates (Eq. 3.1 & Eq. 3.2).

The entry *'maxorder_recipient'* contains the highest stream order of the adjacent downstream reactor(s). Usually, this number will be the stream order of the current reactor incremented by 1, but a higher number may appear in a looped river net. Based on this information, TRAM decides at which stage in the computation the output load hydrographs of the current reactor can be removed from memory.

```
;This data section declares a stirred
;tank reactor (str) called 'SampleLake'.
;Because its stream order is 1, the list
;of upstream sections is empty. Also, no
;parallel sections which share the same
;inflow can exist.
;The highest stream order of an adjacent
;downstream reactor equals the current
;stream order incremented by one.
[SampleLake]
  reactor= str
  stream_order= 1
  upstream_sections= -
  parallel_sections= -
  maxorder_recipient= 2

;This data section declares a plug-flow
;reactor (reactor = pfr) with the name
;'PFR_3'. The PFR is located downstream
;of the confluence of two other reactors
;called PFR_1 and PFR_2, i.e. it has two
;upstream neighbors.
[PFR_3]
  reactor= pfr
  stream_order= 10
  upstream_sections= PFR_1,PFR_2
  parallel_sections= -
  maxorder_recipient= 11

;The reactor 'PFR_5' is located just
;downstream of a flow split. It shares
;the input from reactor 'PFR_4' with the
;parallel reactor 'PFR_6'.
[PFR_5]
  reactor= pfr
  stream_order= 12
  upstream_sections= PFR_4
  parallel_sections= PFR_6
  maxorder_recipient= 13
```

Figure 3.6: *Extract of an extensively commented network description file showing the declaration of a stirred tank and two plug-flow reactors.*

As mentioned in Sect. 3.1.3, the network description file can be generated from GIS data using a utility program. For simple networks it can also be prepared manually.

3.6.4 Preprocessing of hydrodynamic information

It follows from the description of the transport algorithms in Sect. 3.5.2 and Sect. 3.5.3 that TRAM must be supplied with time series of some basic hydrologic variables. For conservative trans-

[9] The number of reactors that can be simulated with TRAM is not limited.

port modeling, only hydrographs of the inflow rate and the storage volume of a reactor need to be known. However, a reasonable formulation of many turnover processes requires information on additional hydrologic variables to be available (see Table 3.3).

It is the task of the preprocessing utilities TRAMP-STR and TRAMP-PFR to create and store time series of all hydrologic variables which can be accessed later on by TRAM. Basically, the preprocessors merge two types of information:

1. Hydrographs of water surface elevation and flow.

2. Data on channel and lake geometry (cross-sections, streamlines, bathymetry).

The benefit from using the preprocessors is twofold: First of all, it is guaranteed that TRAM can be used independently from any specific hydrodynamic model. Because only the hydrographs of flow and water surface elevation are required as input data and derived variables (such as water depth, wet perimeter, etc.; see Table 3.3) are computed by the preprocessors, TRAM could also be run using raw observation data.

The second benefit from the use of the preprocessors TRAMP-STR and TRAMP-PFR emerges if a large number of simulations with the same hydrological boundary conditions are carried out for a system. In this case it would be a considerable waste of time if TRAM was computing values of the derived hydrologic variables from geometry and stage/flow data anew for each model run.

Hydrograph preprocessing for STR

The functioning of the hydrograph preprocessor for stirred tank reactors is illustrated in Fig. 3.7. The required digital elevation model of the lake bottom can be derived from a bathymetry map (Fig. 3.8) by vector to raster conversion using GIS[10]. It is absolutely essential that the same bathymetric map is used for deriving the geometric input data for both TRAM and the hydrodynamic model in order to avoid inconsistencies[11].

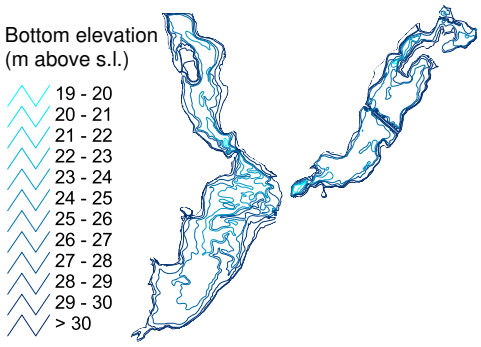

Figure 3.8: *Bathymetric map of three lakes on the Lower Havel River.*

As Fig. 3.7 shows, the preprocessor TRAMP-STR temporarily creates lookup tables from which the derived hydrologic variables can be queried for each water surface elevation in the observed range. This speeds up the preprocessing significantly if input hydrographs contain many values or if the elevation grid has a high ground resolution.

In the current version of the preprocessor, only the reactor's surface area, not the true bottom area is computed. For shallow lakes (and only those can be represented as STR), the two values cannot differ very much. Also, in the formulation of sediment-water interactions the projection of the bottom area must be used which is identical to the surface area.

Hydrograph preprocessing for PFR

The preprocessor TRAMP-PFR is similar to TRAMP-STR as it computes time series of derived hydrologic variables from geometry information and stage/flow hydrographs. However, the spectrum of the derived variables is different and cross-section data form the geometric data base. The overall functioning of the TRAMP-PFR utility is illustrated in Fig. 3.9.

[10] The elevation model is read using the ASCII-grid format.

[11] Disregard of this may cause inaccurate results in transport modeling, but it does *not* affect the overall mass balance.

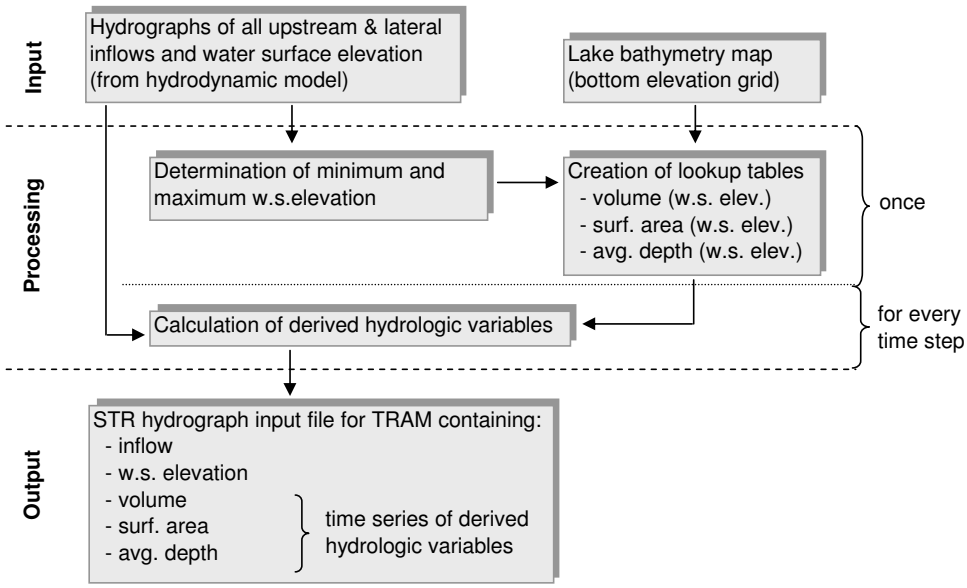

Figure 3.7: *Generation of TRAM's hydrograph input file for a stirred tank reactor by the preprocessing utility TRAMP-STR.*

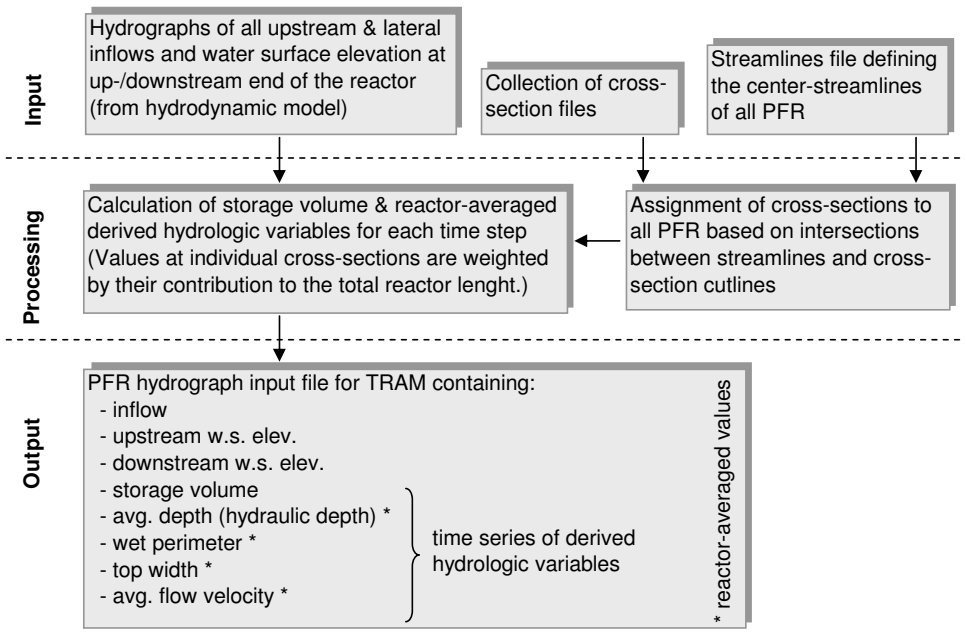

Figure 3.9: *Generation of TRAM's hydrograph input file for a plug-flow reactor by the preprocessing utility TRAMP-PFR.*

Fig. 3.10 shows a detailed sketch of a plug-flow reactor with a definition of cross-section parameters. For each time step in the input hydrographs, the water surface elevation at the individual cross-sections is estimated by linearly interpolating between the given values at the upstream and downstream reactor end. Then, the stage-dependent parameters A (cross-section area), W (top width) and P (wet perimeter) can be determined for each cross-section. Using the information on A, the storage volume V of the PFR with n cross-sections can be computed from Eq. 3.16.

$$V = \sum_{i=1}^{n} A_i \cdot \Delta x_i \tag{3.16}$$

Reach-averaged values of the derived hydrologic variables P and W as well as the average depth D and the average flow velocity U are estimated according to Eq. 3.17–Eq. 3.20. In these equations Q is the reactor's inflow rate and Δx_T is the total length of the PFR, i.e. $\Delta x_T = \sum \Delta x_i$. It is pointed out that one must not derive further composite variables from P, W, D, and U since their interrelationships are non-linear for natural cross-sections. For example, $W \cdot D$ does not yield a proper value for the reach-averaged cross-section area if the reactor's geometry is non-uniform.

$$P = \sum_{i=1}^{n} P_i \cdot \frac{\Delta x_i}{\Delta x_T} \tag{3.17}$$

$$W = \sum_{i=1}^{n} W_i \cdot \frac{\Delta x_i}{\Delta x_T} \tag{3.18}$$

$$D = \sum_{i=1}^{n} A_i/W_i \cdot \frac{\Delta x_i}{\Delta x_T} \tag{3.19}$$

$$U = \sum_{i=1}^{n} Q/A_i \cdot \frac{\Delta x_i}{\Delta x_T} \tag{3.20}$$

Similar to the utility for stirred tanks, TRAMP-PFR is able to process the information for all simulated plug-flow reactors at once. This is because the streamline file (see Fig. 3.11) defines the spatial position of all simulated PFR. Also, the program is supplied with a list of all cross-sections covering the entire simulated river network.

```
Jungfernsee%Westteil
3368854.940765, 5810239.634686
3368769.867465, 5810346.498471
...
3368175.421993, 5811112.224841
3367899.609369, 5811273.430393
END
SPK%BrueckeDesFriedens
3367899.609369, 5811273.430393
...
3367183.050019, 5811609.579583
END
END
```

Figure 3.11: *Shortened sample of a streamlines file describing the spatial position of two plug-flow reactors. The reactor names are followed by a sequence of x,y coordinates that define the streamlines' nodes (here in a UTM system). This notation complies with the 'generate format' of ESRI's GIS.*

#Xcoord	Ycoord	Elevation
3348829.37	5814123.39	29.27
3348827.89	5814125.99	28.99
3348826.40	5814128.60	28.94
...	...	...
3348168.01	5815282.83	28.41
3348166.52	5815285.43	28.44

Figure 3.12: *Shortened sample of a three-column cross-section file with UTM coordinates assigned to each elevation record.*

For cross-sections to be automatically assigned to the correct reactors and for determining their exact positions within the PFR, the cross-section data should have a full spatial reference (3D data) as shown in Fig. 3.12. The use of spatially referenced cross-sections is advisable anyway if a hydrodynamic model with GIS data import capabilities like HEC-RAS (USACE, 2002) is applied.

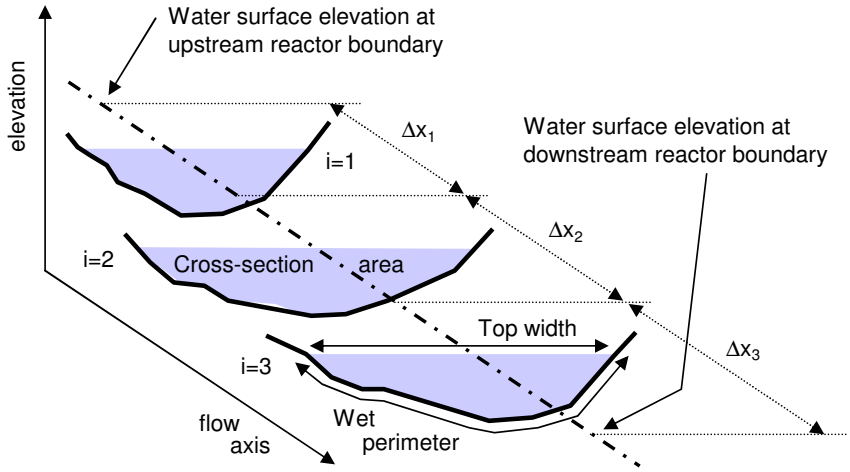

Figure 3.10: *Schematic of a plug-flow reactor whose channel geometry is described by three cross-sections. The symbol Δx_i denotes the reach length corresponding to the cross-section with index i.*

Fig. 4.17 shows the plug-flow reactor's streamlines as well as the corresponding cross-section cutlines for a part of a river network.

3.6.5 Definition of the turnover model

As mentioned in Sect. 3.3.3.2 the preprocessing program TRAMP-CODEGEN is used for translating the user-supplied description of the turnover model into FORTRAN code. This program must be supplied with two ini-files (one for PFR, another one for STR) containing all information of the process matrix, i.e. component and process names, stoichiometry coefficients and process rate expressions (see Table 3.1 on page 31). These files are called the 'process definition files'. In order to facilitate their preparation, especially with respect to the writing of the process rate expressions R_j (see Sect. 3.3.2), a special but simple language is used.

3.6.5.1 Language elements

The language comprises variables, constants, terms, numbers, functions, operators, and conditional expressions.

Variables

Generally, variables change their values during simulation. As described in Sect. 3.3.3, TRAM knows different types of variables such as component concentrations, hydrologic variables, and boundary conditions. Variable names for components and boundary conditions can be chosen freely but in case of components, the first character of the name has a special meaning. If it is a dollar sign ($), the component is implicitly declared immobile but it is mobile otherwise. If used in expressions, variable names must always be enclosed in brackets. Valid variable names are for example *'[aVariable]'*, *'[NO3]'*, *'[NO3_N]'*, or *'[$SedimentP]'*. The names of the hydrologic variables are fixed according to Table 3.3 (page 34). The simulation time can be assessed by the variable name 'unixtime'.

Constants

The values of constants do not change during simulation. Constant names may consist of any characters but within expressions, their names must be enclosed in angle brackets. Valid constant names are for example *'<aConstant>'* or *'<k_2>'*.

Numbers

Constant values can alternatively be written as common floating point numbers. This may be useful for converting units but the use of constants

(see above) should be preferred. While constants are read from input files and their values can easily be modified, hard-coded numbers are fixed once TRAM is compiled.

Terms

A 'term' can be used to temporarily store the result value of an expression. The result value should always be assigned to a term name if an expression appears in multiple other expressions. This prevents the waste of computer time as the original expression is evaluated only once and thereafter the term name can be used as a substitute for it. Also, the storage of intermediate results by the use of terms makes complicated process rates easier to write and to debug. A term name may consist of the characters a–z, the digits 0–9, and the underscore only. In other words, term names must be legal FORTRAN identifiers. If terms are referenced in expressions, their names must be enclosed in curly braces, e.g. *'{aTerm}'*. The expression which is assigned to a term name may contain references to previously defined terms but no cyclic references.

Conditional expressions

In some cases it is desirable to use conditional expressions in the formulation of the process rates. A conditional expression always starts with the sequence *'|if| (condition) |then| (expression)'* which can be followed by an *'|elseif| (condition) |then| (expression)'* branch and/or by *'|else| (expression) |endif|'*. The conditions must be enclosed by parenthesis and the old-style FORTRAN comparison operators like *.lt., .ge., .eq.* must be used. It is important to realize that functions containing conditional expressions are often discontinuous and the convergence of numerical integrations may be hindered.

Functions and operators

In addition to the items listed above, expressions may contain all FORTRAN intrinsic functions with a scalar return value (e.g. *log, exp, min, max*). Also supported are the four standard operators, the double asterisk for power operations, and, of course, parenthesis.

```
[Processes]
  Namelist= Growth, Settling, Recycling

[SimulationVariables]
  Xdis  = 0.1  # the dissolved nutrient (g/m3)
  Calg  = 2.0  # phytoplankton carbon (g/m3)
  $Cset = 1.0  # settled phytoplankton (g/m2)

[Constants]
  g = 1.0/86400  # pot. growth rate (1/s)
  k = 0.02/86400 # decay rate (1/s)
  Hx = 0.01      # half saturation (g Xdis /m3)
  theta = 1.045  # temp.-depend. of growth (-)
  Qxc = 0.025    # X:C ratio in plankton (-)
  u = 0.1/86400  # settling velocity (m/s)
```

Figure 3.13: *Part of a process definition file containing the declaration of process names, components and constants. The corresponding process matrix is given in Table 3.2.*

3.6.5.2 Sections of a process definition file

In the following paragraphs, the contents of the process definition file are discussed. All presented examples (Fig. 3.13–3.17) refer to the sample process matrix from Table 3.2 in Sect. 3.3.2.

Part 1

The first sections of the process definition file (Fig. 3.13) are used for declaring the names of the considered turnover processes and simulated components as well as the names of constants. As the example in Fig. 3.13 illustrates, numeric values must already be assigned to the component concentrations and constants. It is important to realize that these values are in no way used in later simulations. The values become relevant onlywhen the mass balance of the process matrix is automatically checked as described in Sect. 3.6.5.3. Hence, guessed values of the correct magnitude are sufficient.

Part 2

The names of boundary condition variables are declared in the next sections of the process definition file (Fig. 3.14) and – in order to enable mass balance checks – values are assigned to them. Also, test values are set for the hydrologic variables

```
[BoundaryConditionVariables]
  T = 20.0          # water temperature (°C)

[HydrologicVariablesEstimates]
  INFLOW = 10.0     # inflow rate (m3/s)
  WSELEV = 30.0     # water surf. elevation (m)
  ADEPTH = 2.0      # average depth (m)
  SFAREA = 1.0e+06  # surface area (m2)
  VOLUME = 2.0e+06  # volume in reactor (m3)
```

Figure 3.14: *Part of a process definition file in which boundary condition variables are declared and values used in mass balance checks are assigned. The corresponding process matrix is given in Table 3.2.*

```
[ReferenceVolumes]
  Xdis  = [VOLUME]  # water body volume (m3)
  Calg  = [VOLUME]  # water body volume (m3)
  $Cset = [SFAREA]  # bottom area (m2)

[ReferenceElementFactors]
  Xdis  = 1.0
  Calg  = 0.025  # the stoichiometry factor Qxc
  $Cset = 0.025  # the stoichiometry factor Qxc
```

Figure 3.15: *Part of a process definition file containing information which is used in the calculation of mass balances. The corresponding process matrix is given in Table 3.2.*

which are automatically provided by TRAM rather than being defined by the user (see Table 3.3). As the names of the hydrologic variables suggest, the example of Fig. 3.14 corresponds to a stirred tank reactor.

Part 3

The information in the ini-file sections shown in Fig. 3.15 is only evaluated in mass balance checks of the user-supplied process matrix. In the section *'ReferenceVolumes'* a domain must be specified for each of the simulated components. In general, the domain of dissolved or suspended mobile components is the volume of the water column. This means that the total mass of such a component in a STR can be calculated as the product of the concentration and the volume of the water column, given by the hydrologic variable *'[VOLUME]'*. For immobile components, different domains are possible: For instance, a component's mass can be related to the surface area (g m^{-2}) as this is the case with component C_{set} in Fig. 3.15. Then, the required entry is a reference to the variable *'[SFAREA]'* (see Table 3.3). Alternatively, the component's mass may be related to the volume of a certain sediment layer (g m^{-3} of sediment) and the entry would be *'[SFAREA] * <t>'*, where *'<t>'* represents a user-defined constant for the layer's thickness. In the case of non-particulate components which are dissolved in the sediment's pore water, concentrations are also given in g m^{-3} but the calculation of the total mass requires the concentration to be multiplied by both the volume of the sediment layer and the porosity. The reference volume could then be defined as *'[SFAREA] * <t> * <p>'* where *'<p>'* is again a reference to a user-defined constant. Alternatively, both the thickness of the sediment layer and the porosity could be declared as variables.

Since sediment-bound components are currently not supported in plug-flow reactors, the reference volume for all simulated components in a PFR is equal and should be set to unity.

In the section *'ReferenceElementFactors'* factors can be supplied with which the component concentrations are multiplied when mass balances are computed. By means of these factors, certain components can be excluded from a balance (factor zero), they may be included (unity) or stoichiometric characteristics can be accounted for (e.g. NO_3^- could be converted to NO_3^--N). In the example shown in Fig. 3.15, the mass balance is computed for the nutrient X and the conversion factor Q_{XC} must be used in order to account for the nutrient mass stored in the phytoplankton and the settled material which are both defined in units of g carbon m^{-3} (C_{alg}, C_{set}).

Part 4

In this section of the process definition file, the process rates R_j ($j = 1 \ldots m$) for all m processes are assembled and assigned to named terms. An example corresponding to the process matrix of Table 3.2 is shown in Fig. 3.16. Syntax highlighting greatly facilitates the distinction of variables, constants, and terms.

```
[Terms]

  # Nutrient limitation of growth rate (-)
  limit_x = [Xdis] / ([Xdis] + <Hx>)
  # Temperature limitation of growth rate (-)
  limit_t = <theta> ** ([T]-20.0)
  # Process rate for growth (g Calg / s)
  R_grw = <g> * {limit_t} * {limit_x} * [Calg]

  # Process rate for settling (g Calg / s)
  R_set = <u> * [SFAREA] / [VOLUME] * [Calg]

  # Process rate for recycling (g Cset / s)
  R_rec = <k> * [$Cset]
```

Figure 3.16: *Part of a process definition file illustrating the use of 'terms' for storage of the process rates and intermediate results. The corresponding process matrix is given in Table 3.2.*

```
[Growth]
  Xdis  =   {R_grw} * <Qxc> * (-1.0)
  Calg  =   {R_grw}
  $Cset =   0.0

[Settling]
  Xdis  =   0.0
  Calg  =   {R_set} * (-1.0)
  $Cset =   {R_set} * [VOLUME]/[SFAREA]

[Recycling]
  Xdis  =   {R_rec} * <Qxc> * [SFAREA]/[VOLUME]
  Calg  =   0.0
  $Cset =   {R_rec} * (-1.0)
```

Figure 3.17: *Part of a process definition file containing the differential equations which describe the change in the components concentrations over time due to the considered turnover processes. The corresponding process matrix is given in Table 3.2.*

Part 5

In the final sections of the process definition file, the derivatives of the component's concentrations with respect to time are supplied (Fig. 3.17). Note that the differential operator d/dt is not written but only the components' names appear as key names on the left hand sides. As Fig. 3.17 shows, the contribution of each process is written down separately for all components. This has several advantages over writing the full differential equation for each component as a single expression. First of all, it brings clarity and makes error tracing easier. Secondly, the mass balance can be computed separately for each of the conversion processes which again facilitates debugging. For a process matrix involving n simulated components and m processes, $n \times m$ equations must be supplied, each taking a separate line.

As mentioned in Sect. 3.3.2, the transport terms must not appear in the right hand side expressions supplied here as TRAM takes them into account automatically if necessary.

3.6.5.3 Preprocessing of the process definition file

As mentioned in Sect. 3.3.3, the preprocessor TRAMP-CODEGEN basically creates two FORTRAN files which become part of TRAM's source code. While one source file declares variables and constants names only, the other contains the function to compute the derivatives of the components' concentrations.

In addition, the preprocessor generates a third FORTRAN source file. The compilation of this auxiliary file yields a small separate executable which computes the mass balance for each of the processes using the test values that were assigned to the various variables and constants. It is recommended to always build and run this executable as it provides the best means to verify the consistency of the complex information contained in the process definition file. If this auxiliary source file is not compiled without errors, the compilation of TRAM will fail too, and the process definition file must be revised. Automatic comments in the generated source file make it rather easy to locate the cause of the error in the process definition file.

The output of the mass balance verification program for the sample file shown in Fig. 3.13–Fig. 3.17 is illustrated in Fig. 3.18. The zero values in the summary rows 'balance' indicate that the presented process definition file (and thus the process matrix from Table 3.2) provides a closed description of the mass balance of the nutrient X. The booleans in the rightmost column indicate for which components the calculation of a mass balance is activated by setting the reference element factor (see Fig. 3.15) to a non-zero value.

```
*********************************************
   Process | Variable |   Derivative | Active?
*********************************************
    growth |     xdis | -0.10522E+01 |    TRUE
    growth |     calg |  0.10522E+01 |    TRUE
    growth |    $cset |  0.00000E+00 |    TRUE
-----------+----------+--------------+---------
           |  Balance |  0.00000E+00
*********************************************
  settling |     xdis |  0.00000E+00 |    TRUE
  settling |     calg | -0.57871E-01 |    TRUE
  settling |    $cset |  0.57871E-01 |    TRUE
-----------+----------+--------------+---------
           |  Balance |  0.00000E+00
*********************************************
 recycling |     xdis |  0.57870E-02 |    TRUE
 recycling |     calg |  0.00000E+00 |    TRUE
 recycling |    $cset | -0.57870E-02 |    TRUE
-----------+----------+--------------+---------
           |  Balance |  0.00000E+00
*********************************************
```

Figure 3.18: *Output of the preprocessor-generated program which verifies the process definition file by computing mass balances for the simulated processes (see Table 3.2 for the corresponding process matrix).*

```
[u]
  * = 0.1
  @Group1 = 0.15
  Reactor1 = @Group1
  Reactor2 = @Group1
  Reactor3 = 0.2
```

Figure 3.19: *Part of an ini-file defining the values of a constant u. The name of the constant is given in the section header. In the example, u is individually set to a value of 0.2 for a reactor called 'Reactor3'. A common value of u=0.15 is assigned to the reactors 'Reactor1' and 'Reactor2'. This is achieved by specifying another key name at the right hand side instead of a numerical value. For all reactors whose names do not explicitly appear as key names, the default value of 0.1 is used. The reserved key name for specifying the default is the asterisk.*

3.6.6 Values of constants and initial concentrations

In principle, the values of constants appearing in the turnover model can be set individually for each reactor in order to reflect spatial heterogeneities in the river system. However, often it is desirable to set or to modify a parameter for a whole group of reactors with similar characteristics or even for all reactors in the model domain. How this can be conveniently accomplished by the use of ini-files is demonstrated by Fig. 3.19 which shows a sample part of a constants file. Initial concentrations of the components are specified in a separate 'initial conditions file' whose structure is identical with the 'constants file'.

3.6.7 Time series data

TRAM reads all time series files in a standard ASCII format with date and time being formatted in the form 'DD.MM.YYYY hh:mm:ss'. Hence, time series files can conveniently be created by spreadsheet software or data base queries. Apart from the preprocessor-generated hydrographs addressed in Sect. 3.6.4, different groups of time series data can be distinguished.

Time series of external loads

The passing of loads from a reactor to its downstream neighbors is managed by TRAM automatically. Apart from these loads, every reactor may experience the input of additional external loads, e.g. due to a discharge of waste water. In a 'boundary condition management file', which is just another ini-file, times series of such additional loads can be assigned to each reactor for all mobile components.

The specification of additional input loads is optional in general, but load hydrographs must necessarily be assigned to reactors with a stream order of 1, i.e. for the upstream boundaries of the model domain. If multiple load hydrographs for the same component are assigned to a reactor, their values are added up.

Time series of other boundary conditions

In addition to the specification of load boundary conditions for the simulated components, non-load boundary conditions can also be defined in the the boundary condition management file. For example, time series of water temperature must be assigned to each reactor if the water temperature was declared a boundary condition variable in the turnover model (see Sect. 3.6.5).

Time series of observed concentrations
For each simulated component and each reactor, time series of observed concentrations can be specified. If this is done, TRAM computes a set of goodness-of-fit measures and writes them to an output file which can be used for assisting model calibration.

3.6.8 Simulation control parameters

Information on TRAM's basic simulation control parameters is provided below. The parameters can either be read from a keyword-driven text file or they can be specified at the command line. Command line arguments always take precedence. If both alternatives are not used, TRAM prompts for interactive input.

Simulation time window
Dates have to be specified when the simulation should start and end. Furthermore, a date can be supplied from which point onwards TRAM outputs detail intermediate results. This is useful when errors in the user-supplied description of turnover processes or other input data need to be tracked down.

Simulation time step
The simulation time step (given in seconds) determines at which time interval the values of the simulated variables are actually computed. It also controls the temporal resolution of a reactor's export-load hydrograph and it sets the maximum possible temporal resolution of TRAM's standard output files.

It is important to know that this parameter also determines the time interval at which the values of user-specified boundary condition variables are updated. Furthermore, the supplied value serves as an initial estimate of the time increment to be used by TRAM's numerical integration routines.

Useful guidelines for selecting the appropriate simulation time step are:

- The value should be equal or less than the temporal resolution of all user supplied boundary condition time series (e.g. preprocessor-generated hydrographs or time series of additional user-defined variables). This is to make sure that TRAM actually considers all fluctuations in the boundary conditions.
- The value must not be greater than the desired resolution of the model output but it can be smaller of course.
- A rather small value should be chosen if large changes in the numerical values of simulation variables are expected within short periods of time (highly dynamic systems). Choosing a too large value may result in unnecessary adjustments of the time increment in the numerical integration routines.

It is a good idea to compare model results generated with a different simulation time step in order to find the optimum value for a specific application.

Numerical solver parameters
Several parameters have an influence on the numerical solution. First of all, the required accuracy in numerical integrations must be specified[12]. Another input parameter is the smallest tolerable time step (seconds) to be used in the numerical integration. TRAM terminates with an appropriate error if the automatically adjusted step size falls below this threshold. In many applications, step sizes in the order of seconds or less indicate inconsistencies in TRAM's input data (bad process formulation, inappropriate units of constants, etc.). Finally, there is an option to switch between the Runge-Kutta solver which is fast but not stiffly stable and the Rosenbrock integration algorithm.

River network data
Along with the name of the network description

[12]The accuracy is equivalent to the maximum fractional error in a simulated variable for an integration step. Depending on the application and the chosen time step, a value of 10^{-4} or less may be appropriate.

file (see Sect. 3.6.3) stream orders must be supplied at which TRAM should start and finish the simulation. As discussed in Sect. 3.6.3, specifying an initial stream order k which is greater than 1 requires that the export load hydrographs of all upstream reactors (stream orders $< k$) were written to disk in a previous model run.

Hydrograph directories
The names of two directories must be specified, where TRAM searches for the reactor's hydrograph files prepared by the preprocessors TRAMP-PFR and TRAMP-STR (see Sect. 3.6.4).

Further input files
File names need to be specified for the initial conditions file, the constants file (Sect. 3.6.6) and the boundary condition management file (Sect. 3.6.7). In addition, the name of an ini-file must be given by which the output of simulation details is controlled. For example, the output of hydrographs can be switched on and off and the creation of a detailed logfile can optionally be suppressed. Also, debug printouts may be enabled for a specific reactor and time through settings in this file.

Finally, the name of another ini-file is required which assigns time series of observed concentrations to specific reactors and components for goodness-of-fit computations.

Output files and directories
A directory must be given where all model results (Sect. 3.7) and TRAM's log file are to be stored. The file names for simulation results and export load hydrographs are automatically generated based on the reactor's names. In addition, a file must be specified where goodness-of-fit parameters are written to.

3.7 TRAM's output

Standard output
As standard, TRAM creates a detailed output file for each reactor containing time series of all variables (component concentrations, hydrologic variables, boundary conditions). In the case of multi-component simulations for large networks and long time periods, the amount of output data becomes large and the writing of detailed output files can therefore be optionally suppressed for selected (or even all) reactors. As all output files are plain, tab-separated ASCII text they can readily be imported into spreadsheets, a data base, or visualization and statistics software such as GNUPLOT or 'R'.

Hydrographs of export loads
In general, the output load hydrographs of a reactor are stored in memory and the corresponding memory is not deallocated before all downstream reactors which receive these loads as input have been processed. However, TRAM can be asked to save the output loads of selected reactors to disk, which is useful if the simulation is to be restricted to a part of the river network. If the output load hydrographs of all reactors with stream orders $< k$ were written to disk, subsequent simulations can be started at stream order k instead if 1.

Validation results
As mentioned earlier, TRAM automatically outputs goodness-of-fit parameters if observation data are provided for certain simulated components and reactors. These measures include the mean error ME, the mean absolute error MAE, and the mean absolute percentage error MAPE, the root mean square error RMSE, the square of Pearson's correlation coefficient RSQR, and the efficiency after Nash & Sutcliffe (1970). In order to assess the quality of a simulation, it is worth looking at a multiple of these parameters as their sensitivity to certain types of errors is different (Legates & McCabe Jr., 1999). The author personally prefers to inspect the ME as it shows the bias in the unit of the variable, the MAPE because it is instructive, and the efficiency (Eq. 4.34) since the values are easy to interpret.

TRAM also outputs statistics of the observed data and the corresponding simulated values such as variances, percentiles, and extremes.

3.8 Possible enhancements of the current model version

This section addresses some known limitations of the current version of TRAM which should be resolved in the future.

Immobile components in plug-flow reactors
Currently, the only way to simulate immobile components in river or channel sections is to represent these sections by a tanks-in-series model, i.e. by a series of properly sized STR. In the future, the plug-flow routine (Sect. 3.5.3) should be enabled to also handle immobile components. In this context, an internal spatial discretization of plug-flow reactors needs to be introduced in order to account for the fact that the water travels downstream while the bottom sediment, to which immobile components are attached, remains in place.

Distributed input loads from non-point sources
At present, load boundary conditions are generally attached to the upstream end of a plug-flow reactor. Thus, for approximating the lateral input of mass from non-point sources, a plug-flow reactor needs to be subdivided into a series of PFR, each receiving a fraction of the total load. A revised version of TRAM should be able to account for spatially distributed load boundary conditions.

Withdrawal of water
A future version of TRAM should be able to simulate the withdrawal of water due to seepage or pumping. Currently, only makeshift solutions are available, like the use of parallel branches with near zero return flow.

Stratified stirred tanks
Very recent investigations on the Havel River (Becker, 2006) emphasized the relevance of temporary stratification even in lakes of small depth. In a future revision of TRAM, a concept for representing such events should be considered. For example, stirred tank reactors might be discretized into a variable number of layers. The vertical fluxes between the layers would need to be estimated from information on water temperature and wind speed, possibly using stochastic methods.

Time series processing
As pointed out in Sect. 3.4, time series are approximated by step functions in the current version of the model, i.e. each time interval is represented by a constant average value. In order to enhance the accuracy of turnover computations (nonlinear terms) and to reduce numerical diffusion in the transport schemes, an alternative representation should be considered. The use of piecewise linear functions is a possible option.

XML-based input files
The '.ini'-format (Sect. 3.6.1), which is used for most of TRAM's input, is excellent for storing tabular data. For managing more complex data structures, such as the definition of the turnover model (Sect. 3.6.5.2), the XML format would be a better alternative.

3.9 The source code

TRAM is written entirely in FORTRAN 95 which is an up-to-date procedural computer language which is comparable to C with respect to execution speed. The current model version was built using the free G95 compiler (www.g95.org, 2006). The use of this compiler guarantees that TRAM can be used and modified by anyone, without restrictions.

As this is supported by G95, the source code makes use of some features of the FORTRAN 2003 standard which is available as a draft (ISO/IEC, 2003). Most important is the availability of allocatable arrays in derived types. This allows for the creation of fully dynamic record types without using pointers. If such types are stored in module files together with specific constructor, destructor and data handling routines, a well structured, rather object-oriented source code is obtained. The contents of such a FORTRAN module is virtually equivalent to a class definition.

In order to facilitate maintenance and to allow for uncomplicated modifications of TRAM's

sources, some coding conventions were introduced.

- Subroutines and functions were grouped into modules. In this way, non-specific parts of the code were well separated from the actual TRAM code.
- All input and output data of functions and subroutines are passed as arguments. Global variables are not used at all. This guarantees that the effect of local code modifications remains predictable.
- Explicit declaration was used for all variables.
- All involved arrays are dynamically allocated.
- No reliance is given to compiler options (e.g. variable initialization is always done explicitly, the kind of real data is always specified, etc.)
- The code contains comments at crucial locations and identifiers were given associative names.
- Compiler specific language extensions were used in rare cases only, such as for retrieving command line arguments or for executing shell commands. Wrapper routines were used in order to facilitate a replacement of these non-standard FORTRAN features when another compiler is used or TRAM is ported to another platform.

Chapter 4

Model application to the Lower Havel River

4.1 Objectives of modeling

The ultimate motivation for applying TRAM to the Lower Havel River follows from the outline of the research project presented in Fig. 4.1. A condensed overview of this project has already been given in the introduction to this thesis. In summary, it was aimed at analyzing the efficiency of different options for controlling eutrophication of the Havel River and its tributaries. These options were focused on the elements nitrogen and phosphorus and different scenarios with reduced emissions from point and non-point sources were set up. Since the Water Framework Directive requires the 'good ecological status' to be achieved until 2015, the time frame for scenario analyses was 2003–2015.

The impact analysis involved the simulation of the river basin's water and nutrient budgets for the scenarios with the mesoscale hydrological catchment models SWIM (Krysanova et al., 2000) and ArcEGMO-Urban (Biegel et al., 2005). By nature, these models are not capable of adequately representing hydrological features of individual water bodies and nutrient turnover in the aquatic environment.

Consequently, TRAM was set up as an extension to the above mentioned catchment models for the river section introduced in Sect. 4.2. Using the reactor concept (Sect. 3.1.1) TRAM allowed for the representation of the river network and the geometric features of individual water bodies with a grade of detail that is adequate to the spatial scale. It was the task of the underlying hydrodynamic model to describe the flow distribution in the river system and the apparent influence of river regulation.

Previous studies on nutrient dynamics of the Havel River (Hoffmann, 1999; Schettler, 1995) have shown that the process of phosphorus remobilization from sediments strongly influences the observed P concentrations. Furthermore, Behrendt & Opitz (2000) demonstrated the significance of nitrogen retention in river systems. Based on the results of Kozerski et al. (1999), significant retention effects must also be expected for the Lower Havel River.

Consequently, a first objective of modeling was to carry out a system analysis in order to find out to what extent nutrient concentrations are actually controlled by internal turnover. The focus of the analysis was on the magnitude and the seasonal pattern of nitrogen retention and phosphorus retention/release. Because TRAM does not consider any conversion processes by default, an appropriate description of N and P turnover in the Lower Havel River had to be established first (Sect. 4.4). In this context, an 'appropriate description' is one which balances simplification and reliability. The search for an acceptable compromise was certainly the crux of modeling.

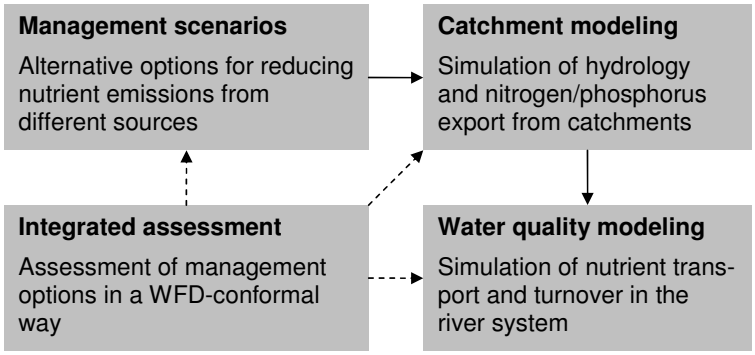

Figure 4.1: *Basic outline of the research project 'Management Options for the Havel River Basin'.*

As shown in Fig. 4.1, the suggested management options had to be evaluated using a WFD-conformal water quality classification. Thus, the final objective of modeling was to provide estimates of the N and P concentrations in the study river under moderately changed management as a basis for inter-scenario comparison and the assessment of management options.

Last but not least, the model study presented in this chapter was a baptism of fire for the concepts underlying the newly developed simulation tool TRAM.

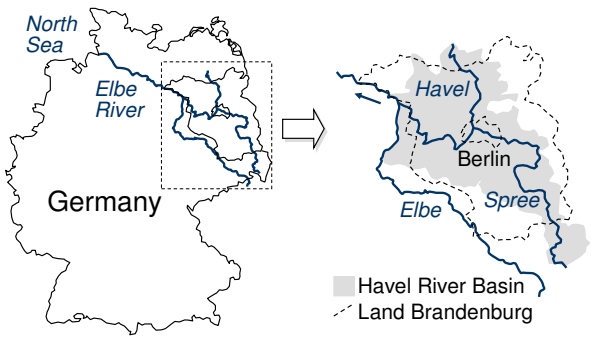

Figure 4.2: *Location of the Havel River Basin within Germany.*

4.2 Introduction to the study site

4.2.1 Hydrology

With a catchment size of about 24100 km^2, the Havel River is one of the major tributaries of the Elbe River (Fig. 4.2). The total river length is 325 km but the difference in elevation between source and mouth is only 41 m. The average slope of the riverbed is 0.13‰ (Naumann, 1995).

The largest tributary is the Spree River which joins the Havel just downstream of Berlin. At the confluence, the catchment size of the Spree River exceeds that of the Havel by a factor of about three (Fig. 4.4). While the Havel itself is a pure lowland River, the Spree River has its source in the hills of Upper Lusatia at an altitude of 478 m.

On their course both the Havel and the Spree River pass a number of flushed lakes. Downstream of the Berlin metropolitan area, the Havel enters a river-lake system with a total length of about 40 km (Fig. 4.3). This river section is marked in Fig. 4.4 as 'study area' and a more detailed map is given in Fig. 4.5. Most of the lakes are shallow (mean depth 3.5 m) and polymictic, i.e. they experience continuous mixing of the water column. The large cross-sections in lakes and widened channels as well as the lowland topography cause flow velocities to be generally low. Due to additional river regulation by weirs, the slope of the water surface at mean flow

Figure 4.3: *View over a lake-like bay of the Havel River in Potsdam city.*

is about 0.006‰ only and flow velocities may drop to near-zero values in dry periods during summer.

The mean specific discharge of the Havel River at the Ketzin gage (see Fig. 4.4) is 4.6 l s^{-1} km^{-2}. Compared with other German river basins (Naumann, 1995) this is a rather low value (e.g. Elbe at Wittenberge: 5.6, Oder at Eisenhüttenstadt: 6.1, Rhine at Kaub and Danube at Ingolstadt: 15.1 l s^{-1} km^{-2}). The low value of 4.6 l s^{-1} km^{-2} appears even more remarkable if one takes into account that the discharge of the Havel River was artificially increased in the past due to drainage of the Lusatian coal mining areas (Spree catchment).

Basic hydrologic parameters for the Ketzin gage (label 6 in Fig. 4.4 and label Hv0195 in Fig. 4.5) are summarized in Table 4.1. Like at many other gages along the Havel River, discharges are measured by the ultrasonic method. Nevertheless, even the gage operators regard measurements as highly uncertain during periods of low flow. Attempts to measure flow rates at some ungaged locations of the Havel River by induction sensors had to be given up by the author. However, the measurements led to the insight that, at low discharge, the flow is heavily controlled by wind and navigation. In some lakes, low-frequency oscillations of the water table (so-called seiches) are caused by wind action.

For most of the time water levels are exclusively controlled at the weirs and gates (see Fig. 4.4). Target water levels and their seasonal variation are negotiated every year by the navigation and water authorities, fishermen, farmers, environmentalists, and residents. Since the Havel is a waterway under federal control, the navigation requirements usually have priority. The difference in target water levels for the summer and the winter period is only 10–15 cm at the Brandenburg weir (shown at the very left of Fig. 4.5).

Due to the lowland topography as well as retention in lakes and impoundments, flood waves of the Havel River are generally smooth. Even at the mean annual flood the water surface slope is only 0.9 cm km^{-1} (period 1993-2002; WSA, 2003). The estimated discharges with return periods of 5, 20, 50, and 100 years are 151, 167, 202, and 216 m^3 s^{-1} at the Ketzin gage.

The Havel River is low in suspended sediments since erosion rates are low and much of the transported material is deposited in lakes. With respect to the Spree tributary, the inland delta 'Spreewald' is an additional huge sediment trap. The bottom sediments of the Havel River are mainly sandy. In lakes and dead zones organic mud is deposited on top of the fluvial substrate.

4.2.2 The eutrophication problem

The major water quality problem of the Lower Havel River with its many interconnected lakes is eutrophication. Consequently, water quality classification focuses on the trophic state rather than on saprobity.

Various methods of trophic state classification for lakes exist (e.g. Carlson, 1977; Vollenweider & Kerekes, 1982) and comparable schemes for plankton dominated rivers have recently been developed (Behrendt & Opitz, 1996; Behrendt & Mischke, 2002; LAWA, 2002). Most of them use either statistical values of phosphorus and nitrogen concen-

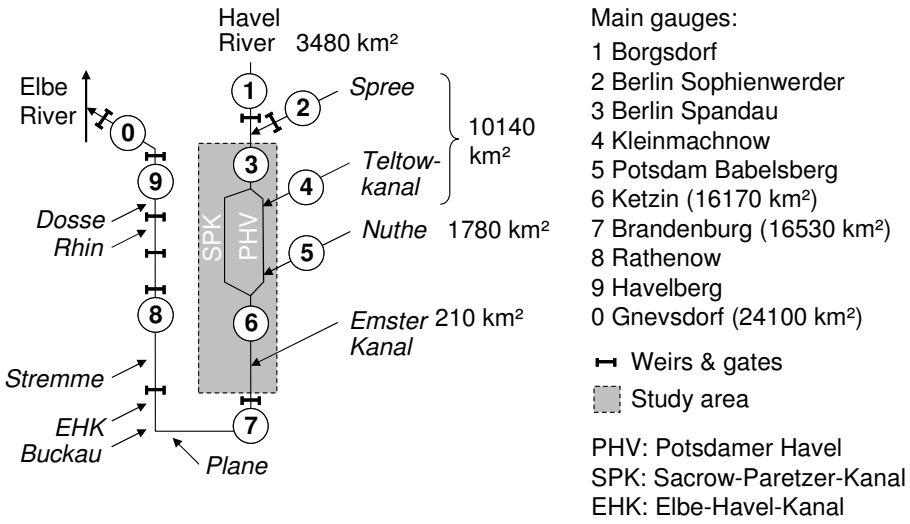

Figure 4.4: *Schematic representation of the Lower Havel River between Berlin Spandau and its mouth at Gnevsdorf. Shown are the main tributaries (italic names; all are heavily regulated) and the major gaging stations (numbers) with their corresponding catchment areas. Highlighted is the study area between Berlin Spandau and the city of Brandenburg. The 'Potsdamer Havel' represents the original course of the river while the 'Sacrow-Paretzer-Kanal' is an artificial shortcut channel designed for navigation.*

Table 4.1: *Flow statistics of the Havel River at the Ketzin gage for the hydrological years 1988–2004. All values in $m^3\ s^{-1}$. Source of raw data: Wasser- & Schifffahrtsamt Brandenburg.*

	Nov	Dec	Jan	Feb	Mar	Apr	May	Jun	Jul	Aug	Sep	Oct	Year
Year of appearance	'88	'94	'94	'94	'88	'88	'94	'94	'95	'02	'94	'02	
HQ	120	139	176	179	185	170	185	122	105	123	103	97	185
MHQ	77	93	101	110	116	97	75	60	51	43	55	60	130
MQ	58	69	82	91	93	82	53	40	31	26	38	45	59
MNQ	41	45	59	64	67	55	27	18	14	10	19	29	7
NQ	11	21	14	21	40	20	3	0	0	1	1	12	0
Year of appearance	'04	'97	'97	'97	'04	'93	'00	'03	'03	'03	'03	'04	

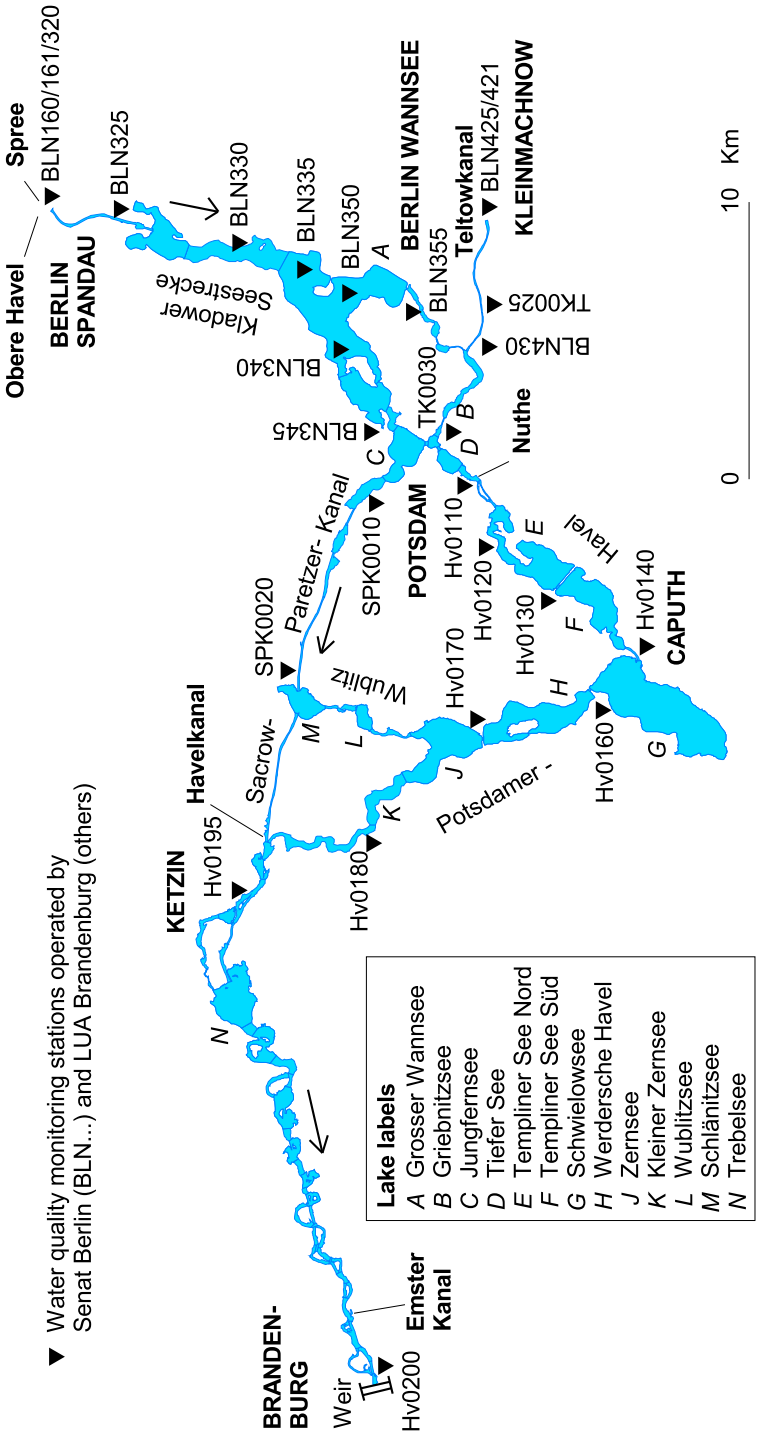

Figure 4.5: *Detailed map of the river-lake system between Berlin Spandau and the city of Brandenburg. Names of major tributaries are given in bold, city and village names in capitals.*

Table 4.2: *WFD-conformal water quality assessment scale for the Havel Lakes with respect to phosphorus from LUA (2005a). The total phosphorus concentrations are annual average values in $\mu g\ l^{-1}$. The class 'high' represents the reference conditions without anthropogenic disturbance.*

State	High	Good	Moderate	Poor	Bad
TP	<97	97–172	172–305	305–538	>538

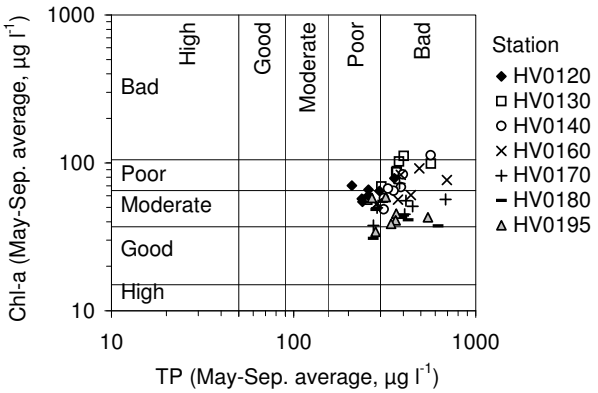

Figure 4.6: *Water quality of the Potsdamer Havel Lakes according to the classification suggested by Behrendt & Mischke (2002) based on average values of chlorophyll-a and total phosphorus over the vegetation period (May–September). Each data value represents a single year of the period 1998–2004.*

trations (focus on the causes) or parameters like Secchi-depth or chlorophyll-a (focus on the consequences). Some classification schemes make use of both kinds of indicators. The application of the assessment scale suggested by Behrendt & Mischke (2002) is illustrated in Fig. 4.6. According to Mietz & Vietinghoff (1994) all lakes of the Potsdamer Havel shown in Fig. 4.5 belonged to the hypereutrophic type at the beginning of the 1990s.

With the implementation of the European Water Framework Directive in 2000, the standards for trophic state evaluation changed. It became necessary to assess the 'ecological state', i.e. the deviation between the current ecological conditions and reference conditions, expected in the absence of anthropogenic disturbances. For the lakes of the Havel catchment, an assessment scale for the chemical parameter phosphorus was developed by LUA (2005a). It is based on a paleolimnetic analysis of diatom skeletons in undisturbed sediment cores. This scale (see Table 4.2) is less stringent than the one from Fig. 4.6 and the recent quality state of the Havel Lakes downstream of Berlin is classified as 'moderate'. Within the research project 'Management Options for the Havel River Basin' the scale from LUA (2005a) was used for its compatibility with the requirements of the WFD.

It is important to understand that the high trophic level of the Havel River is favored by several factors: River morphology, catchment hydrology, and the excessive input of nutrients.

Influence of hydrological conditions

According to the classification of German rivers and lakes (LAWA, 2003), the lakes of the Lower Havel River belong to type 12 (calcium-rich, non-stratified lakes of the lowland with residence times of 3–30 days and a volume quotient[1] VQ greater than 1.5 m^{-1}).

The volume quotient is a key parameter in the identification of potentially natural nutrient concentrations (LUA, 2005a). The larger VQ is, the higher is the expected in-lake nutrient concentration in steady state. In the case of the lakes shown in Fig. 4.5, the volume quotients are large. For example, VQ is 550 m^{-1} for Lake Schwielowsee. In addition, short residence times of the water (see Fig. 4.7) guarantee a constant delivery of nutrients from the catchment.

Finally, elevated nutrient concentrations over the vegetation period are favored by the absence of summer stratification. While settled nutrients are temporarily trapped in the hypolimnetic layer of stratified lakes, an efficient recycling throughout the whole year occurs in shallow water bodies.

[1]The volume quotient VQ ($m^2\ m^{-3}$) relates the size of a water body's catchment area to its volume.

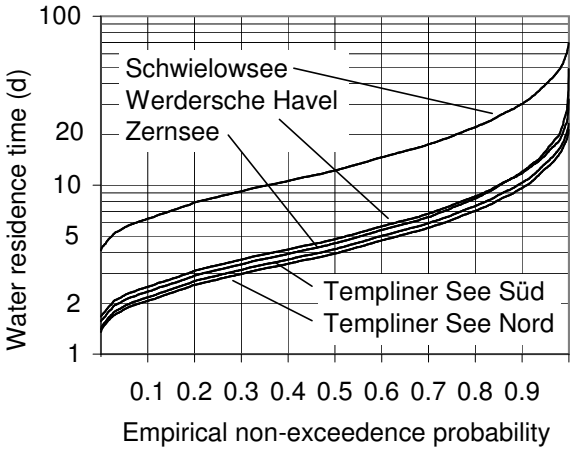

Figure 4.7: *Period-of-record duration curves of the water residence time (days) in lakes of the Potsdamer Havel. Period: 1995-2004.*

Impacts of nutrient loading

Anthropogenic eutrophication is primarily caused by elevated nutrient emissions from the catchment. As Table 4.3 illustrates, both point and non-point sources contribute to the pollution of the Havel River in significant shares. Because many sewage treatment plants were equipped with enhanced P elimination in the mid of the 1990s, the contribution of P emissions from non-point sources is expected to have increased compared to Table 4.3 while the total emissions declined.

The predominant non-point sources of phosphorus are polluted groundwater, erosion, and wash-off from urban areas (LUA, 2002). In the case of nitrogen, groundwater pollution as well as emissions from drained areas are most important. The total emissions have declined by about 66 % (P) and 47 % (N) when comparing the periods 1993–1997 and 1983–1987 (LUA, 2002). With respect to phosphorus, point-source emissions were primarily reduced due to the use of phosphorus-free detergents and enhanced elimination in wastewater treatment. With regard to nitrogen, the shift in the contribution of different sources is much less pronounced.

Although external nutrient loading decreased in the 1990s, the concentrations of phosphorus and nitrogen are still elevated (Fig. 4.8). In the case of phosphorus, this is not only due to ongoing emissions from point and non-point sources but also due to internal loading. A large phosphorus pool has accumulated in the lake sediments over the past decades (Rohde, 1995). Today, after partial reduction of external P loads, the excess phosphorus of the sediments is slowly being released. The resulting delay in the recovery of water quality is a common phenomenon (Jeppesen et al., 1991; Kozerski & Kleeberg, 1998; Søndergaard et al., 2003).

4.2.3 Water quality overview

At the monitoring stations shown in Fig. 4.5, surface water quality is inspected fortnightly by the state environmental authorities (LUA Brandenburg, Berliner Senat). At selected locations, daily data from automatic samplers are available; these samples are analyzed for a greater number of physical, chemical, and biological parameters including water temperature, pH, conductivity, oxygen, total N and P, organic nutrient fractions, nitrogen species, and chlorophyll.

Fig. 4.8 illustrates the trend in the annual averages of nutrient and chlorophyll-a concentrations at four monitoring stations in the period 1990–2004. Obviously, there was a continuous decline in all nitrogen species with a remarkable drop in ammonium until the mid of the 1990s. This is certainly the result of a successful sewage treatment policy. The latter focused on a reduction in total N emissions but also aimed at emitting the residual inorganic N in oxidized form (NO_3^-) rather than as oxygen-depleting and potentially toxic NH_4^+. Possibly, the disproportional drop in ammonium concentrations is intensified by the NH_4^+preference in phytoplankton uptake.

Compared to nitrogen, phosphorus concentrations show a different pattern. At the mouth of the Teltowkanal and downstream monitoring stations a significant drop in TP could be observed in the

Table 4.3: *Phosphorus and nitrogen emissions (E_P, E_N) at selected gages after LUA (2002). Presented are total emissions (t a^{-1}) and the estimated contribution of non-point sources (%) in the period 1993–1997.*

River	Gage	E_P (t a^{-1})	% diffuse	E_N (t a^{-1})	% diffuse
Obere Havel	Henningsdorf	78	65	1766	88
Spree	Berlin Mühlendammschl.	413	53	10498	54
Nuthe	Potsdam Babelsberg	58	59	1181	84
Havel	Ketzin	712	55	17984	50
Havel	Brandenb. Mühlendamm	722	55	18186	51

first half of the 1990s. Thereafter, no clear trend in TP can be identified and also the concentrations of dissolved phosphorus do not exhibit a continuous decline. The above mentioned process of internal P loading provides a reasonable explanation for this observation.

In eutrophic rivers there are strong seasonal dynamics in many water quality parameters. Fig. 4.9 displays the seasonality of both nutrients and chlorophyll based on data from 1998–2004.

With respect to water quality management, knowledge of the factors that currently control aquatic primary production is fundamental. A look at Fig. 4.9 reveals that the concentration of dissolved phosphorus, which limits algal growth in many rivers and lakes, is too high to restrict the annual maximum in primary production. In fact, there is a significant increase in the concentrations of soluble reactive phosphorus (SRP) due to internal loading and weak dilution in summer rather that a depletion by algal uptake. Dissolved phosphorus concentrations are much lower in early spring only. Though Sas (1989) states that only average SRP concentrations lower than 0.01 mg l^{-1} over the entire vegetation period can indicate phosphorus limitation of the phytoplankton, half-saturation concentrations used in Michalis-Menten type growth models (Bowie et al., 1985) suggest that the low SRP levels in spring might have some minor effect.

According to the present understanding, peak primary production is likely to be controlled by two other factors: self-shading and possibly temporary nitrogen shortage.

The effect of self shading can be illustrated by a simple numerical example. According to the law of Lambert-Beer, light extinction is a first order process and the underwater light intensity I at depth z is related to the intensity at the water surface I_0 by Eq. 4.1, with E being the extinction coefficient.

$$I(z) = I_0 \cdot e^{-Ez} \tag{4.1}$$

In eutrophic waters low in suspended solids, the extinction coefficient for photosynthetically active radiation (PHAR) is primarily controlled by the chlorophyll concentration. Various empirical formulas exist for estimating E as a function of the chlorophyll concentration and a widely used model is presented by Ambrose et al. (2001). A rule of thumb for estimating E from the Secchi-depth z_{Secchi} is provided by Witter (2002) with $E = 1.5/z_{Secchi}$. If the background extinction E_0 is assigned a value of 0.7 m^{-1} both cited approaches fit the data from the Havel River quite well. Using Eq. 4.1, the function $I(z)$ can now be plotted for different chlorophyll levels. Fig. 4.10 reveals that about 90% of the available light is extinguished in the first meter of the water column at a chlorophyll-a concentration of 75 μg l^{-1} (recall the data from Fig. 4.9). Thus, in a well-mixed shallow lake of 2.5 m depth, the algae are exposed to less than 10% of the near-surface light intensity for $3/5$ of the daylight period.

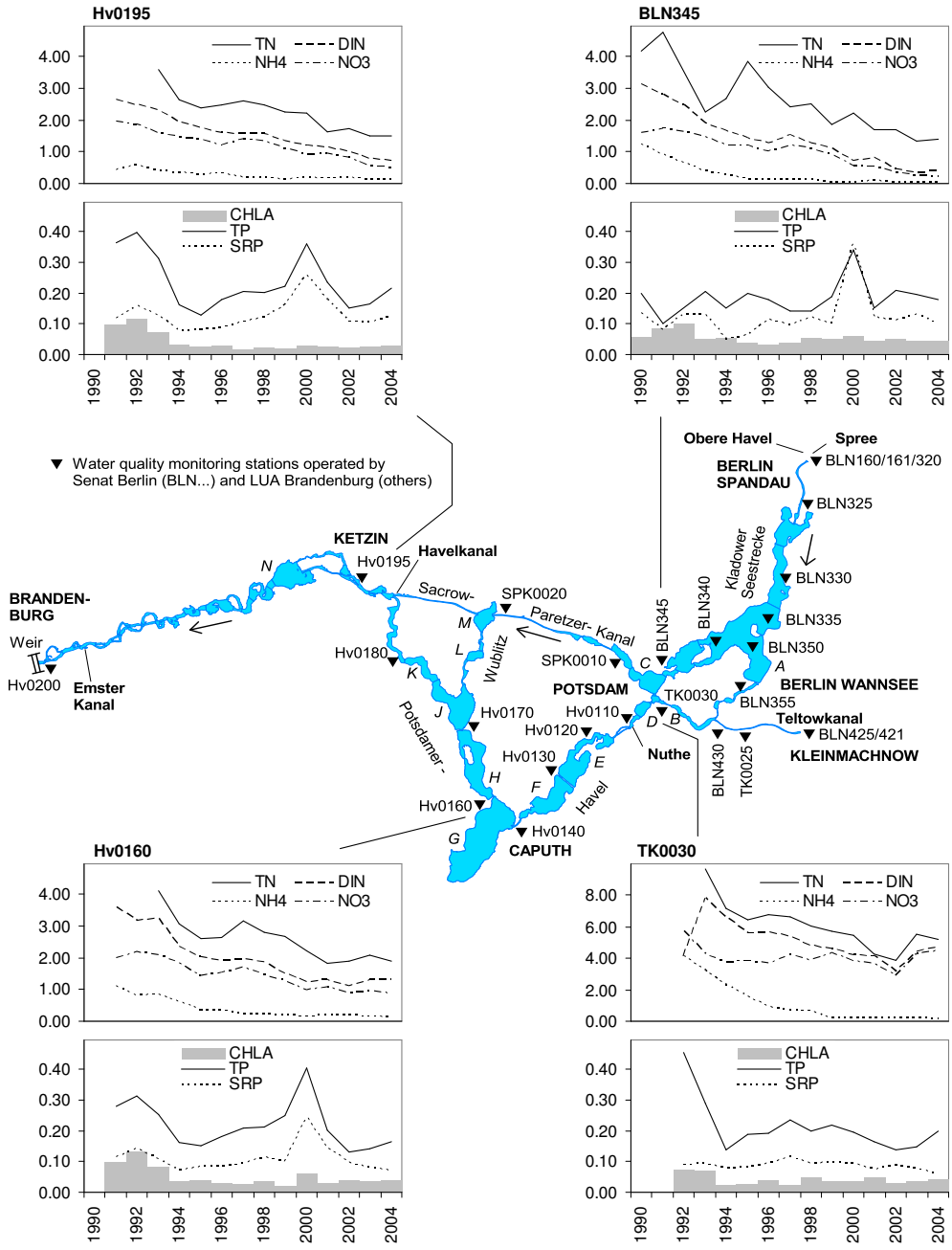

Figure 4.8: *Trend in the annual average concentrations (medians; mg l^{-1}) of the key variables chlorophyll-a (CHLA), total and dissolved phosphorus (TP, SRP), total nitrogen (TN), dissolved inorganic nitrogen (DIN), and the DIN species NO_3^--N and NH_4^+-N (given as N) at four monitoring stations near Potsdam. The stations are Krughorn (BLN345), Teltowkanal - Paschabrücke (TK0030), Potsdamer Havel - Baumgartenbrücke (HV0160), and Ketzin - Fähre (HV0195). Note that the scale for nitrogen concentrations at station TK0030 differs from the other charts. The phosphorus peak in 2000 is a result of extraordinarily high P remobilization from sediments (see Fig. 4.36 in Sect. 4.5.1.)*

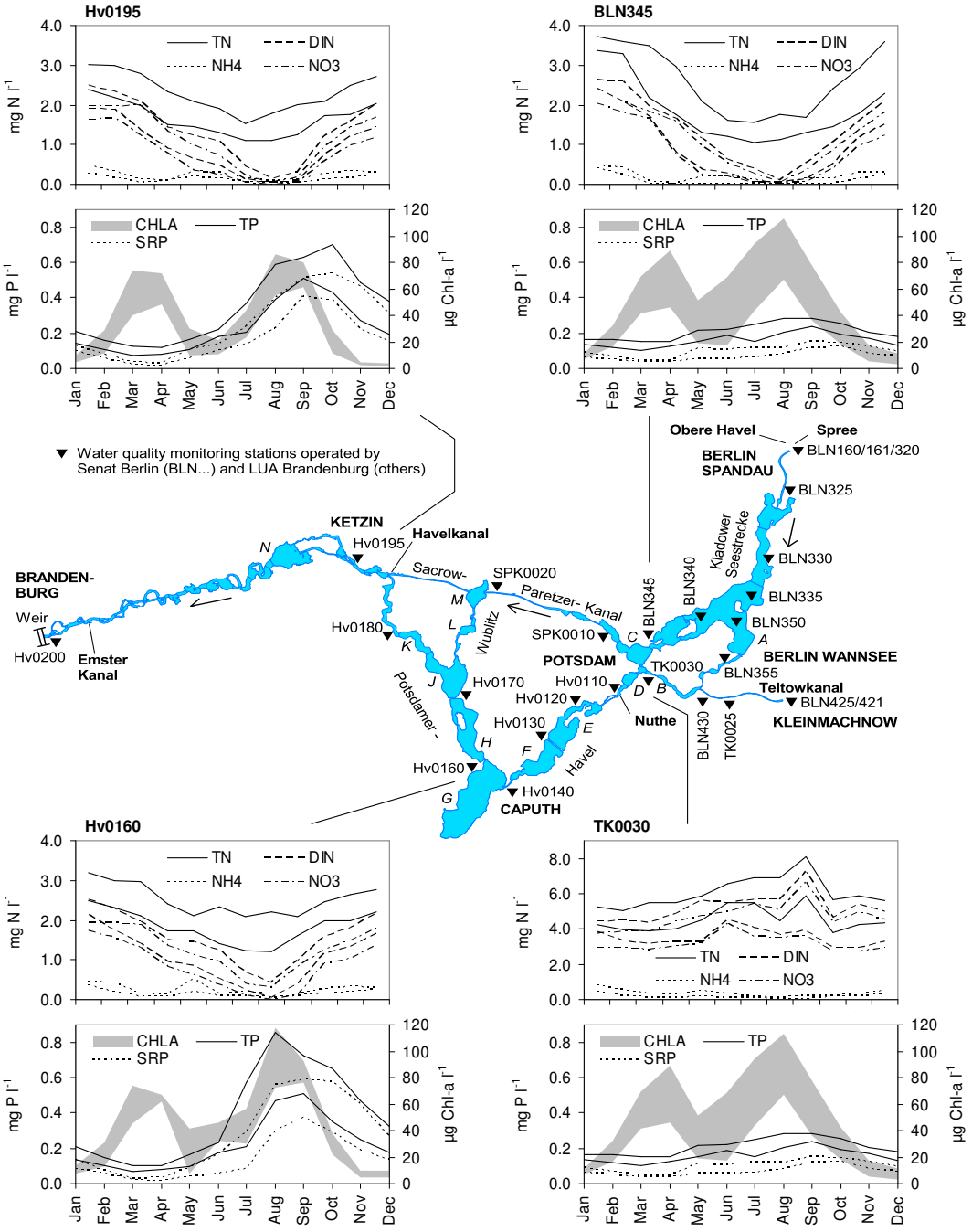

Figure 4.9: *Seasonality in the concentrations of chlorophyll-a (CHLA), total and dissolved phosphorus (TP, SRP), total nitrogen (TN), dissolved inorganic nitrogen (DIN), and the DIN species NO_3^--N and NH_4^+-N (given as N) at the four monitoring stations shown in Fig. 4.8. In order to illustrate the variability in the data, the upper and lower quartiles are shown for each parameter and each month, i.e. 50% of the observed values fall in the range between the two corresponding lines or within the grey band, respectively. Note that the scale for nitrogen concentrations at station TK0030 differs from the other charts.*

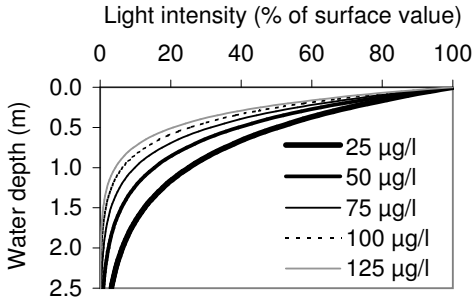

Figure 4.10: *Underwater PHAR intensity as percentage of the intensity just below the air-water interface at different levels of chlorophyll-a in $\mu g\ l^{-1}$.*

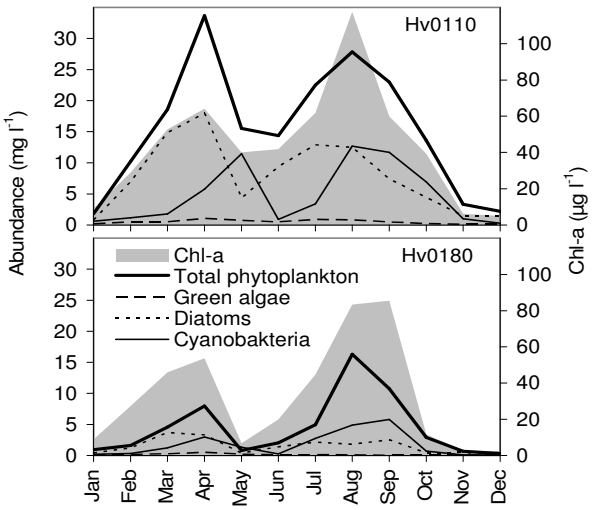

Figure 4.12: *Concentration of chlorophyll-a (shaded area; $\mu g\ l^{-1}$) and abundance of the major phytoplankton groups (lines; mg l^{-1}) upstream and downstream of the Potsdamer Havel Lakes (see Fig. 4.5 for the locations Hv0110 and Hv0180). Shown are monthly medians for the period 1996–2002.*

As mentioned above, shortage of available nitrogen (DIN) in summer might contribute to the limitation of phytoplankton growth. According to present understanding, two mechanisms of DIN removal are important: the depletion of NH_4^+ and NO_3^- by algal uptake as well as denitrification. While the first process obviously changes the pelagic DIN concentrations, the effect of denitrification is believed to be more indirect. As denitrification is largely bound to oxic–anoxic interfaces in the sediment, it attenuates the recycling of settled organic N rather than affecting the pelagic NO_3^- concentration directly.

For the time being, N limitation of algal growth can only be suspected based on correlation analysis. Fig. 4.11 (left chart) indicates that, during the vegetation period, higher concentrations of chlorophyll-a correspond to higher concentrations of dissolved inorganic N. A similar relationship between chlorophyll and available phosphorus (SRP) could not be found (Fig. 4.11, right chart), underpinning the oversupply of P.

Though N limitation seems plausible when looking at the left chart of Fig. 4.11, one must not confuse correlation and causality. In fact, the average DIN concentrations during the vegetation period are quite high (recall Fig. 4.9) when compared to the threshold of 0.1 mg l^{-1} which is required for N-limitation according to Sas (1989). Hence, Fig. 4.11 is likely to show a spurious correlation to some extent. A possible explanation is a gradient in DIN (in space and/or time) that correlates with a shift in the species composition of the phytoplankton, with different species exhibiting different cellular chlorophyll levels. Additional disturbing factors must be considered when analyzing DIN-chlorophyll correlations such as loss processes (e.g. grazing) or nitrogen fixation by cyanobacteria. Nutrient addition experiments (e.g. Weithoff & Walz, 1999) or an analysis of cyanobacteria species would be required in order to verify the hypothesis of temporary nitrogen limitation.

The share of different taxonomic groups and the seasonal pattern of phytoplankton abundance in the Lower Havel River are illustrated in Fig. 4.12. Diatoms and cyanobacteria dominate the phytoplankton throughout the year. Both groups are well adapted to low light intensities which makes them competitive at high chlorophyll levels (e.g. Scheffer et al., 1997).

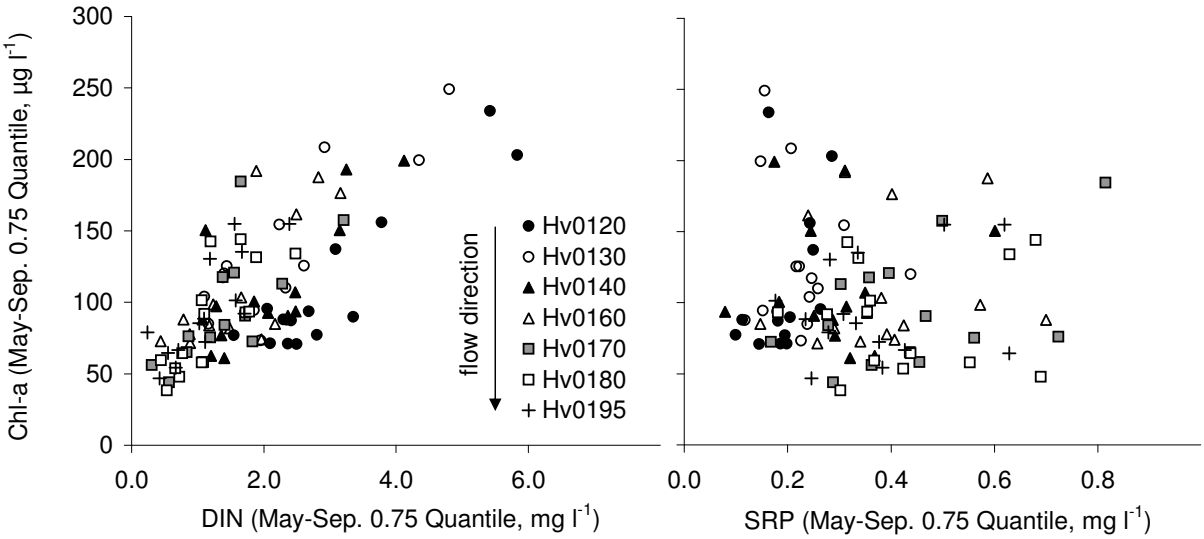

Figure 4.11: *Correlation between the upper quartiles of dissolved nutrient concentrations (nitrogen as DIN, phosphorus as SRP) and the upper quartiles of chlorophyll-a (Chl-a) in the vegetation period May–September. Note that each data point represents one single year of the period 1992–2004. Also note that the data for each monitoring station Hv0120–Hv0195 are plotted with a different style in order to show that (for nitrogen) correlations exist at each single monitoring station and not only due to a spatial trend of decreasing DIN and Chl-a concentrations from upstream to downstream monitoring stations.*

The time lag between the peaks of cyanobacteria and diatom biomass (Fig. 4.12, upper chart) probably results from higher growth rates of the latter group which typically dominates the phytoplankton in early spring (Sommer et al., 1986). A high proportion of cyanobacteria in summer is also typical for eutrophic lakes due to the ability to cope with high grazing pressure, high turbidity, and possibly shortage of nitrogen.

The significant drop in phytoplankton concentrations in May–June is a phenomenon observed in many lakes (e.g. Noges et al., 1998). Grazing of zooplankton and an adaptation of the algae community to decreased flushing and higher temperatures are believed to be of importance.

Fig. 4.12 displays a decrease in phytoplankton concentrations through the Potsdamer Havel Lakes from monitoring station Hv0110 to Hv0180 which is contrary to observations in many other river-lake systems (e.g. Kneis, 2002). For the time being one can only speculate on the causes. For example, light limitation might be more severe in the lakes than in upstream reaches like the Teltowkanal because of increased depth and less turbulence[2]. A spatial gradient in zooplankton abundance[3] or a decrease in DIN (denitrification, settling) and/or silica (settling) along the flow path could be alternative explanations.

The shift in the ratio of chlorophyll-a and algal biomass is pointed out again in Fig. 4.13. The significant increase in this ratio from monitoring station Hv0110 to Hv0180 shows an adaptation of the phytoplankton's cell-internal pigment concentration to low underwater irradiance. This fact corroborates that light availability is in fact a ma-

[2]The effect of turbulence on primary production was demonstrated by Gervais et al. (1997).

[3]Since zooplankton growth rates are low compared to algal growth rates, the buildup of zooplankton takes more time. Hence, one should expect an increase in zooplankton and a reduction in its prey (algae) during the passage of a river-lake system.

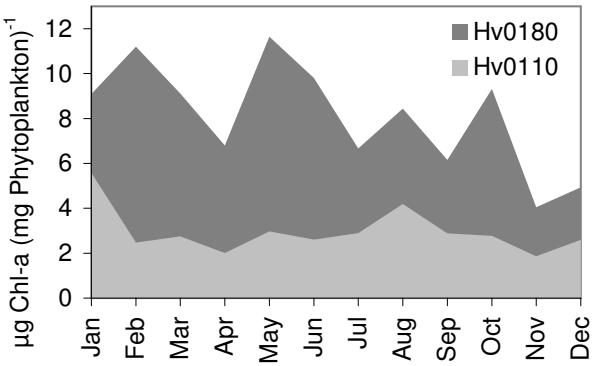

Figure 4.13: *Chlorophyll-a content of total phytoplankton biomass (μg Chl-a (mg Phytoplankton)$^{-1}$) upstream (Hv0110) and downstream (Hv0180) of the Potsdamer Havel Lakes. Shown are monthly medians for the period 1996–2002.*

jor controling factor for primary production in the Lower Havel.

4.3 Hydrodynamic submodel

As mentioned in Sect. 3.2, the hydrodynamics are not computed by TRAM but by an external software. In the presented application, the one-dimensional, unsteady hydrodynamic model HEC-RAS (USACE, 2002) was used for computing flow rates and stages in the river-lakes system shown in Fig. 4.5. This model proved to be particularly suitable for several reasons:

- RAS handles looped systems, i.e. river networks with multiple parallel flow paths.
- The software supports the import of geometry data via an ASCII-interface. It is therefore possible to import the geometric data (cross-sections, stream lines, channel junctions, bank lines, levee positions, ineffective areas[4]) in an automated way using GIS and/or other external utilities. This greatly speeds up the creation of hydrodynamic models for spatially large domains.
- The program's GIS capabilities allow for a visual overlay of the river network as represented in RAS with TRAM's network of reactors. This makes it easy to identify those cross-sections where stage and flow data must be recorded for later use by TRAM's preprocessors.
- Software utilities are available for extracting the desired information (e.g. hydrographs at a certain location) from large model outputs in a very efficient manner (see Sect. 4.3.4).
- HEC-RAS is widely used because it is freely available and well documented.

4.3.1 Sources and preprocessing of geometry data

For creating the geometry input file for HEC-RAS, data from different sources were combined.

Sonar data

Cross-section data from sonar measurements were made available by the navigation authorities for the river section between the mouth of the Havelkanal near Ketzin and the downstream model boundary at the city of Brandenburg. Since sonar and GPS measurement were combined, the data have a full spatial reference (3D coordinates).

Data from an existing model

For the river section between Berlin-Spandau (upstream boundary at the confluence of Spree and Havel) and Krughorn (flow split upstream of Potsdam), cross-section data were extracted from the geometry data base of the water surface profile calculation model HYDRAX[5]. Some further parameters such as the cross-sections of bridges were also taken from this source. Since HYDRAX uses 2-dimensional cross-section data (offset from left bank, bottom elevation), the data had to be georeferenced, based on river station information. To

[4] Areas which are inundated at high stage but which do not contribute to the active cross-section area (ponding areas).

[5] The data were provided by the federal water authorities.

do so, the cross-section cut lines[6] were drawn in the GIS and the 3-dimensional position of each elevation measurement was recomputed by a utility program Xs2dToXs3d.

Topographic maps

For the lakes of the Potsdamer Havel, contour lines of the bottom elevation were digitized from topographic maps with a scale of 1:10000 (see Fig. 3.8). The information was converted into cross-section data by another utility (ContourToXs3d). Data on levee positions were also taken from digital topographic maps.

Digital elevation model

Since the sonar data were recorded from a boat, shore line positions as well as elevation data for the floodplain are (with some exceptions) lacking. In order to allow for a continuous unsteady simulation including floods, floodplain elevations were extracted from a digital elevation model (DEM) which was made available by project partners. The location and extent of ineffective areas were also estimated based on the DEM.

How all data (bed elevations, floodplain elevations, levee positions, stream lines, etc.) from different sources were merged into one single data base is exemplified in Fig. 4.15. Basically, the sonar data which are present as point data (x, y, elevation) were automatically converted to short line segments oriented parallel to the channel. The same was done with floodplain elevation data extracted from the DEM along specified paths. Finally, the cut lines, defining the position of the individual cross-sections, were drawn in the GIS. Other information like streamlines, bank positions and levees were drawn as lines as well. The different line data sets were then exported from the GIS and preprocessed by a FORTRAN program Gis2Ras developed by the author. This utility collects all elevation data along the cross-section cut lines by looking for intersections with the mentioned line segments representing elevation data.

[6] Top view of a cross-section.

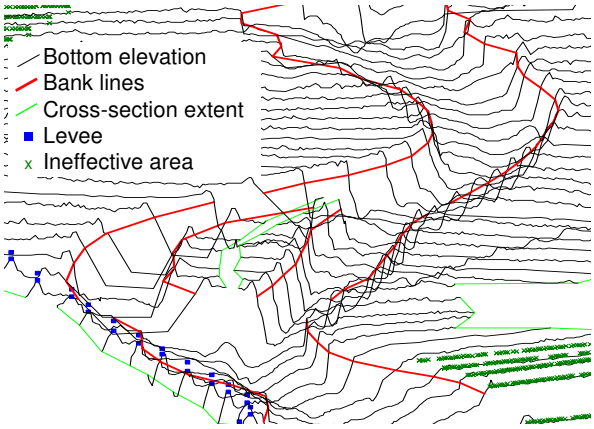

Figure 4.15: *A section of the Lower Havel River displayed in HEC-RAS's 3D-viewer.*

In the same way, bank and levee positions etc. are identified for all cross-sections.

The final result of the geometry preprocessing is shown in Fig. 4.15 and Fig. 4.16. The complete HEC-RAS data base for the studied section of the Lower Havel River comprises about 1100 cross-sections and 27 junctions.

It should be noted that the Havel Lakes are represented in the model by ordinary channels, not by reservoirs. This is necessary because the lakes' water surface elevation is entirely controlled by the weir at Brandenburg (see Fig. 4.5). Hence, no stage-discharge relationships exist at the lakes' outlets which could be used for computing the outflow rates as a function of stage. In the existing HYDRAX model, the lakes are also represented by channel sections.

4.3.2 Boundary conditions

The two major upstream boundary conditions of the hydrodynamic model are the inflows at Berlin-Spandau (Upper Havel, Spree) and Kleinmachnow (Teltowkanal). The smaller tributaries (Nuthe, Havelkanal, Emster Kanal) appear as lateral inflows as does infiltrating groundwater. Because of the large water surface area, evaporation was also taken into account. Compared to the discharges of

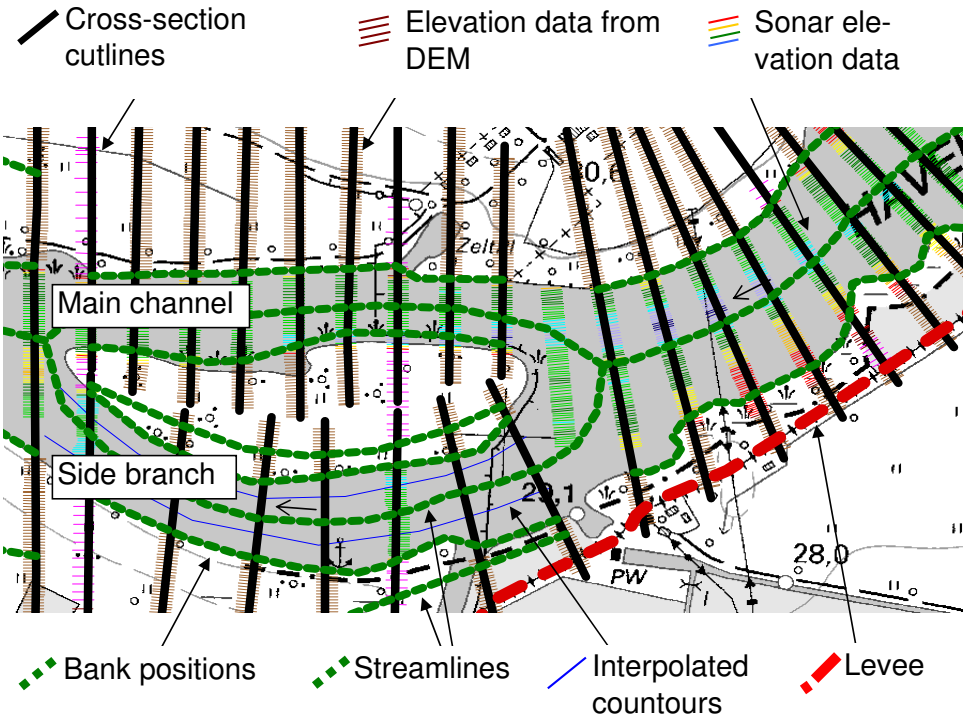

Figure 4.14: *Illustration of geometry data preparation for HEC-RAS in the GIS. Elevation information is shown by arrays of short line segments oriented parallel to the channel. At this site, they were taken from two sources: the DEM (brown lines) and from the sonar data (colored lines, elevation increases from dark blue to red). The original elevation data (point data) were converted to the line segments shown in order to facilitate the digitizing of the intersecting cross-section cutlines (bold black lines perpendicular to the river).*

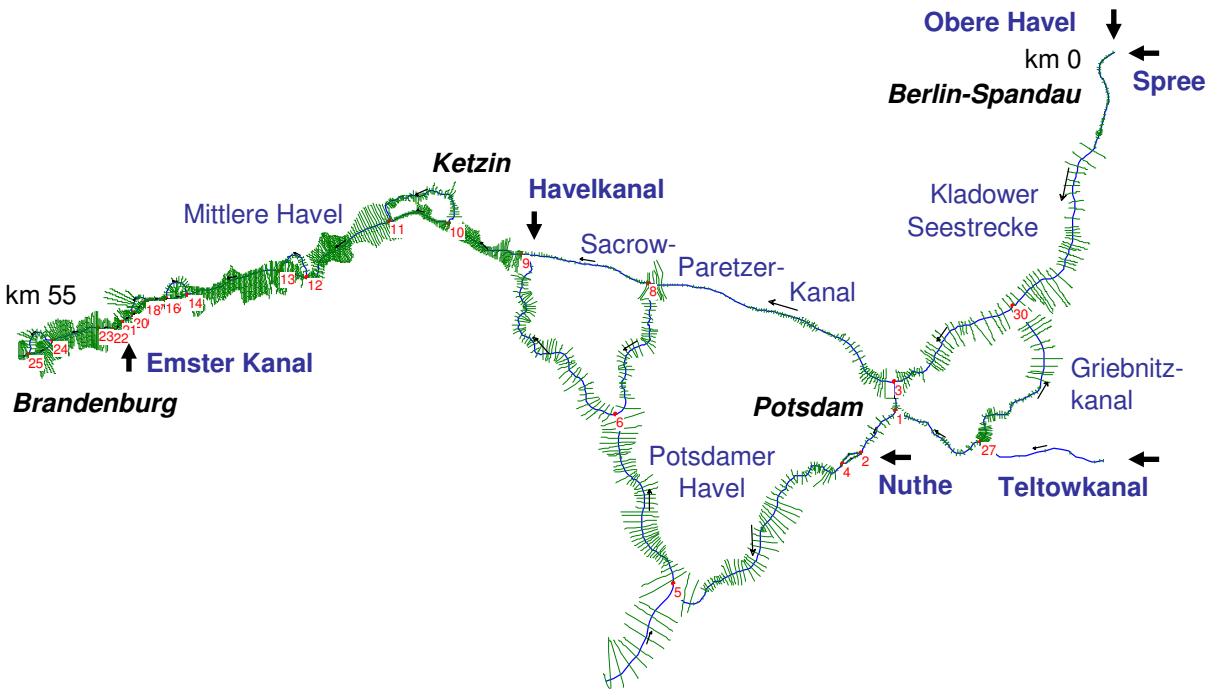

Figure 4.16: *The Havel River between Berlin-Spandau (river station 0) and the city of Brandenburg (km 55) as represented in HEC-RAS. The distance refers to the connection via the Sacrow-Paretzer-Kanal. The total length of the Potsdamer Havel side branch is approximately 29 km. Blue lines represent the reaches, green lines show the cross-section cut lines and red numbers identify channel junctions. The names of tributaries (inflow boundary conditions) are printed in bold. Note the smaller distance between adjacent cross-sections in the western part of the model domain resulting from better data availability (sonar data). Also note how the large dead zone of Lake Schwielowsee (in the very south of the Potsdamer Havel) was represented in the model by a dummy tributary.*

Table 4.5: *Error statistics for the hydrodynamic simulation in the calibration period (1988–2000) and four subsequent years (Q: flow rate, W: water surface elevation). ME: mean error, MAE: mean absolute error, NSE: Efficiency after Nash & Sutcliffe (1970).*

Variable	Period	ME	MAE	NSE
Q at Ketzin	88–00	2.79	7.68	0.92
(m^3 s^{-1})	01–04	1.48	6.23	0.94
W at Spandau	88–00	0.00	0.03	0.96
(m)	01–04	0.03	0.04	0.87

the tributaries Upper Havel, Spree, Teltowkanal, and Nuthe, the other boundary conditions are of minor importance only. At the downstream boundary of the model domain, the time-variable water surface elevation at the Brandenburg weir was predefined. Table 4.4 summarizes how the boundary condition values were obtained for the calibration period and scenario simulations in the period 2003–2015.

4.3.3 Model calibration

Estimates of the channel roughness were adopted from the existing HYDRAX model. A comparison of observed flow rates and water surface elevations with simulated values at the gages Ketzin, Potsdam, and Berlin-Spandau indicated satisfying agreement. After some further calibration runs, a value of K_{st}=37 $m^{1/3}$ s^{-1} was chosen for the main channel and the floodplain was assigned a value of K_{st}=15 $m^{1/3}$ s^{-1} with K_{st} being the reciprocal of Manning's n. Some goodness-of-fit parameters for the calibration period and four additional years are shown in Table 4.5.

4.3.4 Exchange of data between the hydrodynamic model and TRAM

Before data can be exchanged between HEC-RAS and TRAM, the geometry of both models needs to be overlayed first. This is necessary in order to identify the cross-sections (or external inflow locations) in the hydrodynamic model which correspond to boundaries of TRAM's reactors. Practically, this was done by loading a projected image or shape file of the TRAM reactor network into HEC-RAS's geometry viewer as a background (see Fig. 4.17). For each of TRAM's reactors, the river stations of the most upstream and downstream cross-section were determined. At these locations, stage and flow hydrographs were extracted from the HEC-RAS output.

Because a long-term hydrodynamic simulation produces a huge amount of output data, HEC-RAS saves its simulation results in a binary format using a specially designed data storage system (HEC-DSS). For exporting the required stage and flow hydrographs at the identified 'linking' cross-sections from the HEC-DSS, the DSSUTL utility[7] was used. The exported data served as input for TRAM's preprocessing utilities TRAMP-PFR and TRAMP-STR which were introduced in Sect. 3.6.4.

It should be noted that the comparison of model geometries for creating the list of HEC-RAS's output locations is the only manual step. The actual transfer of information between the two models is fully automated. Data exchange is a matter of minutes once all preprocessing tools are configured.

4.4 Water quality submodel

For a proper understanding of the nutrient turnover model presented in Sect. 4.4.3, some basic knowledge of the fate of nitrogen and phosphorus in the aquatic environment is indispensable. Consequently, a short introduction to nutrient cycles (Sect. 4.4.1) and P turnover (Sect. 4.4.2) is given, before the model approaches taken are addressed in Sect. 4.4.3.

[7] DSSUTL allows for very efficient retrieval and formatting of mass data from the HEC-DSS when run in batch mode. The program is freely available from the HEC.

Table 4.4: *Boundary conditions of the hydrodynamic model (Q=flow, W=water surface elevation) and corresponding data sources.*

Boundary condition	Type	Observation period (1988–2004)	Scenario simulations (2003–2015)
Obere Havel	Q	Measured flow rates at the gages Berlin-Freybrücke und Berlin-Stößenseebrücke (sum of Obere Havel and Spree) [a]	Flow rates simulated by the catchment model SWIM [d]
Spree	Q	see above	Observed flows for the period 1988–2000 at the Sophienwerder gage corrected for a trend as predicted by BfG (2003)
Teltowkanal	Q	Measured flow rates at Kleinmachnow [b]	Observed flows for the period 1988–2000 at the Kleinmachnow gage corrected for a trend as predicted by BfG (2003)
Nuthe	Q	Measured flow rates at Potsdam-Babelsberg [c]	Flow rates simulated by the catchment model SWIM [d]
Havelkanal	Q	Estimated seasonally variable flow rates [e]	Flow rates simulated by the catchment model SWIM [d]
Emster Kanal	Q	Monthly averages, estimated from the discharges of the Nuthe River and the ratio of catchment sizes	Flow rates simulated by the catchment model SWIM [d]
Groundwater infiltration	Q	Estimated from model error at gage Ketzin	Flow rates simulated by the catchment model SWIM [d]
Evaporation	Q	Computed by the PENMAN-Equation (DVWK, 1996)	see left
Weir Brandenburg (upper gage)	W	Observed data	Monthly target values after WSA (2003) taking into account exceedance during floods

[a] Provided by Senatsverwaltung für Umwelt und Stadtentwicklung Berlin
[b] Provided by Wasser- und Schifffahrtsamt Brandenburg
[c] Provided by Landesumweltamt Brandenburg
[d] Provided by A. Habeck, Potsdam Institute for Climate Impact Research
[e] Löper, G. (WSA Brandenburg), pers. comm.

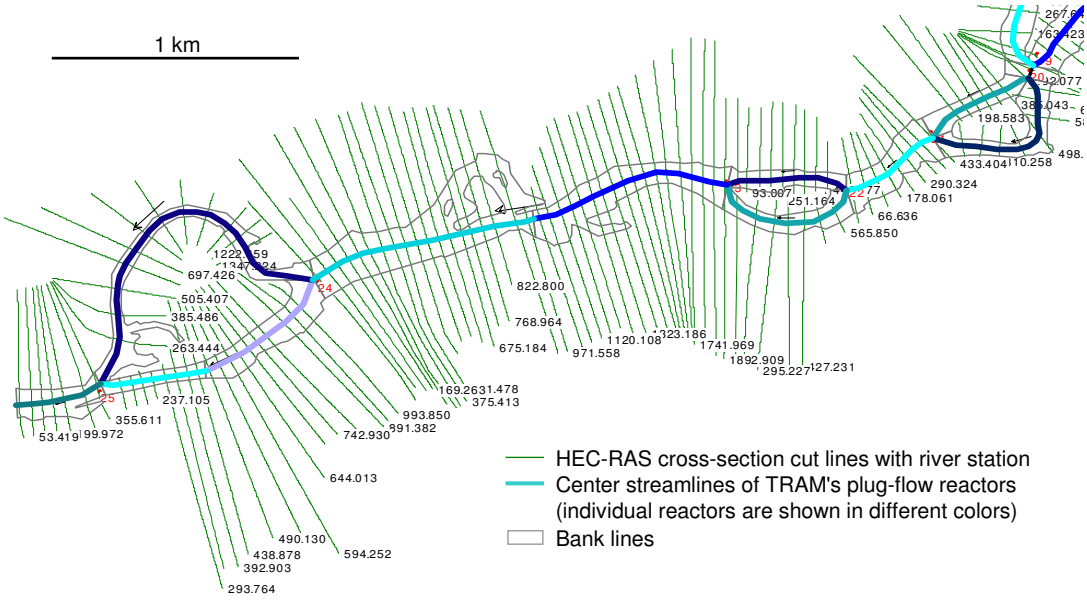

Figure 4.17: *Visual overlay of the geometry of the HEC-RAS model with TRAM's network of reactors. The comparison of the model's geometries is necessary in order to identify those 'linking' cross-section, for which stage and flow hydrographs must be exported from the hydrodynamic model as input for TRAM's preprocessors TRAMP-PFR and TRAMP-STR.*

4.4.1 Simplified outline of the aquatic nutrient cycle

A generalized chart of the nutrient cycle in a shallow, non-stratified aquatic environment is shown in Fig. 4.18. While many processes equally affect both N and P, there are also some important differences.

Common features of the N and P cycle
Both nitrogen and phosphorus are affected by the major turnover processes listed below.

- Dissolved inorganic nutrients (orthophosphate, NH_4^+, NO_3^-) are taken up by the autotrophic phytoplankton but also by bacteria feeding on dissolved organic material low in nutrients.
- The phytoplankton is the basis of a food chain with zooplankton and fish as higher trophic levels. Due to filtration by zooplankton, bacterial and particulate organic matter (detritus) is partly included in this food chain.
- Nutrients are lost from all trophic levels. Excretion of nutrients from the consumers (zooplankton, fish) recharges the pool of dissolved inorganic nutrients directly. Particulate organic matter and released dissolved organic matter must first be mineralized before the nutrients they contain become available for uptake again.
- Particulate organic matter from the plankton and detritus pool is subject to settling which results in a transfer of nutrients to the sediment. In the active upper layer with high microbial activity, nutrients recycling takes place and the dissolved forms (mainly orthophosphate, NH_4^+, NO_3^-) are released to the pore water. They may be transfered back into the pelagic zone via diffusion and other transport processes (see Sect. 4.4.2.2).
- Some part of the settled organic matter is lost to the deeper sediment layers by bioturbation and continued deposition of fresh mate-

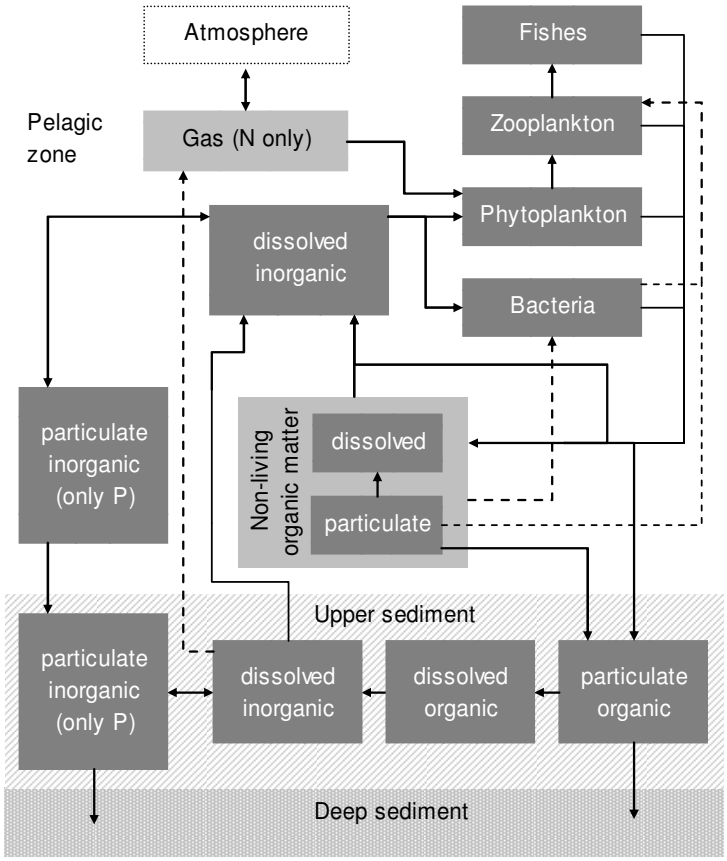

Figure 4.18: *Generalized flow chart of the nutrient cycle in a non-stratified water body. It should be noted that the biological groups are not homogeneous but each of them consists of multiple species with different stoichiometry which is not necessarily constant in time. The organisms in the sediment are not explicitly considered in the chart.*

rial (burial). This fraction forms the muddy sediments which can be found in many eutrophic lakes.

Major differences between N and P

Since nitrogen does not form insoluble minerals, the particulate inorganic fraction can usually be neglected unless the sorption of NH_4^+ to suspended clay minerals is of special relevance. In the case of phosphorus however, sorption to mineral surfaces and the formation of insoluble minerals is important (see Sect. 4.4.2.1). This partly explains why phosphorus is usually stored in sediments in greater quantities compared to nitrogen. Particulate inorganic phosphorus may also be subject to settling when P is sorbed to suspended sediment or precipitation with calcite occurs.

In contrast to phosphorus, nitrogen may not only be removed from the system by burial in the sediment but also by gaseous losses in the form of N_2 or N_2O. This process is believed to be mostly bound to the sediment, as oxic conditions (nitrification) and anoxic conditions (denitrification) must be present in close vicinity (Scheffer, 1998). Ammonia volatilization is believed to be less significant in natural waters as long as the pH is not very high.

Another interesting feature of the nitrogen cycle is that some groups of cyanobacteria are able to take up dissolved N_2 and to reduce it to form organic N. Thus, the atmosphere is not only a nitrogen sink but it can also become a source.

Unlike phosphorus, dissolved inorganic nitrogen appears in different oxidation levels (NH_4^+, NO_2^-, NO_3^-). Dissolved inorganic phosphorus however is always present as phosphate, with the actual species depending on the pH. In chemical analysis, ortho-phosphate can hardly be isolated from colloidal phosphates (Lampert & Sommer, 1993) and the concentration of molybdate reactive phosphorus (SRP) is commonly used as an estimate of DIP.

In most freshwater systems, the nutrient which limits primary production is phosphorus, because the DIP concentration in equilibrium with sorbents and phosphate minerals is low. As discussed in Sect. 4.2.3 the situation in the Havel River has shifted towards nitrogen limitation due to high external P input and phosphorus remobilization from sediments.

Options for simplification

For modeling, it is important to know which of the nutrient pools and interactions shown in Fig. 4.18 are most relevant and which may be neglected. At this point, some knowledge of the energy flow in food webs is helpful. After Begon et al. (1996), the transfer efficiency TE which relates the biomass production P of the consumers at the trophic level n to the production of the prey at trophic level $n-1$, i.e. $TE = P_n/P_{n-1}$, is typically in the range 0.02–0.24. Often 0.1 is used as a standard estimate. This figure indicates that only about 10% of the energy is transfered from one trophic level to the next while 90% is lost due to respiration and incomplete assimilation. In consequence, the biomass – and thus the amount of stored nutrients – at the level of the primary producers (phytoplankton) is much higher than that at higher trophic levels. Exceptions may occur only if the system is far from steady state, e.g. during mass developments of zooplankton.

In many models, the nutrient pools associated with consumers are consequently neglected. The dynamics of the zooplankton is of interest only, because it controls algal mortality. The three major pools of nutrients in the water column are therefore (1) phytoplankton, (2) dead organic material and (3) dissolved inorganic nutrients (e.g. Ambrose et al., 2001). While nutrient storage in microbial biomass is often not explicitly modeled, it must be taken into account in systems with large input of allochtonous organic matter such as polluted rivers (see e.g. Reichert et al., 2001).

In the sediment, the nutrients stored in organic matter, dissolved nutrients in the pore water as well as the inorganically bound fraction are all relevant.

Whether the burial of nutrients in the deep sediment must be taken into account depends on many criteria. The error from neglecting this process will probably be small if,

- the simulation time period is short compared to the quotient of the burial velocity (m s^{-1}) and the thickness of the considered upper sediment layer (m),
- the majority of the organic matter is mineralized in the top sediment due to high microbial activity,
- the formation of inorganic compounds which are stable in the reduced environment of the deep sediment is less important.

In principle, the burial velocity can be assessed from data on the rate of sediment net growth but it is difficult to measure under natural conditions.

4.4.2 Phosphorus storage in sediments and remobilization

Because the release of phosphorus from the bottom sediments of the Havel Lakes is of great significance for its present and future water quality, the theory of storage and remobilization is presented in more detail in the following paragraphs. The topic is rather complex because multiple fractions of sedimentary P exist, each exhibiting different stability with respect to the ambient conditions such as pH, redox-potential, and temperature. In Sect. 4.4.2.1 only those P fractions are addressed which are known to be of relevance in the sediments of the Havel Lakes (see Schettler, 1995).

The situation is further complicated by the occurrence of multiple mechanisms which govern the transport of sedimentary phosphorus back to the water column. The mechanisms of P remobilization are covered by Sect. 4.4.2.2.

4.4.2.1 Phosphorus fractions

Iron-bound phosphorus

In many freshwater sediments, a considerable amount of the total phosphorus is bound to iron. For the Lower Havel River, this has been proven by Knösche (2006a). Two different kinds of binding need to be distinguished: adsorption and the formation of minerals (Jacobsen, 1978; Smits & Van der Molen, 1993).

Most important for phosphate sorption are iron-III hydroxides and oxides, e.g. $Fe(OH)_3$ and FeOOH (goethite). The sorption capacity of amorphous, freshly precipitated Fe hydroxides is higher than that of aged, crystalline forms such as goethite due to a greater specific surface area. In sorption experiments, Jacobsen (1978) found a strong negative correlation between the sorption capacity of iron hydroxides and the pH. This was explained by the positive charge of hydroxide surfaces at low pH ([Fe]-OH + $H^+ \rightarrow$ [Fe]-OH_2^+) which favors the sorption of the phosphate anion.

At low redox potentials, iron-III is reduced and the hydroxides dissolve, e.g. according to Eq. 4.2. The formerly adsorbed phosphate is released into the pore water.

$$Fe(OH)_3 + e^- \rightleftharpoons Fe^{2+} + 3OH^- \qquad (4.2)$$

After Jacobsen (1978) the released Fe^{2+} may precipitate again, e.g. as siderite ($FeCO_3$) or hydroxysiderite after reaction with bicarbonate, as pyrite (FeS_2) if sufficient sulfide is present, or vivianite ($Fe_3(PO_4)_2$). The formation of vivianite might explain why the phosphorus binding capacity of iron-rich but reduced sediments is still significant (e.g. Kozerski, 1977; Schellenberger et al., 1983). Vivianite was shown to be present in the Havel sediments (Schettler, 1995) and in their SWITCH model Smits & Van der Molen (1993) attributed the phosphorus binding in deeper (reduced) sediment layers to $Fe_3(PO_4)_2$ precipitation. The mineral strengite ($FePO_4$) is presumably irrelevant as it is only stable at high levels of Fe^{3+} which correspond to oxic conditions and low pH.

The following hypotheses summarize the present understanding of how phosphorus is bound to iron in sediments and how it is released.

- Under oxic conditions, Fe-III hydroxides provide a very high phosphate sorption capacity. The sorption capacity decreases with increasing pH and the mineral age. In sediments, oxic conditions can be found in the uppermost layer due to the penetration of oxygen and nitrate from the water column.
- The thickness of the oxidized surface layer is subject to seasonal variation. In winter, when microbial activity is low and oxygen solubility is high, the critical depth, where the consumption of electron acceptors equals the supply from the water column, moves downwards. Thus, the oxidized layer with high P sorption capacity increases to a thickness of a few millimeters to centimeters.
- In eutrophic lakes, the oxidized layer may vanish altogether during summer. After the electron acceptors O_2, NO_3, and manganese-IV (see Stumm & Morgan, 1996, for the sequence of consumption) become depleted, the iron-III hydroxides are reduced and Fe^{2+} together with the formerly sorbed phosphate is released. Some part of the Fe^{2+} may precipitate in different minerals. If vivianite is formed, a fraction of the released phosphate may be rebound. After Kozerski (1977) the reduction is a rather slow process. It is therefore hypothesized that sudden peaks in the sediment P release originate from fast mineralization of fresh organic matter under anoxic or near-anoxic conditions rather than from the dissolution of P-sorbents.
- The pH, which modifies the sorption capacity, is subject to seasonal and spatial variation as well. Whereas high values (up to 9 and above) may occur in the water column of eutrophic lakes during the day, the pH decreases in the sediment due to CO_2 production. Thus, mineralization causes two opposite effects: On the one hand, the P sorption capacity is reduced due to iron reduction. On the other hand, the sorption capacity of the remaining Fe-III hydroxides should increase due to the pH effect.
- The deeper layers of the sediment are permanently reduced. Information on the binding of phosphorus to iron in this zone is scarce. The formation of vivianite provides a possible explanation for correlations between the iron and phosphorus content even in the deeper sediment.

The above discussion revealed how complex the binding of phosphorus to iron in natural sediments is. All of the relevant P-Fe compounds are sensitive to the microbial activity via pH and redox potential. This results in a considerable temporal variation in the P-binding capacity, especially in the uppermost sediment. Simple sorption models, e.g. built on the Langmuir isotherm, are therefore inappropriate. Furthermore, one must not overlook that concurrent reactions such as the precipitation of calcium phosphate may interfere with the iron related mechanisms (see Golterman (1988) and Golterman (1995a) for a revised view).

Calcium-bound phosphorus

Stumm & Morgan (1996) list the following minerals composed of calcium and phosphate: $CaHPO_4$, $Ca_4H(PO_4)_3$, $Ca_{10}(PO_4)_6(OH)_2$, $Ca_{10}(PO_4)_6F_2$, $CaHAl(PO_4)_2$ but further forms such as $Ca_3(PO_4)_2$, $Ca(H_2PO_4)_2$ are known to exist. Furthermore, the chemosorption of PO_4^{3-} to surfaces of calcite ($CaCO_3$) is possible, but Jacobsen (1978) has shown that the formation of hydroxyapatite is quantitatively more important.

In calcium rich natural waters[8], hydroxyapatite ($Ca_{10}(PO_4)_6(OH)_2$) is the predominant form because it is less soluble than other calcium phosphates. The existence of apatite minerals in sediments of the Lower Havel River (Lake Breitlingsee) was proven by x-ray spectrometry (Schettler, 1995). The formation and dissolution of hydroxyapatite is often written as

[8] Commonly called *hard waters* because Ca^{2+} is often a major species contributing to hardness.

$$Ca_5(PO_4)_3(OH) \rightleftharpoons 5Ca^{2+} + 3PO_4^{3-} + OH^-$$

where all stoichiometric factors have been divided by two. The solubility product K_L of $Ca_5(PO_4)_3(OH)$ is in the range 10^{-50} to 10^{-60}. Golterman (1995b) suggests to use pK_L=50, since it best explains the PO_4^{3-} concentrations found in the hardwater rivers Rhine and Rhone (Golterman & Meyer, 1985).

Using the known pK_L, the concentration of PO_4^{3-} in equilibrium with hydroxyapatite can be computed according to Eq. 4.3 [9]. To do so, the concentration of Ca^{2+} as well as OH^- must be given.

$$K_L = \frac{[Ca^{2+}]^5 \cdot [PO_4^{3-}]^3 \cdot [OH^-]}{[Ca_5(PO_4)_3OH]} \qquad (4.3)$$

Eq. 4.3 predicts the equilibrium concentration of PO_4^{3-} only. At pH values normally occurring in surface waters, the dissociation equilibrium of the species $H_2PO_4^-$ and HPO_4^{2-} must be taken into account if the total concentration of dissolved inorganic P (DIP) is to be computed. As indicated by Eq. 4.4 and Eq. 4.5, these equilibria are pH-dependent as well.

$$K_{d\ H_2PO_4^-} = \frac{[HPO_4^{2-}] \cdot [H^+]}{[H_2PO_4^-]} \qquad (4.4)$$

$$K_{d\ HPO_4^{2-}} = \frac{[PO_4^{3-}] \cdot [H^+]}{[HPO_4^{2-}]} \qquad (4.5)$$

The second and third dissociation constants of phosphoric acid are approximately $pK_{d\ H_2PO_4^-}$= 7.2 and $pK_{d\ HPO_4^{2-}}$= 12.3 at 25°C (Stumm & Morgan, 1996; Hellmann, 1999). Polynomials for the temperature dependence of both constants are presented in Golterman & Meyer (1985). Eq. 4.3, Eq. 4.4, and Eq. 4.5 can now be combined to yield the DIP concentration in equilibrium with hydroxyapatite at a given pH and Ca^{2+} concentration. If DIP is defined as

$$[DIP] = [PO_4^{3-}] + [HPO_4^{2-}] + [H_2PO_4^-]$$

one arrives after some algebra at Eq. 4.6.

$$[DIP] = \sqrt[3]{\frac{K_L}{[Ca^{2+}]^5 \cdot [OH^-]}} \cdot \left(1 + \frac{[H^+]}{K_{d\ HPO_4^{2-}}} + \frac{[H^+]^2}{K_{d\ HPO_4^{2-}} \cdot K_{d\ H_2PO_4^-}}\right) \qquad (4.6)$$

The concentration of $[OH^-]$ and $[H^+]$ in Eq. 4.6 can be substituted by the pH according to

$$[OH^-] = 10^{(pH - pK_{d\ H_2O})}$$
$$[H^+] = -log_{10}(pH)$$

with $pK_{d\ H_2O}$ being the dissociation constant or 'ionic product' of water ($pK_{d\ H_2O} \approx$ 14; see Golterman & Meyer (1985)).

The solution of Eq. 4.6 for a range of common pH and Ca^{2+} concentrations is presented in Fig. 4.19. As the figure shows, the concentration of DIP in equilibrium with hydroxyapatite is very sensitive to changes in the pH. A change in the pH by one degree ($\Delta[H^+]$= 10), changes the DIP concentration by up to two magnitudes.

Due to the strong influence of the pH, a considerable seasonal variation of DIP in the sediment pore water must be expected. This is because the sediment pH is affected by the activity of microorganisms which release acidifying substances such as CO_2 and NH_4^+ into the pore water. The biological activity increases with temperature and the supply of freshly settling organic matter[10]. Thus, the

[9] The brackets around the species symbols stand for the respective activities but in solutions of low ionic strength (low total ion concentration), activities and concentrations are virtually equal. Note that molal concentrations (mol kg^{-1} of H_2O) are used here. Also note that the activity of the solid phase in the denominator of Eq. 4.3 equals unity.

[10] The dependence of the pH on freshly settled degradable organic matter is corroborated by an observed negative correlation between pore water pH and chlorophyll-a in the Havel sediments (data from R. Knösche).

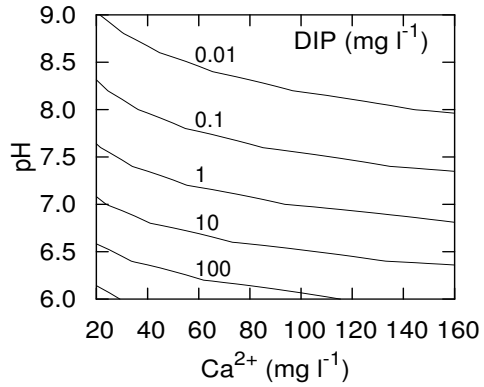

Figure 4.19: *Total concentration of dissolved inorganic phosphorus (DIP) in equilibrium with hydroxyapatite as a function of pH and dissolved calcium. The plot was drawn with an apatite solubility constant of pK_L=50 and a temperature of 20° C. Note that concentrations are given in mg l^{-1}, not as molalities as in Eq. 4.6.*

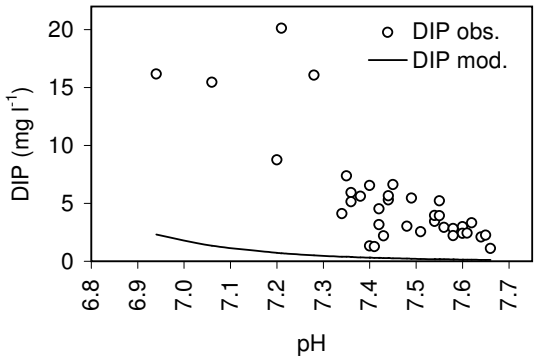

Figure 4.20: *pH and DIP concentration in the pore water of 19 sediment samples (0–6 cm) from the Potsdamer Havel collected in November 2005 (R. Knösche). The solid line shows the theoretical DIP concentration in equilibrium with hydroxyapatite as a function of the pH at a Ca^{2+} concentration of 90 mg l^{-1} and a temperature of 10 °C. A good model fit would require the Ca^{2+} concentration to be as low as 18 mg l^{-1}.*

dissolution of hydroxyapatite at lower pH in summer provides another potential explanation for the observed sediment P release in the Havel Lakes.

The application of the apatite model (Eq. 4.6) to 19 sediment samples from the Potsdamer Havel collected in November 2005 by R. Knösche is presented in Fig. 4.20. Sediment pH values in the range 6.9–7.7 ($\overline{x}$= 7.45, SD= 0.16, n= 19) were observed in the top 6 cm. The corresponding calcium concentrations were not measured. However, in the Potsdamer Havel, Ca^{2+} levels of about 90 mg l^{-1} are found with only little seasonal variation and it seems reasonable to assume a similar value for the pore water of the upper sediment.

According to Fig. 4.20, the DIP concentration in the pore water of the sediments is apparently (at least not permanently) in equilibrium with hydroxyapatite. Because the overall existence of $Ca_5(PO_4)_3OH$ was proven by Schettler (1995), it seems likely that its formation is a rather slow process which is unable to buffer massive release of P from mineralization. The simulation results of Hoffmann (1999) indicate that the apatite-equilibrium can explain the observed P concentrations during the winter period.

Organic phosphorus

The organic matter (OM) in sediments is spread over different fractions. The largest part consists of particulate OM which originates from the settling of organisms and detritus. Some degradable part of the OM is taken up by consumers and heterotrophic bacteria. In the latter case, the particulate OM must first be hydrolyzed to dissolved OM with the help of enzymes. Another smaller part of the sedimentary OM is stored in the biomass of autotrophic organisms such as nitrifying bacteria or autrotrophic denitrifiers.

The recycling of organic carbon to CO_2 (oxic conditions) or CO_2 and reduced compounds such as methane (anoxic conditions) is the result of the organisms' respiration. Respiration and hydrolysis of OM as well as excretion finally result in the release of nutrients according to the stoichiometry of the organic matter.

To illustrate how the concentration of organic phosphorus (and nitrogen) in the sediment is regulated, a simple mass balance equation can be written. If the organic P concentration in the sediment (g P m^{-3} sediment) is denoted $P_{org,sed}$ and $P_{org,pel}$

(g P m^{-3}) is the corresponding concentration in the pelagic zone, one arrives at Eq. 4.7.

$$\frac{dP_{org,sed}}{dt} = \frac{u \cdot V_w}{z_w \cdot V_s} \cdot P_{org,pel} - k \cdot P_{org,sed} \quad (4.7)$$

The first term describes the input to the pool of sedimentary organic P by settling, where u (m s^{-1}) is the settling velocity, z_w (m) is the depth of the water column, and V_w/V_s is the ratio of the volume of the water column and the considered sediment layer, respectively. The second term describes the conversion of sedimentary organic P to dissolved inorganic P by microbial degradation with k (s^{-1}) being a temperature dependent rate constant. Solving Eq. 4.7 for steady state and assuming $V_w/V_s \approx z_w/z_s$ with z_s being the thickness of the sediment layer yields Eq. 4.8.

$$P_{org,sed*} = \frac{u}{k \cdot z_s} \cdot P_{org,pel} \quad (4.8)$$

Thus, the steady state concentration of sedimentary organic P ($P_{org,sed*}$) increases linearly with the concentration of organic P in the pelagic zone and the settling velocity u. An inverse dependence on the decay rate k and the thickness of the (mixed) sediment layer is predicted.

It should be kept in mind that the sediment conditions turn from oxic to anoxic at high concentrations of degradable organic matter (including $P_{org,sed}$). If such a change in the redox milieu occurs, the value of k will change too. Hence, Eq. 4.7 is actually a nonlinear equation because the value of k is not independent from $P_{org,sed}$.

Furthermore, the use of a single rate constant k does not take into account the heterogeneity of organic matter. Differences in the degradability of the OM fractions are better reflected by a multi-rate approach (e.g. Carignan & Lean, 1991) which, however, requires more parameters to be known.

Identification of the P fractions

In practice, it is difficult to determine how the total amount of sedimentary phosphorus is distributed over the different fractions. A number of sequential extraction procedures are discussed in the literature (Hieltjes & Lijklema, 1980; Psenner et al., 1984). Unfortunately, these procedures are costly and their applicability to a large number of samples is therefore limited. Less complicated extraction schemes distinguishing acid and base soluble phosphorus only have been developed therefore (Schettler, 1995). The drawback of simplification is a loss of information. For example, treatment with 0.24 N H_2SO_4 is believed to extract all inorganically bound P from a mud sample without discriminating the calcium and the iron bound fraction (Keizer & Sinke, 1992; Knösche, 2006b).

4.4.2.2 Remobilization processes

Diffusion

If phosphorus is released from one of the above mentioned fractions due to desorption, dissolution, excretion, or hydrolysis, an increase in the phosphate concentration of the pore water occurs. If the released phosphate is not sorbed, precipitated, or taken up by organisms again, it is subject to diffusive transport. The specific vertical flux rate J (g m^{-2} s^{-1}) is related to the spatial concentration gradient (g m^{-3} m^{-1}) by the sediment bulk diffusion coefficient D_s (m^2 s^{-1}) according to Fick's first law (Eq. 4.9). The reduction in diffusion area by the sediment particles is taken into account by the dimensionless porosity ϕ.

$$J = -\phi \cdot D_s \cdot \frac{dC}{dx} \quad (4.9)$$

The bulk diffusion coefficient D_s in Eq. 4.9 is related to the more fundamental molecular diffusion coefficient in pure water D_m by the turtuosity θ and the constrictivity δ (Eq. 4.10).

$$D_s = D_m \cdot \frac{\delta}{\theta^2} \quad (4.10)$$

The turtuosity is the ratio of the true travel length between two locations (around particles) and the

straight distance between the locations. According to Maerki et al. (2004), the squared turtuosity θ^2 can be estimated from the porosity ϕ by Eq. 4.11.

$$\theta^2 = F \cdot \phi \tag{4.11}$$

The factor F is the 'formation factor' and represents the ratio of the bulk electric resistivity and the resistivity in the pore water alone. Often, F is simply estimated from the porosity by $F = a \cdot \phi^{-m}$ where a is a constant close to one and m is a value in the approximate range 1.2–3. For sandy freshwater sediments Maerki et al. (2004) fitted the empirical relation $F = 1.04 \cdot \phi^{-1.21}$.

Combining Eq. 4.10 and Eq. 4.11 and inserting into Eq. 4.9 finally yields Eq. 4.12 for calculating the diffusive flux rate in the sediment.

$$J = -D_m \cdot \frac{\delta}{F} \cdot \frac{dC}{dx} \tag{4.12}$$

The diffusion coefficient in water D_m is specific for each molecule and the influence of temperature can be described by the Einstein equation (Eq. 4.13).

$$\frac{D_m(T_1)\, V_a(T_1)}{T_1 + 237} = \frac{D_m(T_2)\, V_a(T_2)}{T_2 + 237} \tag{4.13}$$

In this relation, T (°C) is the temperature and $V_a(T)$ (kg m^{-1} s^{-1}) is the dynamic viscosity[11]. Molecular diffusion coefficients for a number of ions can be found in Li & Gregory (1974) or Carignan & Lean (1991).

If Eq. 4.9 is combined with the one-dimensional mass balance equation to yield Fick's second law,

[11] The dynamic or 'absolute' viscosity $V_a(T)$ is related to the kinematic viscosity V_k (m^2 s^{-1}) by $V_a(T) = V_k \cdot \rho(T)$ with ρ being the density of water (kg m^{-3}). For temperatures T in the range 0–30°C the density is approximately $\rho = 1000 - 0.00653 \cdot (T - 3.98)^2$. The kinematic viscosity V_k (m^2 s^{-1}) can be approximated by $V_k = 1.78 \cdot 10^{-6}/(1 + 0.0337 \cdot T + 0.221 \cdot 10^{-3} \cdot T^2)$ with T in °C after Preissler & Bollrich (1985).

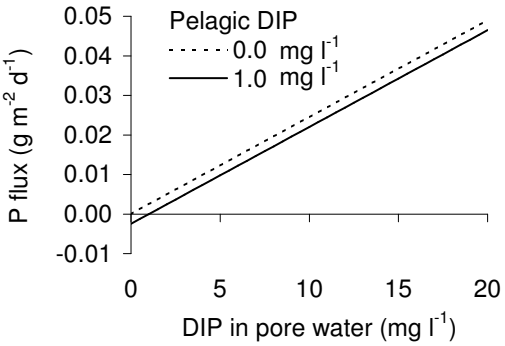

Figure 4.21: *Calculated phosphorus flux rates at the sediment water interface (g m^{-2} d^{-1}) according to Eq. 4.12. The molecular diffusion coefficient of phosphate was set to 7.17·10^{-10} m^2 s^{-1} which is the average of the individual coefficients for the species HPO_4^{2-} (7.34·10^{-10} m^2 s^{-1} at 25° C) and $H_2PO_4^-$ (8.46·10^{-10} m^2 s^{-1} at 25 ° C) after transformation to 20° C. The mixing length dx was set to 0.01 m, the porosity ϕ was assigned a value of 0.85, δ = 1, and $F = 1.04 \cdot \phi^{-1.21}$.*

it can be used for calculating the vertical phosphorus flux in a sediment column. Eq. 4.9 can furthermore be used for estimating the flux through the sediment-water interface (Ramm & Scheps, 1997; Lavery et al., 2001). In the latter case, the gradient can either be computed from measured pore water concentrations at two different depths near below the sediment surface or one can directly use the difference between the pelagic and the pore water concentration at a certain depth.

Fig. 4.21 shows calculated phosphorus flux rates at the sediment-water interface for pore water concentrations between 0 and 20 mg l^{-1} DIP and pelagic DIP levels of 0 and 1 mg l^{-1}. One must not forget that the computed flux rates account for molecular diffusion only. In natural sediments concurring processes occur which may be – at least temporarily – much more effective (see following paragraphs). Also, porosities are highly variable in both space and time.

In models which approximate the upper sediment as a single layer (e.g. Hoffmann, 1999), the concentration gradient dC/dx for sediment-

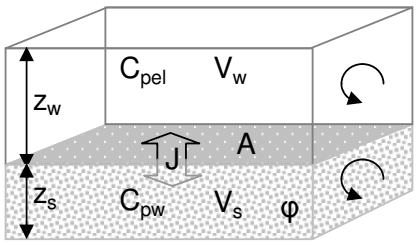

Figure 4.22: *Schematic representation of a water-sediment system. C_{pel}: concentration in the water column, C_{pw}: corresponding concentration in the sediment pore water, z_w, z_s: depth of water and sediment, V_w, V_s: volume of the water column and total volume of the sediment layer, A: interface area, ϕ: sediment porosity.*

water flux calculations is approximated by $(C_{pw} - C_{pel})/(0.5 \cdot z_s)$. Here, z_s is the thickness of the considered layer, C_{pw} is the average pore water concentration, and C_{pel} is the concentration in the water column (see Fig. 4.22).

Using Eq. 4.12, the change in the water column's concentration may be expressed by Eq. 4.14 and the change in the pore water concentration follows Eq. 4.15.

$$\begin{aligned} \frac{d}{dt} C_w &= J \cdot A / V_w \\ &= J / z_w \\ &= \frac{2 \cdot D_m \cdot \delta}{z_s \cdot z_w \cdot F} \cdot (C_{pw} - C_{pel}) \end{aligned} \tag{4.14}$$

$$\begin{aligned} \frac{d}{dt} C_s &= -\, J \cdot A / (V_s \cdot \phi) \\ &= -\, J / (z_s \cdot \phi) \\ &= -\, \frac{2 \cdot D_m \cdot \delta}{{z_s}^2 \cdot \phi \cdot F} \cdot (C_{pw} - C_{pel}) \end{aligned} \tag{4.15}$$

Sediment mixing

Bioturbation refers to the mixing of the sediment matrix by organisms (Lampert & Sommer, 1993). These might be organisms living in the sediment and feeding on detritus and bacteria, but also fish, stirring up the sediment on their search for benthic prey. The term bio-irrigation refers to the activity of invertebrates (e.g. chironomides) who pump oxygen-rich water into the sediment through biogenic macropores. These mechanisms of random mixing in the upper sediment layer can be modeled in the same way as molecular diffusion but values of the related exchange coefficients are hard to estimate. It is reasonable to assume a dependence on those variables which control benthic bioactivity, e.g. temperature, redox conditions, settling rate of organic matter, occurrence of macrophytes, etc.. According to Mermillod-Blondin et al. (2003) bioactivity also modifies the sediment's porosity. In the SWITCH model (Smits & Van der Molen, 1993) bioturbation was assumed to be a very important process, causing the transport of vivianite from deeper, reduced layers to the upper sediment where the mineral dissolves and the formerly bound P is released.

The deeper sediment zones of eutrophic waters are usually anoxic, since the consumption of electron acceptors by the decay of organic matter exceeds the rate of supply from the water column. Under these conditions, methane is produced from incomplete organic carbon oxidation or the use of CO_2 as electron acceptor. In times of high microbial activity, methane bubbles are formed. When bubbles move toward the sediment surface driven by buoyancy, a directed mixing of particles and pore water takes place.

Resuspension of sediment by wind-induced shear stress contributes significantly to nutrient remobilization in shallow water bodies (Hellstrøm, 1991; James et al., 1997; Welch & Cooke, 2005). Again, several control factors are involved such as wind speed and direction, the lake geometry, as well as the sediment composition, compaction, and its spatial distribution.

Compared to molecular diffusion (Eq. 4.9 & 4.12), the effects of bioturbation, bubbling, and resuspension are much harder to predict. This is a problem, because the apparent dispersion coefficients ($m^2\ s^{-1}$) related to these processes may

be large compared to molecular diffusion coefficients. In present models, remobilization of sedimentary substances by turbation and resuspension is either neglected or a lumped dispersion coefficient is used that covers all mechanisms, including diffusion (e.g. Smits & Van der Molen, 1993).

Further difficulties for modeling sediment phosphorus release arise from the fact that the environmental condition in the sediment and the pelagic zone are different with respect to the pH and the redox potential. For example, dissolved phosphate which is brought to the sediment surface may precipitate there as calcium phosphate due to the increase in pH from deeper sediments toward the surface. Also, if reduced iron (Fe^{2+}) and phosphate are transported to the sediment surface, instantaneous refixation by sorption or precipitation may occur when iron is oxidized in contact with the oxygenated pelagic water.

4.4.3 Representation of nutrient retention and remobilization in TRAM

4.4.3.1 Required degree of simplification

From the discussion in Sect. 4.4.1 and 4.4.2, several conclusions for modeling of the Lower Havel River can be drawn:

Many different mechanisms are responsible for the storage of nutrients in sediments and their remobilization. This is especially true for phosphorus, which – in contrast to nitrogen – forms insoluble inorganic compounds (minerals). Transformation, binding and remobilization processes are all mediated or indirectly affected by microbial activity. How poorly the true mechanisms behind phosphorus release, *after several decades of research*, are actually understood was shown by Golterman (1995a).

Because existing models describe the sediment diagenesis in a greatly simplified, conceptual manner (Van der Molen, 1991; Smits & Van der Molen, 1993; Hoffmann, 1999), they use lumped parameters. Hence, the parameter values integrate the effect of different processes and also compensate for unknown mechanisms. They can only be determined by calibration and it is therefore hard to transfer parameter values from one study site to another.

In order to identify the key processes and parameters of a process-oriented model of nutrient cycling in the sediments of the Havel Lakes, a monitoring of physical and chemical parameters over many years with high spatial and temporal resolution would be required. Since sediment samples are – compared to surface water – hard to collect and more difficult to analyze without disturbing the natural conditions (e.g. anoxia), this is not practically feasible without significant investment of time and money. At present, the only available data on sediment characteristics and nutrient concentrations are those collected by Knösche (2006a) and those published by Schettler (1995).

Finally, the catchment models SWIM and ArcEGMO-Urban, to which TRAM must be coupled for scenario simulations, compute the emissions of total N and P only. Thus, the catchment models cannot provide the required boundary conditions for a complex process model, such as fractions of organic P and N, or species of dissolved inorganic N.

Consequently, a nutrient turnover model for the Lower Havel River must primarily focus on a closed description of the nitrogen and phosphorus mass balance. The bottom sediment and the dynamics of nutrient exchange with the pelagic zone need to be approximated by a strongly simplified approach.

4.4.3.2 Nitrogen retention

According to Jensen et al. (1992b) and Seitzinger (1988), permanent losses of nitrogen may result from two different processes: denitrification and burial of organic N in deeper sediment layers. This is also reflected by Fig. 4.18. Jensen et al. (1992b) found denitrification in lakes to be closer related to the pelagic concentration of total nitrogen than

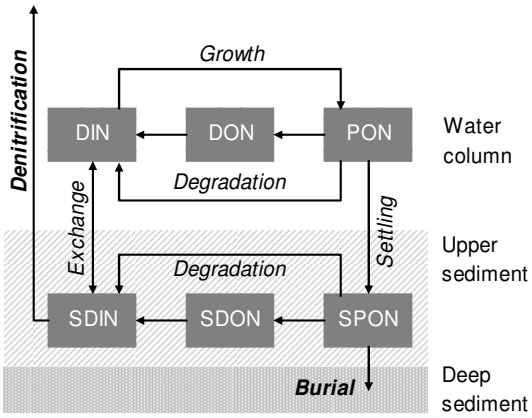

Figure 4.23: *Simplified nitrogen cycle with the two sinks, denitrification and burial. The considered nitrogen fractions in the water column are: PON (particulate organic N), DON (dissolved organic N) and DIN (dissolved inorganic N). The corresponding sediment fractions carry the initial letter 'S'.*

to the pelagic NO_3^- concentration. This indicates that denitrification is in fact mainly bound to the sediment (see Sect. 4.4.1) since it is the particulate fraction of TN which is responsible for the transfer of N from the pelagic to the benthic compartment.

Fig. 4.23 shows a simplified chart of the N cycle that distinguishes three fractions of N in the water column and the sediment. The total nitrogen in the water column (TN) is the combination of particulate organic N (PON), dissolved organic N (DON) and dissolved inorganic N (DIN). The actual distribution of DIN over the species NO_3^-, NO_2^-, and NH_4^+ is neglected. In accordance with Fig. 4.23, the dynamics of these N fractions can be expressed by Eq. 4.16–Eq. 4.19 if the exchange of mass via inflow and outflow is left unconsidered (closed system).

$$\frac{d}{dt}\,TN = \frac{d}{dt}\,PON + \frac{d}{dt}\,DON + \frac{d}{dt}\,DIN \tag{4.16}$$

$$\begin{aligned}\frac{d}{dt}\,PON = &+ k_{grw}\cdot PON\\ &- k_{dw1}\cdot PON\\ &- k_{dw2}\cdot PON\\ &- \frac{u_{nset}}{z_w}\cdot PON\end{aligned} \tag{4.17}$$

$$\begin{aligned}\frac{d}{dt}\,DON = &+ k_{dw1}\cdot PON\\ &- k_{dw3}\cdot DON\end{aligned} \tag{4.18}$$

$$\begin{aligned}\frac{d}{dt}\,DIN = &+ \frac{2\cdot D\cdot\phi}{z_s\cdot z_w}\cdot(SDIN - DIN)\\ &+ k_{dw2}\cdot PON\\ &+ k_{dw3}\cdot DON\\ &- k_{grw}\cdot PON\end{aligned} \tag{4.19}$$

The symbols in Eq. 4.16–Eq. 4.19 have the following meaning: k_{grw}: growth rate of organisms taking up DIN (s^{-1}), k_{dw1}: PON to DON conversion rate (s^{-1}), k_{dw2}: PON to DIN conversion rate (s^{-1}), k_{dw3}: DON to DIN conversion rate (s^{-1}), u_{nset}: settling velocity of PON (m s^{-1}), z_w: depth of the water column (m), z_s: depth of the considered, well mixed sediment layer (m), D: bulk diffusion coefficient for dissolved inorganic N in the sediment pore water (SDIN) given in (m^2 s^{-1}), ϕ: sediment porosity (–). The concentrations of all fractions are expressed in the standard unit (g m^{-3}). Note that Eq. 4.19 contains the implicit assumption that the volume of the water body V_w divided by the volume of the considered sediment layer V_s can be approximated by $V_w/V_s = z_w/(z_s\cdot\phi)$, i.e. the areal extent of the water body and the sediment are assumed to be equal.

Eq. 4.16–Eq. 4.19 can be summarized to yield the TN balance (Eq. 4.20).

$$\begin{aligned}\frac{d}{dt}\,TN = &+ \frac{2\cdot D\cdot\phi}{z_s\cdot z_w}\cdot(SDIN - DIN)\\ &- \frac{u_{nset}}{z_w}\cdot PON\end{aligned} \tag{4.20}$$

Obviously, the DON fraction no longer appears in the TN balance (Eq. 4.20), because the conversion of PON to DON and the decay of DON to DIN is just a redistribution of nitrogen in the water column's total N pool. Only the diffusive exchange of dissolved inorganic N with the sediment (first term in Eq. 4.20) and the settling of the particulate fraction (second term) control the dynamics of TN.

Similar to Eq. 4.17–4.19, three differential equations can be written for the N fractions in the sediment (Eq. 4.21–Eq. 4.23). While the concentration of the sedimentary particulate organic N (SPON) has the unit mass per sediment volume (g m^{-3}), the dissolved fractions in the sediment pore water (SDON, SDIN) are given in mass per volume of pore water (g m^{-3} too).

$$\begin{aligned}\frac{d}{dt}\,SPON = &+ \frac{u_{nset}}{z_w} \cdot \frac{z_w}{z_s} \cdot PON \\ &- k_{ds1} \cdot SPON \\ &- k_{ds2} \cdot SPON \\ &- \frac{u_{nbur}}{z_s} \cdot SPON\end{aligned} \tag{4.21}$$

$$\begin{aligned}\frac{d}{dt}\,SDON = &+ \frac{k_{ds1}}{\phi} \cdot SPON \\ &- k_{ds3} \cdot SDON\end{aligned} \tag{4.22}$$

$$\begin{aligned}\frac{d}{dt}\,SDIN = &+ \frac{k_{ds2}}{\phi} \cdot SPON \\ &+ k_{ds3} \cdot SDON \\ &- \frac{2 \cdot D \cdot \phi}{z_s \cdot z_s \cdot \phi} \cdot (SDIN - DIN) \\ &- k_{denit} \cdot SDIN\end{aligned} \tag{4.23}$$

Most symbols used in Eq. 4.21–Eq. 4.23 were already declared above. The new symbols are: k_{ds1}: SPON to SDON conversion rate (s^{-1}), k_{ds2}: SPON to SDIN conversion rate (s^{-1}), k_{ds3}: SDON to SDIN conversion rate (s^{-1}), u_{nbur}: burial velocity of SPON (m s^{-1}), k_{denit}: rate of N loss from the SDIN pool due to denitrification (s^{-1}). Note that some of the constants cancel out but the possible simplifications have not been adopted for the sake of transparency. As in Eq. 4.19, the assumption $V_w/V_s = z_w/(z_s \cdot \phi)$ was used in the derivation of Eq. 4.23. Furthermore, for Eq. 4.19 to be valid, some part of SDIN must be present as NO_3^- because this is a precondition for denitrification.

If the sediment is in steady state, i.e. no accumulation of nitrogen occurs and no decay of a formerly accumulated nitrogen excess takes place, the left hand sides of Eq. 4.21, Eq. 4.22, and Eq. 4.23 can be set to zero. The steady state equations obtained can, after some rearrangement, be inserted into the TN balance equation (Eq. 4.20) to yield Eq. 4.24.

$$\begin{aligned}&\frac{d}{dt}\,TN = \\ &\frac{z_s}{z_w} \cdot \left(\phi \cdot k_{denit} \cdot SDIN - \frac{u_{nbur}}{z_s} \cdot SPON\right)\end{aligned} \tag{4.24}$$

This equation expresses that, as long as the concentrations of the sedimentary N fractions are in steady state, the change in the water column's TN mass must balance the N losses from the system caused by burial and denitrification. This becomes clear when both sides of Eq. 4.24 are multiplied by $z_w \cdot A$ with A (m^2) being the areal extent of the sediment layer and the water body.

In a next step, the values of SDIN and SPON in Eq. 4.24 can be substituted by steady state solutions of Eq. 4.23 and Eq. 4.21, also making use of Eq. 4.22. If this is done (not presented here), the right hand side of Eq. 4.24 turns out to be a linear function of PON and DIN only. Under the assumption that that PON and DIN are constant fractions of TN, i.e. $PON = \alpha_1 \cdot TN$, $DIN = \alpha_2 \cdot TN$, $DON = \alpha_3 \cdot TN$, $\sum \alpha_i = 1$, Eq. 4.24 simplifies

to Eq. 4.25, with the single parameter k_{TN} (s^{-1}) integrating all remaining constants.

$$\frac{d}{dt} TN = -k_{TN} \cdot TN \tag{4.25}$$

The result of the above calculations can be summarized as follows: Given a constant distribution of TN over the fractions PON, DON, and DIN as well as steady state conditions, the total nitrogen loss in the water column (dTN/dt) can be expressed as a linear function of TN. That is, the effects of both burial and denitrification losses can be merged into a single rate constant as in Eq. 4.25. The value of k_{TN} is likely to be dominated by the effect of denitrification.

It must be noted that the approach described is built completely on linear differential equations, i.e. dependencies of the rate constants on the concentrations were neglected. The linear approach of Eq. 4.25 will certainly be invalid if the TN concentration varies over a very wide range. If for example, the sediment shifts from fully oxic to completely anoxic conditions due to very high settling of PON or vice versa, this would not only alter mineralization constants but also effect nitrification and thus denitrification.

The advantage of the first order equation 4.25 lies in the fact that it describes the retention of nitrogen in terms of TN only and no information on the quantity of the different N fractions or DIN species is required. This simplifies the targeted coupling of TRAM to catchment models, which can only deliver TN loads as boundary conditions. The drawback of simplicity, however, lies in the fact that calibrated values of the rate constant k_{TN} are related to a certain constitution of the TN pool. For example, k_{TN} is expected to show a seasonal variation not only because of the temperature dependence of denitrification but also due to changes in the PON/TN ratio which controls nitrogen settling. In the application presented, the seasonal variability in N retention was accounted for by extending Eq. 4.25 with an Arrhenius term (Eq. 4.26)

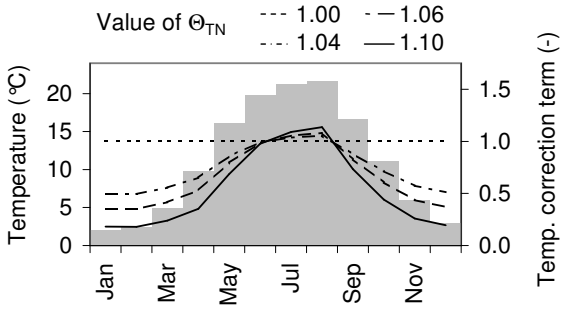

Figure 4.24: *Seasonal variation of the average water temperature at Ketzin (bars) and corresponding values of the temperature correction term $\theta_{TN}{}^{(T-20)}$ (lines) at different values of θ_{TN}.*

where T is the water temperature and θ_{TN} is an empirical coefficient.

$$\frac{d}{dt} TN = -k_{TN} \cdot \theta_{TN}{}^{(T-20)} \cdot TN \tag{4.26}$$

The influence of the temperature correction term $\theta_{TN}{}^{(T-20)}$ on the rate of nitrogen retention is illustrated by Fig. 4.24.

4.4.3.3 Phosphorus retention and release

A simplified scheme of the aquatic phosphorus cycle is presented in Fig. 4.25. The major contrast to the N cycle (Fig. 4.23) is the appearance of the particulate inorganic species PIP and SPIP.

The discussion of nutrient cycles in Sect. 4.4.1 and phosphorus storage in Sect. 4.4.2 revealed how complex the processes of P retention and remobilization actually are. Because data on sediment qualities and their seasonal variability are scarce, the processes and parameters of a detailed sediment model cannot be identified. Thus, similar to the description of nitrogen retention, a greatly simplified, conceptual modeling approach was chosen with two premises in mind:

- The model must reflect the apparent decay of the phosphorus excess which has accumulated in the Havel sediments in past decades.

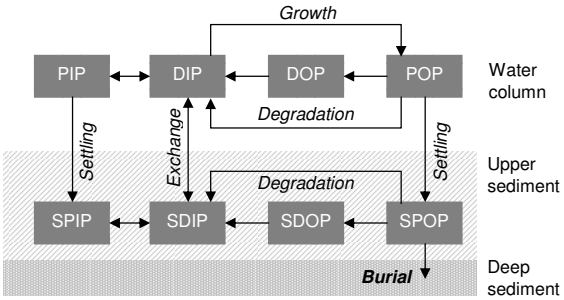

Figure 4.25: *Simplified phosphorus cycle with burial in the deep sediment as a sink. The phosphorus fractions in the water column are: POP (particulate organic P), DOP (dissolved organic P), DIP (dissolved inorganic P) and PIP (particulate inorganic P). The corresponding sediment fractions carry the initial letter 'S'.*

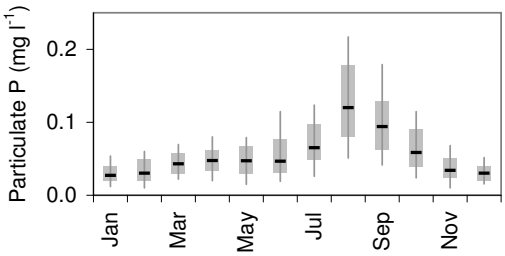

Figure 4.26: *Seasonality of the concentration of particulate phosphorus based on pooled data from the Potsdamer Havel Lakes (1991–2002). The box shows the interquartile range with the median as horizontal line and the 10–90 percentile range as whiskers.*

- The model must take into account the pronounced seasonal variability in P remobilization and retention in order to yield realistic P concentrations during the growth period of algae.

Table 4.6 presents the phosphorus model using the compact matrix notation introduced in Sect. 3.3.2. Only two components are simulated: total phosphorus in the water column (TP) and the total phosphorus in a finite layer of the upper sediment (PS). Because PS integrates the particulate and the dissolved fraction, it is defined in g P per sediment volume.

The three processes considered are the settling of particulate P, the immobilization of sediment P (burial) and the return of sedimentary P into the water column (remobilization). These three processes also form the basis of the 'tier 5' phosphorus retention model developed by Kronvang et al. (2005). Details of the process description are discussed in the following paragraphs while the estimation of parameters and initial values is covered by Sect. 4.4.4.

Settling of phosphorus

Settling of particulate matter is the dominant process of phosphorus transfer from the pelagic zone to the sediment. Its representation in the model requires the particulate fraction of total phosphorus and its effective settling velocity u_{pset} to be known. As illustrated in Fig. 4.25, there are particulate forms of both organic P (plankton, detritus) and inorganic P [12]. In the model presented, these two fractions are not distinguished but the lumped variable PP (particulate P, see Table 4.6) is used, for which measured data are available.

In the model, PP is a boundary condition variable, not a simulated component as in more complex ecological models. Average values of PP are computed from the day of the year using a nonlinear regression model fitted to the data shown in Fig. 4.26.

The fact that the values of PP are predefined, not simulated, must be kept in mind when the model is driven by altered boundary conditions (scenario simulations). The use of PP as a boundary condition is appropriate as long as nutrient concentrations change only slightly and do not result in limitation of plankton growth. In the case of heavily altered external loading, however, there might be a significant drop in phytoplankton abundance. Then a much more complex nutrient-algae model has to be used which includes PP as a simulated component. As a makeshift, the boundary condi-

[12] The settling of organic and inorganic P is often linked because organic particles are involved in the process of calcite precipitation.

Table 4.6: *Process matrix of the phosphorus model for the Havel Lakes (see Sect. 3.3.2 for details on this kind of notation). TP: total phosphorus in the water column (g m^{-3}), PP: particulate phosphorus (g m^{-3}), PS: total phosphorus in the upper sediment layer (g m^{-3} sediment), P_0: P-binding capacity of the sediment (g m^{-3} sediment), u_{pset}: settling velocity of particulate P (m s^{-1}), u_{pbur}: velocity of sediment growth (m s^{-1}), z_w: water depth (m), z_s: thickness of the active sediment layer (m), k_{prem}: flux constant (g P m^{-2} sediment surface s^{-1} (g P excess · m^{-3} sediment)$^{-1}$), $f(T)$: a nonlinear function of temperature T (–).*

Process	Components		Process rate
	TP	PS	
Settling	-1	z_w/z_s	$u_{pset}/z_w \cdot PP$
Burial	0	-1	$u_{pbur}/z_s \cdot PS$
Remobilization	$1/z_w$	$-1/z_s$	$\begin{cases} k_{prem} \cdot f(T) \cdot (PS - P_0) & \text{if } PS > P_0 \\ 0 & \text{if } PS \leq P_0 \end{cases}$

tion variable PP is corrected for the effects of nutrient limitation as described below.

First, the concentration of PP is restricted to $4/5$ of the simulated total P concentration (TP) if the difference $TP - PP$ is smaller than 0.02 mg l^{-1}. The threshold used for the occurrence of P limitation is based on Sas (1989), who found that phosphorus is likely to limit algal growth at DIP concentrations below 0.01 mg l^{-1} during the vegetation period. The increased threshold value of 0.02 mg l^{-1} takes into account that the residual of $TP - PP$ does not consist of DIP only but also contains unavailable dissolved organic P. The factor $PP/TP \approx 4/5$ was derived from observation data at TP concentrations lower than 0.1 mg l^{-1}.

Second, PP is corrected for possible N limitation based on the N:P ratio. According to the Redfield-Ratio (Lampert & Sommer, 1993), the optimum stoichiometric ratio of N and P in algal biomass is approximately 16 which is equivalent to a mass ratio of about 7 (see Klausmeier et al., 2004, for information on the variability). Data from the Havel Lakes indicate a decline in phytoplankton concentrations at a N:P ratio in particulate organic matter of about 6 (see Fig. 4.27).

In order to correct the average concentration of PP for N shortage, it was multiplied by the factor $1/6 \cdot PON/PP$ if $PON/PP < 6$. A reasonable upper-limit estimate for the concentration of particulate organic N (PON) from the simulated TN concentration is $PON \approx 0.5 \cdot TN$. It is implicitly assumed that PP is mostly particulate *organic* P.

The pragmatic correction of the average concentration of particulate P (PP) for phosphorus and nitrogen limitation is summarized in Eq. 4.27–Eq. 4.28. Here, PP_{cP} is the concentration of PP corrected for P shortage and the final estimate PP_{cPN} accounts for both P and N shortage.

$$PP_{cP} = \begin{cases} \frac{4}{5} \cdot TP & \text{if } TP - PP < 0.02 \\ PP & \text{else} \end{cases} \tag{4.27}$$

$$PP_{cPN} = \begin{cases} \frac{0.5 \cdot TN}{6} & \text{if } \frac{0.5 \cdot TN}{PP_{cP}} < 6 \\ PP_{cP} & \text{else} \end{cases} \tag{4.28}$$

Phosphorus burial

The driving force behind phosphorus burial is the continuous settling of fresh material at the sediment surface. In the model, it is assumed that no phosphorus from the deep sediment is transferred back into the upper layer or the water column. Thus, burial irreversibly removes phosphorus from the system.

If vertical heterogeneities in the uppermost sediment layer with high bioactivity[13] are neglected,

[13] This is also called the *active layer*.

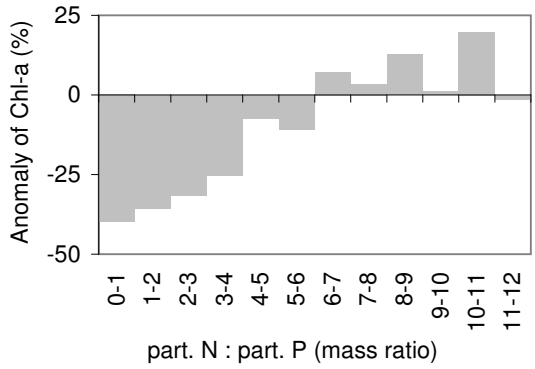

Figure 4.27: *Anomaly in the concentration of chlorophyll-a against the N:P ratio in particulate organic matter. The anomaly A_k for each class k of the N:P ratio was computed as $A_k = Median(C_{k,m}/\overline{C_m} - 1) \cdot 100$. In this definition, $C_{k,m}$ is the observed chlorophyll concentration at a date in month m where the N:P ratio falls into class k and $\overline{C_m}$ is the average concentration of chlorophyll in month m. For example, a value of -25% indicates that – with an empirical probability of 50% – the chlorophyll concentration is lower than 75% of the monthly average. The figure is based on pooled data from the Potsdamer Havel. The number of data in each class is >100 for N:P$\leq$7, it is >50 for N:P$\leq$10, and $\geq$25 for the remaining two cases.*

the rate constant of P loss equals the quotient of the effective sediment growth velocity and the thickness of the active layer u_{pbur}/z_s (Chapra, 1997, see Table 4.6).

Phosphorus remobilization

In accordance with Table 4.6, the influence of phosphorus remobilization on the water column's total P concentration is described by Eq. 4.29

$$\frac{d}{dt}\,TP = \begin{cases} \frac{k_{prem} \cdot f(T)}{z_w}\,(PS - P_0) & PS > P_0 \\ 0 & PS \leq P_0 \end{cases} \tag{4.29}$$

and the corresponding change in the concentration of sediment phosphorus PS follows from Eq. 4.30.

$$\frac{d}{dt}\,PS = -\frac{z_w}{z_s} \cdot \frac{d}{dt}\,TP \tag{4.30}$$

A fundamental assumption of this approach is the linear dependence of P remobilization on the sediment phosphorus excess. The excess is defined as the difference between the current total P concentration PS and a threshold value denoted P_0. Conceptually, P_0 represents the capacity of the sediment for permanent phosphorus storage. As long as $PS \leq P_0$ no remobilization of phosphorus occurs in the model. In other words, it is assumed that all settling phosphorus is being adsorbed or precipitated after mineralization or it is stored in organic form. Phosphorus remobilization begins after the surface sediment has become supersaturated, i.e. if $PS > P_0$.

From sediment analysis (Knösche, 2006a; Schettler, 1995) it is known that a considerable fraction of the sedimentary phosphorus in the Havel Lakes is iron-bound (see Sect. 4.4.2.1). The dependence of the P remobilization from aerobic lake sediments on the iron content was demonstrated by Jensen et al. (1992a). It is therefore advisable not to define P_0 in absolute units (g P m^{-3} sediment), but to use a threshold iron:phosphorus

ratio $r_{p:fe}$ instead. P_0 is then computed from Eq. 4.31

$$P_0 = r_{p:fe} \cdot Fe \tag{4.31}$$

with Fe being the iron content of the sediment (g m^{-3}) and $r_{p:fe}$ being the P binding capacity in g P (g Fe)$^{-1}$. In this way, differences in the P binding capacity of sediments with different Fe content can be taken into account.

The constant k_{prem} in Eq. 4.29 is a scaling parameter that controls how much P is released per square meter and time at a given sediment P excess. The corresponding unit is (g P m^{-2} surface area s^{-1} (g P excess)$^{-1}$ m^3 sediment).

The dimensionless term $f(T)$ was introduced to account for the seasonality of P remobilization. As discussed in Sect. 4.4.2, the intensity of P release should increase with rising bioactivity due to a decline in the redox potential, lowered pH, and turbation effects. Because the activity of microbes and other organisms in the sediment is not simulated, the temperature, which is the ultimate control variable, was chosen as a surrogate parameter.

Model tests revealed that best simulation results can be obtained if P release rates are linked to the average temperature of a previous time period rather than to instantaneous values. In other words, the maximum of sediment P release lags behind the maximum of water temperature. There are multiple plausible explanations for this observation.

Firstly, the maximum abundance of microbes should lag behind the maximum of sediment temperature according to the laws of population growth. Secondly, a delay between the temperature of sediment and water is to be expected. In consequence, the minimum values of redox potential and sediment pH should also be retarded with respect to the temperature maximum. The time lag may be further amplified by the fact that reductable substances other than iron must first be depleted in the sediment before iron itself is reduced and Fe-bound P is released.

After extensive model tests, the term $f(T)$ was defined as in Eq. 4.32

$$f(T) = \theta_{prem}{}^{(\overline{T_7}-20)} \tag{4.32}$$

with $\overline{T_7}$ being the average water temperature of the previous seven weeks and θ_{prem} being a dimensionless calibration parameter.

In summary, the model of phosphorus release is a conceptual one. It assumes a linear dependence of P release on the sediment phosphorus excess which is derived from the phosphorus:iron mass ratio. The seasonality of the phenomenon is accounted for by an empirical model based on the average temperature over of a previous time period.

The behavior of the complete phosphorus model can best be understood by analyzing a steady state situation. If the full expression dPS/dt according to Table 4.6 is set to zero, solving for PS yields the steady state P concentration in the sediment PS* (Eq. 4.33; see Table 4.6 for declaration of symbols).

$$PS^* = \frac{u_{pset} \cdot PP + k_{prem} \cdot f(T) \cdot P_0}{u_{pbur} + k_{prem} \cdot f(T)} \tag{4.33}$$

From Eq. 4.33 two important conclusions can be drawn:

1. The steady state concentration of sediment P increases linearly with the intensity of phosphorus settling.
2. If burial is neglected ($u_{pbur} = 0$) and the settling rate is non-zero, the value of PS* will exceed the storage capacity of the sediment P_0. That means, even in steady state, there is a sediment phosphorus excess. This excess will be greater, the less effective P remobilization is. Only at large values of k_{prem} does PS* approach P_0 and the excess ($PS^* - P_0$) goes down to zero.

For proper application of this phosphorus model, attention should be paid to the following points:

- The computed rate of sediment P release is independent from the concentration of dissolved phosphorus in the overlying water (DIP). Consequently, the model should only be applied in its existing form if the flux rate is insensitive to altered values of DIP. In the sediment of the Havel Lakes, an average pore water concentration (SDIP) of about 4 mg l^{-1} was found in November 2005 (data from Knösche, 2006a). Because the corresponding concentration in the pelagic zone is much lower (about 0.3 mg l^{-1}), the diffusive flux rate would increase by only 4% if DIP was be reduced by as much as 100%.
- The seasonal pattern of P release, which is approximated by the function $f(T)$, is assumed to be unaffected by changes in the sediment P excess. This is reasonable since the bioactivity in the sediment – and thus P release – are basically bound to the seasonal cycle of temperature.
- As mentioned above, the particulate P fraction is a boundary condition variable, not a simulated component. If the model is applied to situations in which a significant reduction in plankton biomass is likely (e.g. due to severe nitrogen shortage or manipulation of the pelagic foodweb), the particulate P concentration needs to be introduced as a simulated state variable. Notice that, at present, a moderate reduction in *total* P is unlikely to cause a reduction in *particulate* P because the system is currently not limited by phosphorus.

It is obvious that the applicability of the chosen model formulation is limited to scenarios with moderately altered boundary conditions. From this point of view, the use of a complex, more process-oriented ecological model would be desirable. However, such a model will only be of greater value if,

1. key parameters of a phytoplankton model have been determined in the field, such as growth and settling rates of functional algae groups,
2. observation data for all simulated variables of a plankton model are available with higher temporal resolution (e.g. daily values),
3. the catchment models to which TRAM is linked are able to provide the complete set of required boundary conditions instead of total N and P loads only,
4. more information on the phosphorus fractions in the Havel sediments and their remobilization mechanisms is available.

4.4.4 Parameter estimation and model performance

4.4.4.1 Calibration strategy

Because the parameters of the nutrient turnover models described above cannot be measured directly, their values had to be determined by calibration. The goal was to achieve a good agreement of observed and simulated TN and TP concentrations at the water quality monitoring stations shown in Fig. 4.5 given the model structures outlined in Sect. 4.4.3.2 & 4.4.3.3.

With the PEST software (Doherty, 2004), a flexible and free optimization tool for automatic calibration of nearly any simulation model is available. The use of such nonlinear optimization algorithms is certainly superior to 'manual calibration' with respect to objectivity and efficiency but its successful application may be less easy (see e.g. Doherty, 2004; Beven, 2000). A complicated shape of the objective function or insufficient precision of the model output may slow down convergence or cause the algorithm to fail completely. A further drawback of unsupervised optimization algorithms lies in the fact that the value of the objective function cannot be tracked over the full parameter space but only along a more or less random path. Another, more practical, problem is the automatic editing of the model's input files by the optimiza-

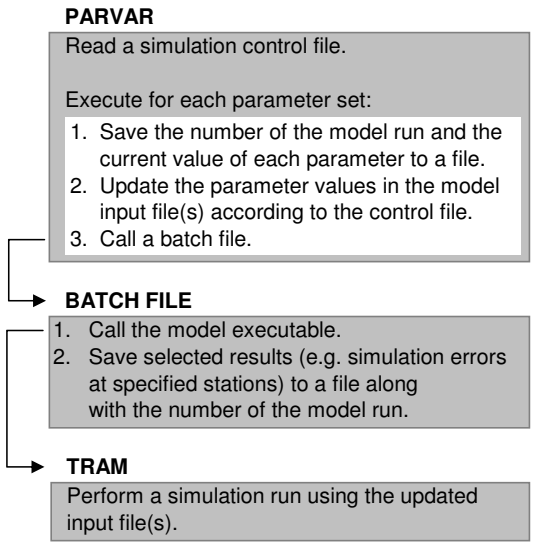

Figure 4.28: *Functionality of the PARVAR utility program used for automatic calibration.*

tion tool. While PEST's low level editing routines provide great flexibility, the risk of producing corrupt data files without notice is quite high.

In order to avoid these difficulties, a utility program PARVAR was designed that facilitates a model calibration by the method of combinatorial scenarios (Granger Morgan et al., 2003) or the Monte Carlo approach[14] . The principle of its application is illustrated by Fig. 4.28.

In a simulation control file, the names of the calibration parameters are specified. For each of the parameters, the following information must be supplied:

- The name of the ini-file from where TRAM reads the parameter value.
- The name of the corresponding data section and keyword (see example in Fig. 3.19).
- A list of values covering the parameter range to be scanned[15].
- Optionally, the name of another parameter can be specified to which the present parameter is tied. In this way, parameter interdependencies can be accounted for and the number of simulations is reduced since the values of both parameters are altered synchronously. In true Monte Carlo simulations with n_p parameters, it may be useful to tie $n_p - 1$ of them to one single master parameter.

After some postprocessing, the information recorded by PARVAR can easily be inspected for the parameter set(s) which gave the best agreement of simulated and observed data.

In the application presented, the model performance was quantified using the efficiency after Nash & Sutcliffe (1970) which is defined as the ratio of the mean square error MSE(p,o) and the observation variance VAR(o) subtracted from unity (symbol NSE; Eq. 4.34). In order to improve the sensitivity of the objective function at low concentrations, the efficiency was divided by the mean absolute percentage error (MAPE) which is computed from observations (o) and predictions (p) according to Eq. 4.35. Further parameters such as the mean error (bias) were logged for each model run. The performance measures were averaged over multiple monitoring locations if necessary.

$$NSE = 1 - \frac{\frac{1}{n}\sum_{i=1}^{n}(o_i - p_i)^2}{\frac{1}{n}\sum_{i=1}^{n}(o_i - \overline{o})^2} = 1 - \frac{MSE(p,o)}{VAR(o)} \tag{4.34}$$

$$MAPE = \frac{1}{n}\sum_{i=1}^{n}\frac{|o_i - p_i|}{o_i} \cdot 100 \tag{4.35}$$

If the number of independent calibration parameters is denoted n_p and $n_v(i)$ values are to be tested

[14] In a Monte Carlo simulation, the parameters are sampled randomly from their distributions. In combinatorial scenario analysis, the test values are predefined instead of being randomly chosen.

[15] No automatic sampling is performed, i.e. for Monte Carlo simulations, the array of random values must be generated externally, based on distribution information.

for the i-th parameter, the total number of simulations n_s follows from Eq. 4.36.

$$n_s = \prod_{i=1}^{n_p} n_v(i) \tag{4.36}$$

Considering the required time for a single simulation[16], the possible number of test values for each parameter is strictly limited. In the case of spatially variable parameters, it is a good idea to split the study area into subsections and to calibrate each of them separately.

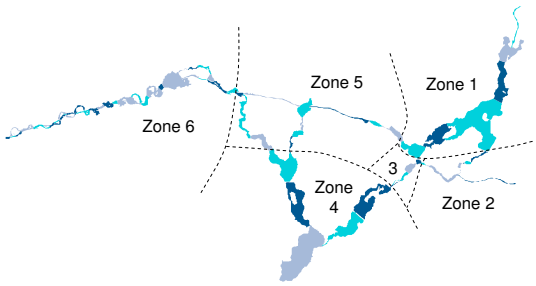

Figure 4.29: *Subdivision of the river network for calibration of the nitrogen retention model. Zone 1: Lake section downstream of Berlin Spandau, 2: Teltowkanal with high sewage load, 3: Zone downstream of the Teltowkanal's mouth, 4: Lake section downstream of Potsdam, 5: Channel section of the Sacrow-Paretzer Kanal, 6: Middle Havel River downstream of Ketzin.*

4.4.4.2 Nitrogen submodel

Parameter estimation

The model was calibrated using observed TN data of the period 1997–2000 and the subsequent 4 years served as validation period. Although total nitrogen is measured since 1995, observation data from before 1997 were excluded because of inconsistencies which might result from a change in measurement practice.

In a first attempt, global values were used for the parameters k_{TN} and θ_{TN}. Since the goodness-of-fit measures obtained were poor, the study area was divided into zones as shown in Fig. 4.29. The goal of subdividing the model domain was to allow for the use of different parameter values for water bodies which were expected to show a different retention behavior. The primary criterion for defining the zones shown in Fig. 4.29 were the hydrological characteristics. Whereas zone 1 and 4 mainly comprise lakes, the remaining zones represent more typical river conditions. The Teltowkanal and the river section downstream of its mouth (zone 2 & 3) were separated because they experience an extraordinarily high nitrogen load from Berlin's wastewater treatment plants. The use of the spatially variable model parameters shown in Table 4.7 improved the model performance (Fig. 4.30) significantly.

According to Table 4.7, nitrogen retention appears to be higher in the lakes (zone 1 & 4) compared to the more typical river/channel sections (zone 5 & 6). The high value of k_{TN} for the Teltowkanal (zone 2) seems to contradict this finding at first glance. However, the increased N retention is likely to result from the high and constant nitrate load (see Fig. 4.9). It is presumed that the nitrogen retention determined in the lakes of the Berliner Havel (zone 1) is somewhat too high because it compensates for an overestimated inflow of water from the polluted Teltowkanal into Lake Wannsee.

Furthermore, the θ_{TN} values greater than one for all separately calibrated zones indicate that nitrogen retention is more effective during summer (recall Fig. 4.24). As explained in Sect. 4.4.3.2, this may partly be attributed to the temperature dependency of denitrification but a seasonal variation in the composition of the TN pool (plankton growth) may also be of relevance. One must keep in mind that the model does not take N fixation by cyanobacteria into account which also affects the seasonality of N concentrations.

[16] A single run with 88 reactors (21 STR, 67 PFR) over a period of 10 years with a maximum time step of 1 day takes 2 minutes on a 2.8 GHz machine.

Table 4.7: *Calibrated parameters of the nitrogen retention model for the six regions shown in Fig. 4.29.*

Zone index	k_{TN} (d^{-1})	θ_{TN} (–)
1	0.025	1.04
2	0.020	1.06
3	0.015	1.10
4	0.010	1.04
5	0.006	1.04
6	0.006	1.06

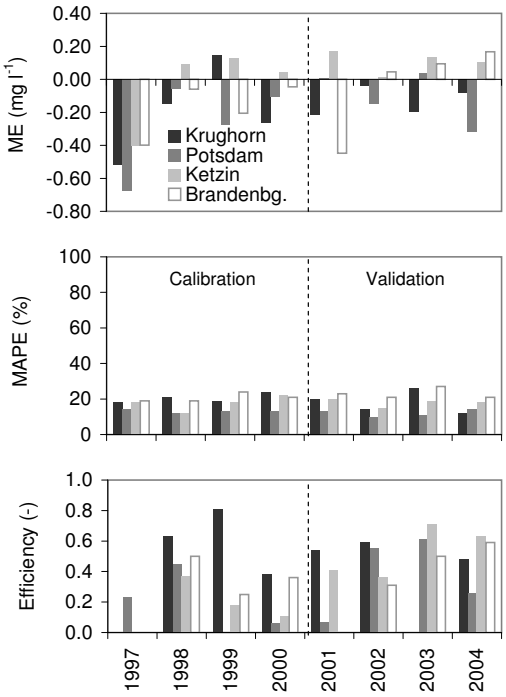

Figure 4.30: *Deviation between simulated and observed TN concentrations at Berlin Krughorn (BLN435), Potsdam Humboldtbrücke (HV0110), Ketzin (HV0195) and Brandenburg (HV0200). The figure shows the mean error or bias (ME), the mean absolute percentage error (MAPE) as well as the efficiency after Nash & Sutcliffe (1970).*

Model performance

The performance of the nitrogen retention model during the period of calibration (1997–2000) and validation (2001–2004) is illustrated in Fig. 4.30. Furthermore, Table 4.9 summarizes the major goodness-of-fit indicators of the nitrogen and phosphorus model.

After Fig. 4.30 and Table 4.9, the model performance measured by the Nash-Sutcliffe efficiency (NSE) is only moderate since the values are generally smaller than 0.6. However, other statistics such as the mean absolute percentage error (MAPE) show that the performance of the very simple nitrogen model is quite satisfactory. In terms of the NSE and the bias (ME), the simulation error during the validation period is even lower than during the calibration period.

With respect to the deviation between observed and simulated concentrations, several sources of errors must be distinguished (refer to Sect. 4.6.5.1 for a comprehensive overview). The nitrogen retention model is certainly subject to structural deficits because many different processes were lumped in Eq. 4.26. Model errors are likely to result from variabilities in the composition of the TN pool, unconsidered boundary conditions and interactions, as well as the total neglect of some processes such as nitrogen fixation. The fact that the model is is not strictly process-oriented has another consequence: Calibration can only identify those parameter sets that fit the data well. A 'true' parameter set however cannot exist from a theoretical point of view.

Another potential source of error are badly estimated nitrogen loads at the systems's inflows. Inaccuracies in discharge values are expected to be rather low, since daily averages were used. Larger errors are likely to result from the coarse temporal resolution of concentration time series requiring interpolation[17]. Finally, errors in individual observations are not unlikely in highly eutrophic systems because the particulate organic fraction of TN is not always homogeneously distributed over a river or lake cross-section. Non-representative

[17] At some stations, daily concentration data were available, whereas only fortnightly data exist for others.

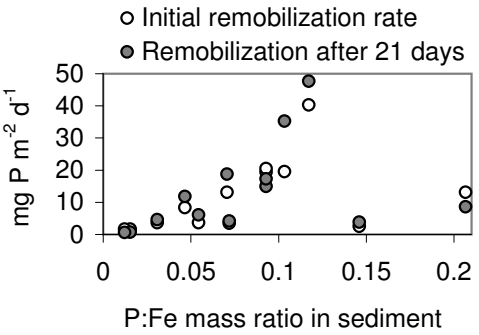

Figure 4.31: *Relationship between phosphorus remobilization under aerobic conditions and the phosphorus:iron mass ratio in the upper sediment (after Jensen et al., 1992a).*

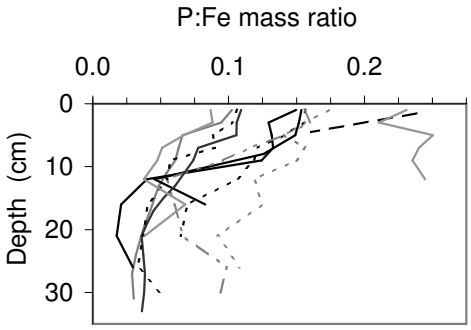

Figure 4.32: *Vertical profile of the P:Fe mass ratio in 11 sediment cores from the Potsdamer Havel Lakes (data from Knösche, 2006a).*

observations distort parameter estimation and (in the case of non-systematic errors) result in poor goodness-of-fit measures.

In the system studied, modeling results are believed to be extra sensitive to errors in the hydrodynamic simulation. This is because the nitrogen load of the Teltowkanal, which is a major source of N, may be differently distributed at two split flow junctions (see Fig. 4.9 and Fig. 4.38). In addition to potential inaccuracies in the flow distribution computed by HEC-RAS, one must not forget that TRAM is unable to properly handle flow reversal (Sect. 3.5.4) which may temporarily occur in some channels of the looped river network.

4.4.4.3 Phosphorus submodel

Determination of the sediment phosphorus excess
A major issue of the phosphorus model is the definition of a reasonable value for the P storage capacity of the sediment expressed by the parameter $r_{p:fe}$. One option is to derive such a value from experimental data. Fig. 4.31 shows the relation between the P:Fe ratio and the rate of P remobilization identified by Jensen et al. (1992a) at values of P:Fe which are comparable to those found in the Havel Lakes.

Based on Fig. 4.31, it is reasonable to assume negligible phosphorus remobilization rates at P:Fe ratios less than $\approx$ 0.025 g P (g Fe)$^{-1}$. However, because of the small number of data, this is a crude estimate only and Fig. 4.31 indicates that P remobilization may also be low at much higher P saturation. In Saxonian reservoirs, Maassen et al. (2005) found a sharp decline in the phosphorus concentration of the pore water at a P:Fe mass ratio of 0.09.

The use of $r_{p:fe}$= 0.025 g P (g Fe)$^{-1}$ is justified by the fact that the phosphorus:iron ratio in the deeper layers of the Havel sediments is somewhat higher than this value (Fig. 4.32). Such a P:Fe ratio slightly above the storage capacity $r_{p:fe}$ can be expected for sediments which were deposited before the period of extensive phosphorus pollution, i.e. when P settling was still low (recall the steady state consideration from Sect. 4.4.3.3). Although the sediment profile data support the presumed magnitude of $r_{p:fe}$, the absolute numerical value remains highly uncertain.

The vertical profile of sediment P can also be interpreted another way: If the P:Fe ratio approaches a $\pm$ constant value in the deep (old) layers of undisturbed core samples, this ratio reflects the historical equilibrium of the sediment with the average pelagic P concentration. Consequently, the amount of P which would potentially be remobilized if P loading was reduced to the historical level can

Table 4.8: *Average concentrations of phosphorus and iron in the uppermost 20 cm of sediment of the sampled Havel Lakes (data for the year 2005 from Knösche, 2006a).*

Lake label from Fig. 4.5	TP ($g\ m^{-3}$)	Fe ($g\ m^{-3}$)	P:Fe ($g\ g^{-1}$)
C	1330	13000	0.103
E	482	4408	0.124
F	543	6706	0.081
G	254	3759	0.076
H	253	4184	0.060

be estimated from the increased P:Fe ratio in the young deposits at the top of the profile. In a similar way, Kleeberg (1995) and Kleeberg & Kozerski (1997) quantified the phosphorus excess in the shallow Lake Müggelsee based on the vertical profile of g P (g DW)$^{-1}$.

Apart from setting the value of $r_{p:fe}$, choosing an appropriate value for the thickness of the active sediment layer z_s (m) is important if the model is applied to a simulation period of several years or decades. After Søndergaard et al. (2003), phosphorus can be remobilized from a depth of up to about 20 cm and this estimate was adopted for the model simulations. The uncertainty of this value is, however, large because it reflects the efficiency of various remobilization mechanisms (see Sect. 4.4.2.2) which may also be highly variable in space.

Because both $r_{p:fe}$ and z_s are sensitive parameters but their values are not well known, it seemed necessary to carry out multiple simulations with both parameters being varied around the estimated values of $r_{p:fe} = 0.025$ g P (g Fe)$^{-1}$ and $z_s = 0.2$ m (see Sect. 4.6.5).

The P excess in the top sediment of the Havel Lakes was estimated from measured P and Fe concentrations (Table 4.8). The initial sediment P concentration at the beginning of the calibration period (1995) was counted back using the values observed in 2005 and average annual net phosphorus export rates as computed from long-term mass balances.

Estimation of further parameters

The four real calibration parameters of the phosphorus submodel are the burial velocity u_{pbur}, the settling velocity u_{pset}, and the parameters k_{prem} and θ_{prem} which control magnitude and timing of P release. A simultaneous calibration of all 4 parameters using the strategy discussed in Sect. 4.4.4.1 was not feasible with respect to the computational effort. Furthermore, the identifiability of all parameters is questionable, given the available observation time series which include only pelagic concentrations but no sediment samples.

Consequently, u_{pbur} was excluded from the calibration and set to a fixed value. Based on sediment growth rates observed in a shallow, hypertrophic Swedish lake (Granéli, 1999) a value of 2 mm a^{-1} was chosen. According to investigations in lakes of Brandenburg (LUA, 2005a) 1 cm slices of sediment core samples integrate the deposits of 2–20 years. The assumed value of 2 mm a^{-1} agrees well with this observation[18].

The remaining three parameters were globally calibrated. Reasonable start values for k_{prem} and θ_{prem} were determined from P-balances of the Havel Lakes (Kneis et al., 2006). An initial guess of the P settling velocity was taken from Bowie et al. (1985). Calibration was carried out using observed data of the period 1995–2000. As with the nitrogen model, data from 2001–2004 were reserved for the purpose of model validation.

It soon became apparent that the settling velocity u_{pset} is barely identifiable given the available observation data. For values of u_{pset} below $\approx$ 0.1 m d^{-1}, the sensitivity of the model was low with respect to any of the computed goodness-of-fit measures. At larger values, the model error increased significantly. Therefore, the parameter u_{pset} was fixed like u_{pbur}. A value of 0.04 m d^{-1} was chosen based on the model performance dur-

[18] For a more reliable estimation of u_{pbur}, cores samples from the Havel should be analyzed for isotopes emitted after the Tschernobyl disaster in future research.

ing winter (Nov-Apr) considering the full period 1995–2004. During summer, u_{pset} was unidentifiable at all because of the compensating effect of P release. The value of 0.04 m d^{-1} is at the lower bound of the data published by Bowie et al. (1985). For shallow, turbulent surface waters a low effective sinking rate is plausible.

Fig. 4.33 shows the response surface of the model with respect to the two remaining free parameters k_{prem} and θ_{prem}. On the one hand, the plot reveals the existence of an optimum parameter set within the range scanned in the simulation. On the other hand, the location of this optimum set obviously depends on the chosen goodness-of-fit criteria.

In addition, the response surfaces do not exhibit steep peaks but a number of parameter sets produced almost equally good results near to the 'best' values, e.g. NSE > 0.69 or MAPE $< 27\%$. The diagonal, ridge-like structure in Fig. 4.33 also shows that a low value of k_{prem} may, to some extent, be compensated by an increased value of θ_{prem} and vice versa. According to the GLUE philosophy (Beven, 2000), a larger number of parameter sets, e.g. those with an efficiency above 0.68, are equally likely. This must be accounted for when the uncertainty of model predictions is assessed (see Sect. 4.6.5).

Based on the maximum quotient of the efficiency and the MAPE obtained, values of k_{prem} = 0.000085 g P m^{-2} d^{-1} (g P excess)$^{-1}$ m^3 and θ_{prem} = 1.35 were selected. Using this set, the sediment P concentrations observed in 2005 were reproduced with a deviation $\leq 14\%$. That is, the simulated cumulative P export from the lakes in 1995–2004 is consistent with the mass balances used for estimating the initial P pool in 1995.

Model performance

The performance of the phosphorus model during the calibration and the validation period is illustrated by Fig. 4.34 and Fig. 4.36. Further goodness-of-fit parameters are listed in Table 4.9.

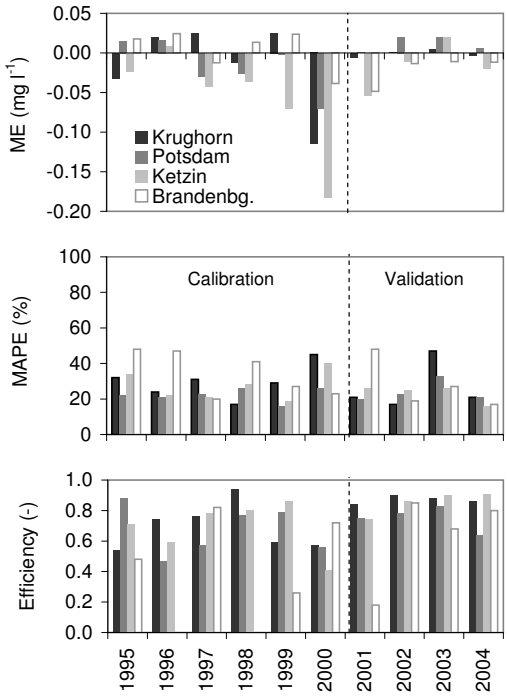

Figure 4.34: *Deviation between simulated and observed TP concentrations during the calibration and validation period (same presentation as in Fig. 4.30).*

With respect to the model efficiency after Nash & Sutcliffe (1970), the phosphorus model performs well and certainly better than the nitrogen retention model. The mean absolute percentage error, however, is larger than for the N model, confirming that a single goodness-of-fit measure is insufficient for assessing the quality of a model. In the present case, the Nash-Sutcliffe efficiency indicates a good fit because the model is able to reproduce the summer peak in the phosphorus concentration. The MAPE, which is less sensitive to the concordance of peaks, weights the error by the absolute values and even small errors are considered severe at low P concentrations.

As in case of the nitrogen model (Fig. 4.30), a better fit was obtained for the validation period than for the period of model calibration. More reliable observation data for recent years might explain this fact.

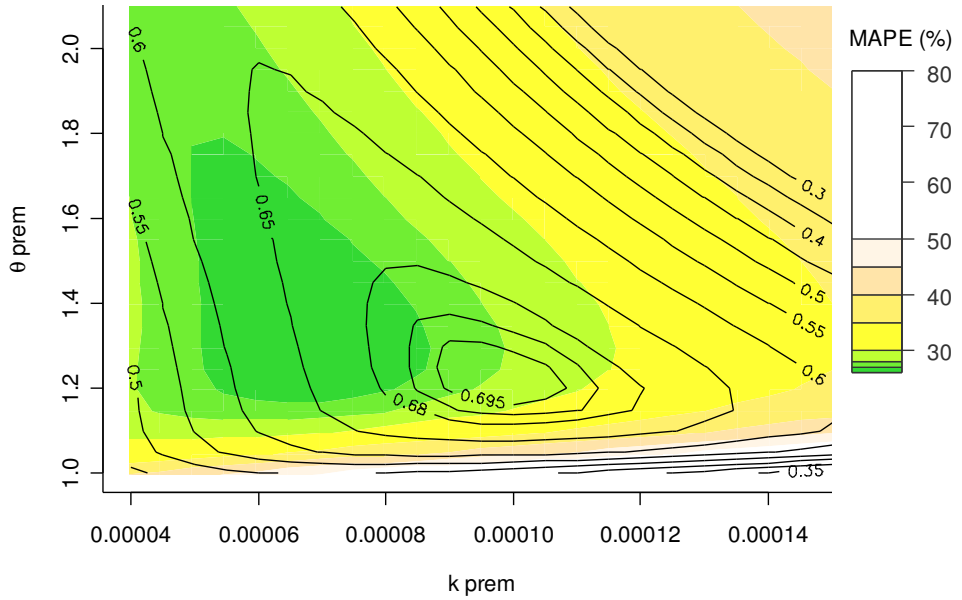

Figure 4.33: *Response surface of the phosphorus model obtained from 529 simulations with k_{prem} in range 0.000040–0.000150 g P m^{-2} surface area d^{-1} (g P excess)$^{-1}$ m^3 sediment and values of θ_{prem} between 1.0 and 2.1. Both parameters were sampled in regular intervals from the corresponding ranges. Contours show the Nash-Sutcliffe efficiency (Eq. 4.34), the mean absolute percentage error (MAPE) is represented by colors.*

Table 4.9: *Performance indicators of the nutrient turnover model at the four monitoring stations from Fig. 4.30 and Fig. 4.34. ME: mean error, MAPE: mean absolute percentage error, NSE: efficiency after Nash & Sutcliffe (1970).*

		Calibration			Validation		
Station	Component	ME (mg l^{-1})	MAPE (%)	NSE (–)	ME (mg l^{-1})	MAPE (%)	NSE (–)
BLN345	TN	-0.20	21	0.45	-0.14	19	0.52
	TP	-0.016	30	0.69	-0.001	26	0.87
Hv0110	TN	-0.29	13	0.33	-0.10	12	0.52
	TP	-0.013	23	0.69	0.011	24	0.78
Hv0195	TN	-0.06	17	0.11	0.10	18	0.59
	TP	-0.048	27	0.68	-0.016	23	0.85
Hv0200	TN	-0.18	21	0.30	-0.03	23	0.37
	TP	0.004	34	0.47	-0.021	28	0.55

The more general sources of simulation errors discussed in conjunction with the nitrogen model (Sect. 4.4.4.2) apply to the phosphorus model too. With respect to the phosphorus model, it is important to recall that the key process – the remobilization of P from sediments – is actually highly variable on different time scales. For example, sediment resuspension during storm events or the depletion of electron acceptors at the sediment-water interface during temporal stratification periods may cause sudden peaks in P remobilization. The model, however, which approximates the seasonality of P release by an empirical temperature function, produces a rather smooth pattern.

An evident example for the large interannual variability in the magnitude of P remobilization is the year 2000 (see Fig. 4.36). In this year, the model dramatically underestimates the phosphorus concentration at all monitoring stations downstream of the Havel Lakes. No significant correlations between the annual residuals and possible control variables such as minimum winter or average summer temperatures, chlorophyll concentrations, etc. could be identified so far.

Finally, one must keep in mind the strong simplification which is due to the approximation of the bottom sediment by a single layer. In reality, most of the sediment parameters are not homogeneously distributed with depth and this is also true for the P:Fe ratio (Fig. 4.32). It is not unlikely that the magnitude of P release is in fact more closely correlated to the P excess at the very top of the sediment rather than to the average excess in a layer of 20 cm thickness. At present, sediment stratification is ignored by the model because processes such as turbation or compaction would need to be simulated otherwise. The corresponding parameters are certainly not identifiable from the available data base.

A quantitative analysis of the uncertainties associated with the phosphorus submodel is presented in Sect. 4.6.5.

4.5 Use of the calibrated model for system analysis

Apart from being used for predicting possible future trends in water quality, the simulation model can also contribute to the understanding of past and present conditions (system analysis). For example, the model allows the retention of N and P to be quantified and seasonal patterns to be evaluated. This can be done in alternative ways:

1. With knowledge of the model's structure, the calibrated parameter values can be interpreted directly.
2. The simulation results of the calibrated model can be compared to those produced by a conservative model, i.e. a model which does not take into account any turnover processes.
3. Finally, the model can be used for calculating mass balances for individual water bodies with high temporal resolution as described in Kneis et al. (2006). In this case, the output of conservative simulations is directly compared with observations, not model results[19].

4.5.1 Significance of phosphorus release

A result of mass balance calculations (third approach from the above list) is shown in Fig. 4.35. Using measured P loads at a lake's inlet, the expected hydrograph of the P load at the lake's outlet was computed, assuming that no retention or remobilization of P would take place (conservative model). The modeled loads at the lake's outlet ($L_{out,sim}$) were then compared with observed values ($L_{out,obs}$) and net export rates (r_{TP}, mg P m^{-2} d^{-1}) were computed according to Eq. 4.37. In this

[19] Note that a direct comparison of observed loads at a lake's inlet and outlet is unsuitable for computing short term mass balances because the residence time of the water is not taken into account.

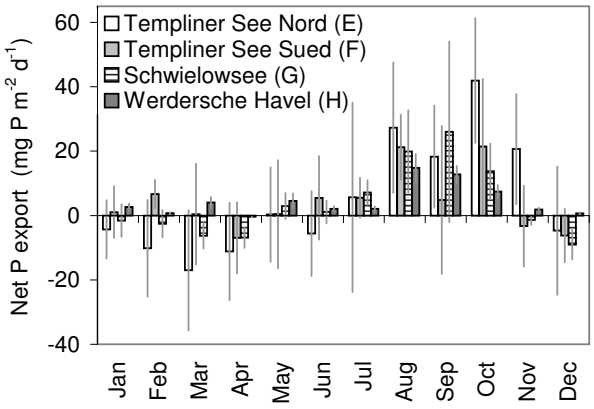

Figure 4.35: *Phosphorus balance of four Havel Lakes during the period 1995–2000. The columns show monthly median values with the 90% confidence interval as whiskers. Lake labels refer to Fig. 4.5.*

context, A (m^2) denotes the lake's sediment surface area.

$$r_{TP} = \frac{86.4 \cdot 10^6}{A} \cdot (L_{out,obs} - L_{out,sim}) \quad (4.37)$$

The near zero or negative values of r_{TP} in winter and early spring indicate that P remobilization is either negligible or it is at least balanced by net phosphorus sedimentation. During the season of increased P remobilization, r_{TP} is greater than zero. According to Fig. 4.35, the rate of sediment P release exceeds the rate of net sedimentation in all of the lakes from July to October. Comparable seasonal patterns and magnitudes of net phosphorus release were reported from Danish lakes (Søndergaard et al., 2002). The fact that r_{TP} is greater than zero when averaged over the whole year clearly indicates that the lakes currently undergo a phase of recovery, i.e. they are loosing P from the sediment.

In Fig. 4.36, the simulation results of the calibrated P model and the output of a conservative model run are presented together with observed data. Summer phosphorus concentrations predicted by the conservative model deviate from the simulation results with consideration of sediment P release by 100% or more. One can conclude that the current P concentrations are increased by this factor compared to a situation with zero P release. This clearly affects not only the studied river section but also downstream waters including several other lakes.

The good agreement between observed and simulated P concentrations during winter, when turnover is less significant, verifies that the system's most relevant boundary conditions have been accounted for. Once more, Fig. 4.36 reveals that a significant part of the observed variance in the TP concentration cannot yet be explained, using the simple model structure described in Sect. 4.4.4.3.

4.5.2 Significance of nitrogen retention

By comparing the simulation results of the calibrated model with the output of a conservative model, the effect of nitrogen retention can be quantified. From Fig. 4.37 it can be deduced that a significant fraction of the total nitrogen which is discharged into the studied river section is subject to retention upstream of the Ketzin gage. For the period 1997–2004 total retention efficiencies of 27% and 28% were identified for the gages Ketzin and Brandenburg, respectively. This results in a significant reduction of the N export to downstream waters. Compared to estimated in-stream retention in a Danish lowland river (Svendsen et al., 1998) nitrogen losses in the Havel River are remarkably high. Since denitrification is most effective at the sediment-water interface (Seitzinger, 1988; Scheffer, 1998), this might be explained by the large surface area of the Havel Lakes.

The identified rates of nitrogen retention were also compared to predictions based on the empirical approach of Behrendt & Opitz (2000). They estimate the quotient of the observed nitrogen load L and the theoretical load due to emissions E using Eq. 4.38

$$\frac{L}{E} = \frac{1}{1 + a \cdot H^b} \quad (4.38)$$

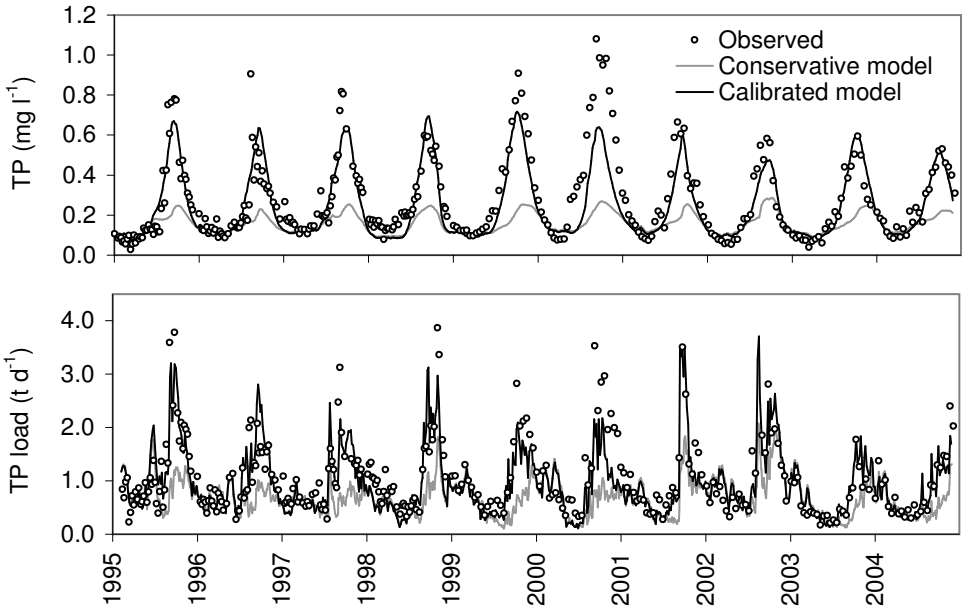

Figure 4.36: *Observed and simulated TP concentrations (mg l^{-1}) and loads (t d^{-1}) at Ketzin (station HV0195 in Fig. 4.5) with and without consideration of phosphorus retention/release.*

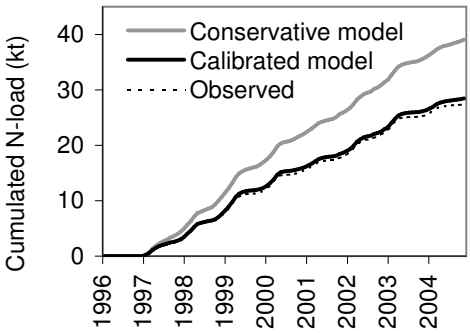

Figure 4.37: *Cumulated load of total nitrogen (kilotons) at Ketzin as computed from observed data and model simulations.*

where a and b are coefficients and H (m a^{-1}) is the hydraulic load. The latter is calculated from the annual runoff (m^3 a^{-1}) divided by the water surface area (m^2). With a reference to the EUROHARP project (Kronvang et al., 2005), Venohr et al. (2003) present values for the empirical coefficients ($a \approx 7.28, b = -1$) applicable to *total* nitrogen retention in lakes. Using the lake area of the studied river section (43 km^2) and a mean flow rate[20] of 30 m^3 s^{-1}, a hydraulic load of $H \approx$ 22 m a^{-1} is obtained. With this figure, Eq. 4.38 predicts a retention efficiency of 25% (L/E=0.75) which is close to values estimated with TRAM.

Apart from showing the magnitude of nitrogen retention, Fig. 4.37 also illustrates that the deviation between simulation and observation is rather small when looking at cumulated TN loads. However, as presented in Sect. 4.4.4.2, the variability in

[20]This estimate is based on the mean flow rate at Ketzin (Table 4.1) taking into account the system's split flow junctions.

TN concentrations is replicated by the model still less accurately.

4.5.3 Visualization of patterns

By merely looking at the time series of nutrient concentrations observed at individual monitoring stations, it is hard to get a holistic impression of the spatial and temporal patterns. Using the calibrated model, these patterns can be visualized in space-time plots like Fig. 4.38. In this case, the model basically serves as an interpolator in space (unmonitored sections) and time (dates between sampling).

A common feature of both panels in Fig. 4.38 are skew structures illustrating the movement of water and nutrients through the system. A particle which enters the system at km 0 at day x passes the downstream model boundary (km 70) at day $x+T$. The dependence of the travel time T on flow rates is reflected by an increased skewness in the diagonal structures during summer and autumn. This is best illustrated by a plot of the characteristics as in Fig. 4.39.

While the temporal fluctuation in the concentrations of TP and TN is high at the system's upstream end (km 0 in Fig. 4.38), the patterns become more smooth in the downstream direction. This is a consequence of dispersion effects in the lakes' large water bodies which are represented in TRAM as completely stirred tanks.

In both panels of Fig. 4.38, a sharp break in the colors at km 18 attracts attention. This steep spatial gradient is caused by the inflow of the Teltowkanal (label 'T'). From the lower panel one can conclude that the Teltowkanal is a major source of nitrogen throughout the year because the concentration strongly increases at it's mouth. A different picture shows up for phosphorus (upper panel). While the P concentration increases downstream of km 18 in spring, there is a significant dilution effect in late summer when the upstream concentrations are elevated due to P remobilization in the lakes of the Berliner Havel.

In contrast to the Teltowkanal, the inflow of the Nuthe River at km 20.5 (label 'N') is of minor relevance only. In the phosphorus plot, one can see a slight increase in the concentrations downstream of the mouth in winter and spring.

Finally, a remarkable temporal shift shows up at km 30 in the phosphorus plot (upper panel). This retardation effect is due to the large residence time of the water in Lake Schwielowsee (recall Fig. 4.7).

The most conspicuous fact about the two panels in Fig. 4.38 is the contrasting temporal pattern of TP and TN concentrations. The peak in the phosphorus concentration appears in late summer due to internal loading and – to a minor extent – because point source emissions are subject to weaker dilution in times of low flow. In the case of nitrogen, the impact of point sources is also pronounced during low flow. This is shown by the peak in TN at km 0 and at the confluence with the Teltowkanal at km 18. However, nitrogen retention results in a significant reduction in summer TN levels downstream of the system's major inflows. The generally higher N concentrations in winter are typical because non-point emissions are highest and retention is lowest during that time.

4.6 Management scenarios

4.6.1 Integration of catchment models and TRAM

During the period of calibration and validation, TRAM was supplied with observed data on flow rates and loads at the system boundaries. These boundary conditions had to be simulated for investigating possible future trends (scenario analysis). For this purpose, the total nutrient loads which enter the system shown in Fig. 4.5 and corresponding flow rates were calculated by the project partners using the hydrological catchment models SWIM (Krysanova et al., 2000) and ArcEGMO-Urban (Biegel et al., 2005). SWIM computes the discharge of tributaries and the corresponding P

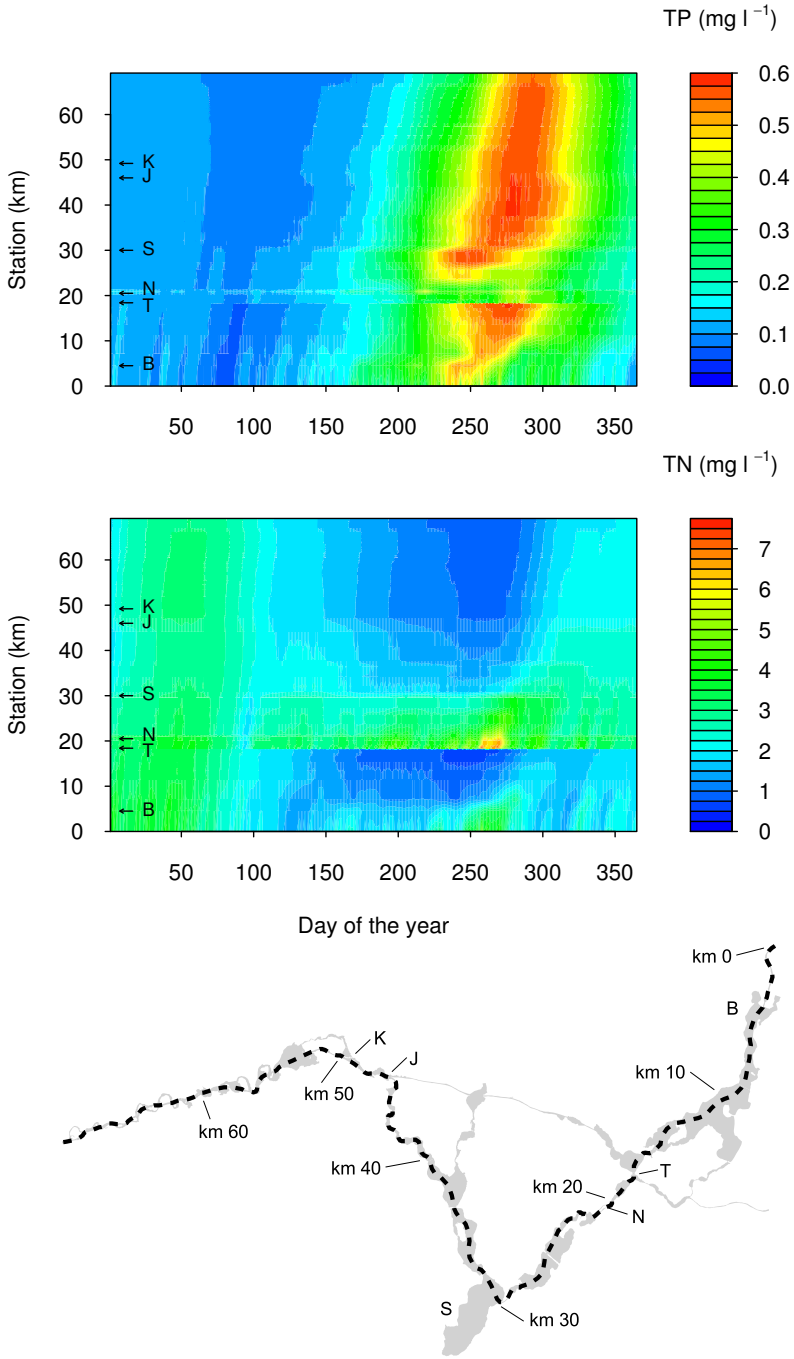

Figure 4.38: *Variation of the concentrations of TP (upper panel) and TN (lower panel) with the season (x-axis) and along a flow path (y-axis). The plots are based on results of the calibrated model for the year 2003 where the simulation matched the observations very well. The selected flow path with major stations is shown in the map below. Label 'B' marks the entry to the lakes of the Berliner Havel, the mouthes of the Teltowkanal and the Nuthe River are labeled 'T' and 'N', respectively. Further labels highlight Lake Schwielowsee ('S'), the confluence with the Sacrow-Paretzer-Kanal at km 47 ('J'), and the Ketzin gage ('K'). See Fig. 4.5 for a more detailed map.*

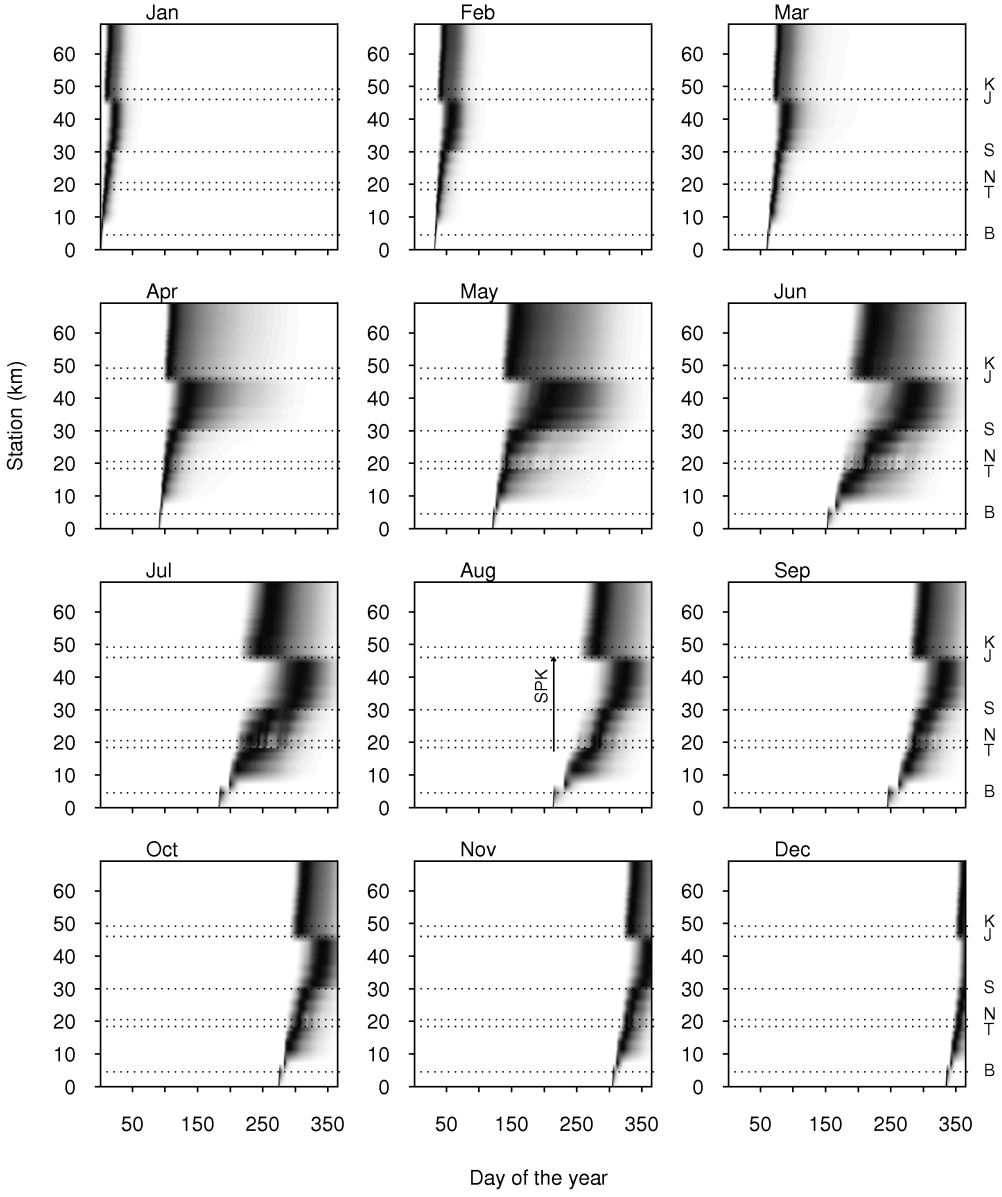

Figure 4.39: *Characteristics illustrating the transport of matter through the river-lake system in the absence of turnover processes. River stations and labels refer to the same flow path as in Fig. 4.38 (see this figure). The plots were produced by simulating the transport of a conservative tracer added at the upstream model boundary (Berlin Spandau) at the first of each month (separate panels). The hydrological boundary conditions correspond to the year 2003 as in Fig. 4.38. In contrast to common plots of characteristics, the spatial distribution of mass is shown for each time step, not only the position of the center of mass. For each river station, concentrations were scaled by the peak concentration at that station in order to eliminate the effect of dilution. The maximum concentration at a station appears in black; white color represents clean water. The arrow labeled 'SPK' indicates the river section which is bypassed by the Sacrow-Paretzer-Kanal (see Fig. 4.5 or 4.38). It is this short cut which causes the conspicuous break in all concentration profiles at km 47.*

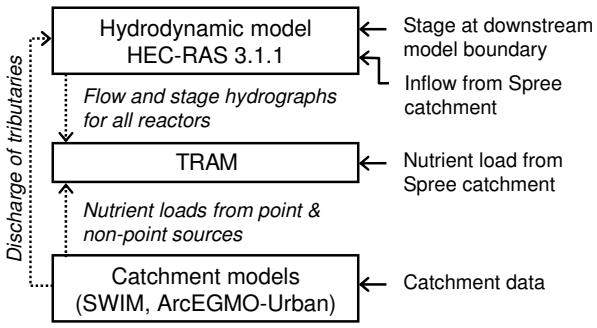

Figure 4.40: *Interaction between the water quality model with the hydrodynamic and catchment model(s). Dotted arrows indicate the exchange of boundary conditions while solid arrows represent external input data.*

Table 4.10: *Average observed nutrient loads (g s^{-1}) in the major tributaries of the Lower Havel River. The evaluated monitoring stations are Sophienwerder (Spree), Henningsdorf (Obere Havel), Kleinmachnow (Teltowkanal) and Potsdam Babelsberg (Nuthe).*

Tributary	Period	TP	TN
Spree	07/94–12/02	3.7	70
Teltowkanal	07/94–12/02	1.9	68
Obere Havel	07/94–12/01	1.4	18
Nuthe	07/94–11/02	1.1	10

and N loads originating from non-point emissions. In contrast, the Urban module of ArcEGMO simulates N and P inputs from point sources only (Biegel, 2005). The interaction between TRAM and the catchment models is illustrated in Fig. 4.40 (see also Table 4.4 on page 72).

For simulating the period 2003–2015, the catchment models were driven by the meteorological boundary conditions of the period 1988–2000, i.e. climate change was not considered in the study.

4.6.2 Runoff and nutrient emissions from non-modeled subcatchments

Since the Spree catchment was not modeled with SWIM or ArcEGMO-Urban, discharge and nutrient loads of the Spree River and the Teltowkanal had to be estimated from other sources (Kneis, 2005). A proper estimation of N and P loads in these two tributaries is essential, as can be concluded from Table 4.10.

For consistency with the other subcatchments, discharges of the Spree River and the Teltowkanal from the period 1988–2000 were extrapolated to the scenario period 2003–2015. The hydrographs were corrected for the predicted negative trend in flow rates which is due to the shut down of open-pit mines in Lusatia (flooding of former mines & reduced drainage) and the operation of newly constructed reservoirs. The relevant trend was derived from predictions of monthly average flow rates in 2003–17 provided by the GLOWA research project (BfG, 2003). Within this period, the effect of climate change underlying the GLOWA simulations is of minor significance only (Rachimow, 2004).

The corresponding loads of phosphorus and nitrogen were estimated using observed load-discharge relationships at the gages Kleinmachnow and Sophienwerder. It was assumed that the observed loads at the two gages reflect both point and non-point emissions. Nutrient loads from diffuse sources are usually correlated with discharge because they are mediated by groundwater exfiltration, (sub)surface stormflow, or drainage. In contrast, nutrient emissions from point sources are expected to be more or less constant. However, a dependence on discharge may appear due to combined sewer overflows or less efficient nutrient elimination in WWTP during winter or storm events. Finally, observed load-discharge correlations at a gage may be influenced by retention and/or remobilization effects. For instance, low flow favors settling and denitrification due to prolonged residence times while particulate P may be remobilized from the river bed at high flow.

The basic equation for computing loads (L) from flow rates (Q) is Eq. 4.39, with L_0 denoting the constant base load from point sources and Q_0 being a discharge threshold above which the effect

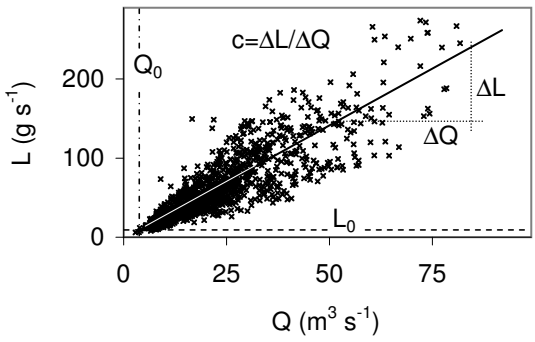

Figure 4.41: *Application of Eq. 4.39 to the relation between total nitrogen loads (L) and discharge (Q) at the Sophienwerder gage (Spree River). In this figure, the model was fitted to the collectivity of data from 1995–2004 for the purpose of illustration. In the actual application, the parameters L_0, Q_0, and c were estimated individually for each month.*

of non-point sources becomes visible. The parameter c represents the slope of the load-discharge relationship for non-point sources. It is identical with the average concentration of diffuse emissions. An application of this type of model is shown in Fig. 4.41. The choice of a linear model was supported by the data sets.

$$L = \begin{cases} L_0 + c \cdot (Q - Q_0) & \text{if } Q > Q_0 \\ L_0 & \text{if } Q \leq Q_0 \end{cases} \quad (4.39)$$

L_0 was estimated from the loads at the smallest observed flow rates (Q_0) at the cited gages. Because the parameter c shows a significant seasonal variation, it was computed separately for each month from observation data of the period 1995/97–2002. It was implicitly assumed that the distribution of Berlin's waste water over the Spree River and the Teltowkanal (including its seasonal modification) remains intact in the future.

4.6.3 Description of the scenarios

4.6.3.1 The base scenario S0

The base scenario called 'S0' assumes that no concerted actions are taken to further reduce nitrogen and phosphorus emissions from point or non-point sources. However, the scenario accounts for some important trends such as a rise in the extent of paved areas as well as the anticipated movement of population from rural to urban areas. The primary aim of this scenario is to approximate the current situation and to provide a basis for inter-scenario comparison.

4.6.3.2 Scenario S1

Scenario 'S1' assumes a reduction in nutrient emissions from all subcatchments modeled with SWIM and ArcEGMO-Urban due to enhanced emission control. This includes the basin of the Upper Havel River, the Nuthe River, minor tributaries downstream of Potsdam, as well as the part of the catchment which drains into the study section via groundwater exfiltration. Potential management actions in the Spree catchment were explicitly excluded in S1, i.e. no enhanced emission control was considered for this part of the river basin.

With respect to point sources, S1 includes the completion of all sewage treatment plants currently under construction as well as upgrades in P elimination techniques to the highest standards in all large and small-scale plants. The corresponding reduction in emissions was calculated by Markus Biegel at IÖR[21] using ArcEGMO's Urban module (Biegel, 2005).

Contrary to phosphorus, the potential for further enhancement of N-elimination in sewage treatment was considered to be insignificant since the officially reported grades of purification are very high already. Thus, the scenario S1 considers further reductions in non-point nitrogen emissions only. In

[21] Institute of Ecological and Regional Development, Dresden

order to simulate this, digital maps of the present land use were reclassified (Jacobs & Jessel, 2003) to reflect a conversion of arable land to grassland and fallow as well as the growing of intercrops in zones with high N losses. The expected reduction in the catchments' N export rates due to the assumed changes in land use was calculated by Anja Habeck at PIK[22] using SWIM.

4.6.3.3 Scenario S2

While management options in the Spree catchment were explicitly neglected in S1, the scenario 'S2' hypothesizes that additional concepts of emission control are also implemented in this part of the river basin. Except for the Spree catchment (see below), the same measures were considered as in S1.

Reduced N exports from the Spree catchment
With respect to nitrogen, it was assumed that non-point emissions from the Spree catchment are reduced similarly to the Nuthe basin. Thus, an equal potential for the application of control measures was assumed. The fundamental equation for computing hydrographs of reduced TN loads in the Spree River and the Teltowkanal under scenario S2 ($L_{tot,S2}$) is Eq. 4.40.

$$L_{tot,S2} = L_{pnt,S0} + L_{dif,S0} \cdot f(mon) \quad (4.40)$$

In Eq. 4.40, $L_{pnt,S0}$ is the hydrograph of the N load due to emissions from point sources under the base scenario and $L_{dif,S0}$ is the corresponding N load attributed to non-point sources. $f(mon)$ represents the average monthly reduction factor of non-point N emissions in the Nuthe catchment obtained from a comparison of the scenarios S1 and S0.

From LUA (2002) information on the average contribution of point and non-point emissions to the total N load is available. Therefore, an advanced approach for determining the unknown fractions $L_{dif,S0}$ and $L_{pnt,S0}$ in Eq. 4.40 from the known hydrograph of the total load $L_{tot,S0}$ can be applied. The basis of this approach is given by Eq. 4.41–Eq. 4.43.

$$L_{tot,S0} = L_{pnt,S0} + L_{dif,S0} \quad (4.41)$$
$$L_{pnt,S0} = L_0 + (L_{tot,S0} - L_0) \cdot k \quad (4.42)$$
$$L_{dif,S0} = (L_{tot,S0} - L_0) \cdot (1 - k) \quad (4.43)$$

Eq. 4.41 simply represents the mass balance. Eq. 4.42 & Eq. 4.43 state that loads above a constant base value L_0 are a linear combination of point and non-point loads. The constant load L_0 was set equal to the N load observed at low flow and the factor k was determined by optimization in order to bring the long-term average proportion of point and non-point sources into agreement with the values reported by LUA (2002).

Reduced P exports from the Spree catchment
The assumed reduction of phosphorus loads in the Spree River and the Teltowkanal is based on a quality target proposed by Senat (2001). According to this management plan, an average concentration of $\approx 80\ \mu$g TP l^{-1} during the vegetation period could represent the 'good status' with respect to phosphorus in the Berlin river system. This value takes into account a natural background P level as well as the morphological characteristics of the Spree-Havel system. Simulations carried out with the MONERIS model (Senat, 2001) support that this target could be achieved if concerted actions were taken. Such actions would need to be focused on a reduction of point source emissions due to enhanced P elimination in sewage treatment – especially in Berlin – and the connection of all households to WWTP. According to the MONERIS simulations, the P emissions from soil erosion and surface runoff are of minor importance, and the potential for further reduction is therefore low. In terms of P loads, a reduction to about 44 % of the current level would be required in order to meet the above mentioned quality target.

For the Spree River and the Teltowkanal, hydrographs of the reduced total P loads $L_{tot,S2}$ were

[22] Potsdam Institute of Climate Impact Research

derived from the hydrographs of the base scenario S0 using Eq. 4.44. In this context $L_{tot,S0}$ is the hydrograph of the total P load in the base scenario S0 and $L_{pnt,S0}$ is the fraction of $L_{tot,S0}$ which is attributed to point source emissions (base load; see L_0 in Eq. 4.39). According to Eq. 4.44, the proportional reduction in the base load (factor 0.44) equals the desired relative reduction in total annual emissions. The parameter k describes the reduction in P loads which exceed the base load. k was determined by optimization with the objective being an average P concentration of 80 μg l^{-1} during April-September (quality target). The values found for k are close to the reduction factor of 0.44 applied to the base load.

$$L_{tot,S0} = 0.44 \cdot L_{pnt,S0} + (L_{tot,S0} - L_{pnt,S0}) \cdot k \tag{4.44}$$

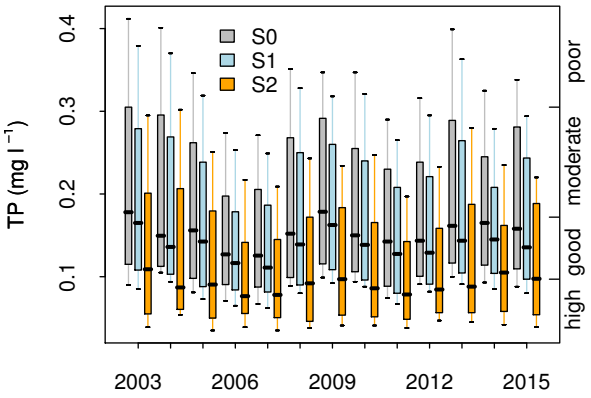

Figure 4.42: *Simulated TP concentrations at the Ketzin gage (see Fig. 4.5) for the management scenarios S0–S2 grouped by years. The box represents the interquartile range with the median value and the full range is shown by whiskers. The classes at the right plot margin refer to the assessment scale from LUA (2005a) but note this scale uses annual (arithmetic) mean values which are not shown.*

4.6.4 Simulation results

4.6.4.1 Phosphorus

Fig. 4.42 displays the statistics of the computed TP concentrations at Ketzin for the 13 simulation years. The results for scenario S1 differ not very much from the base scenario S0 but a pronounced reduction of the TP level was predicted for scenario S2. This can be attributed to the substantial contribution of the Spree catchment to total P loading on the one hand (see Table 4.10) and the assumed drastic decrease in loads on the other hand (Sect. 4.6.2).

When looking at a single scenario, for example S0, Fig. 4.42 indicates a significant variability between years which is clear evidence for the strong dependence of nutrient levels on the hydrological conditions. The highest interannual differences appear in the upper quartiles and maximum values. This fact corroborates that phosphorus concentrations in summer are particularly sensitive to flow variability.

The increased variability in P concentrations in summer as compared to winter times can also be seen in Fig. 4.43. Furthermore, Fig. 4.43 reveals that the proportional change in P levels from scenario S0 to S2 is much greater in winter and spring than in summer, when internal loading strongly controls the phosphorus concentration.

According to the assessment scale from LUA (2005a) presented in Table 4.2, the phosphorus level in the base scenario can be classified as moderate–good. Under scenario S1, the good status is reached in 8 of the 15 simulated years and under scenario S2 the criterion is fulfilled in every single year (see Fig. 4.44).

However, Fig. 4.42 and Fig. 4.43 show that a clear cut classification is difficult because of the large interannual and seasonal variability. Fig. 4.43 gives a good impression how representative the annual mean value of the total phosphorus concentration actually is. From this point of view, an assessment scale which is not built on the annual average alone but takes into account distribution information (e.g. quantiles) would permit a more reliable classification.

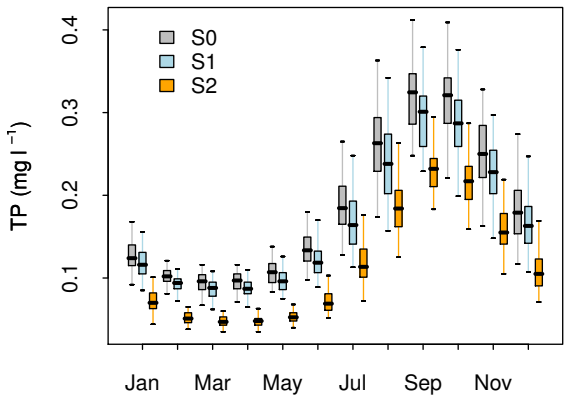

Figure 4.43: *Seasonality of the simulated TP concentration at the Ketzin gage for the three management scenarios S0–S2.*

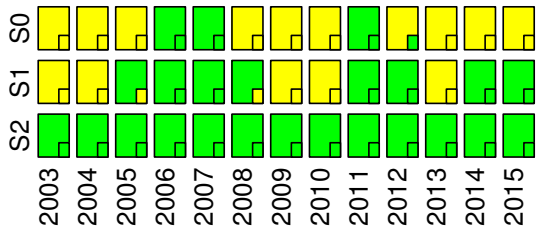

Figure 4.44: *Application of the water quality assessment scale from LUA (2005a) to the simulated phosphorus concentration at Ketzin for scenario S0, S1, and S2 in 2003–2015. In accordance with the WFD convention, green color indicates the targeted 'good status' while yellow stands for 'moderate'. The small inset rectangles show the status which results from applying the scale to the average TP concentration during the vegetation period (April–September) rather than to the annual average.*

The results presented so far all refer to the single station Ketzin located downstream of the Havel Lakes. However, the reduction in phosphorus concentrations is spatially variable as shown by the maps in Fig. 4.45. For example, the change in the TP concentration at Ketzin under scenario S1 (upper map) is almost exclusively attributed to reduced phosphorus loads in the Nuthe River. The lower map shows a very different situation for scenario S2. Here, the assumed reduction in P loads in the Teltowkanal and the Spree River explains most of the changes observed at Ketzin.

4.6.4.2 Nitrogen

Fig. 4.46 and Fig. 4.47 present the statistics of the simulated TN concentration at Ketzin for the three scenarios. The absolute reduction in the TN level from scenario S0 to S2 appears to be somewhat larger than twice the decrease predicted for S1. For both scenarios a greater impact was predicted during winter where the median concentration changes by about 0.2 and 0.5 mg l^{-1} for S1 and S2, in comparison to the base scenario S0. During summer, the predicted changes drop to about 0.1 and 0.2 mg l^{-1} for scenario S1 and S2, respectively.

These seasonal differences primarily result from the significant share of non-point emissions in total N loading. During low flow in summer, the proportional impact of this type of emission declines in favor of point source pollution. The significance of diffuse N sources can also be gathered from the large interannual variability shown in Fig. 4.46 which is greater than the corresponding variability in phosphorus concentrations (Fig. 4.42).

As with phosphorus, the predicted proportional decline in the average N concentration is spatially variable. As indicated by the upper map in Fig. 4.48, the simulated shift in the concentration at Ketzin under scenario S1 (Fig. 4.46 & Fig. 4.47) is mainly caused by reduced nitrogen loads in the Nuthe and the Upper Havel River. In scenario S2, the impact of scenario S1 is superimposed by the

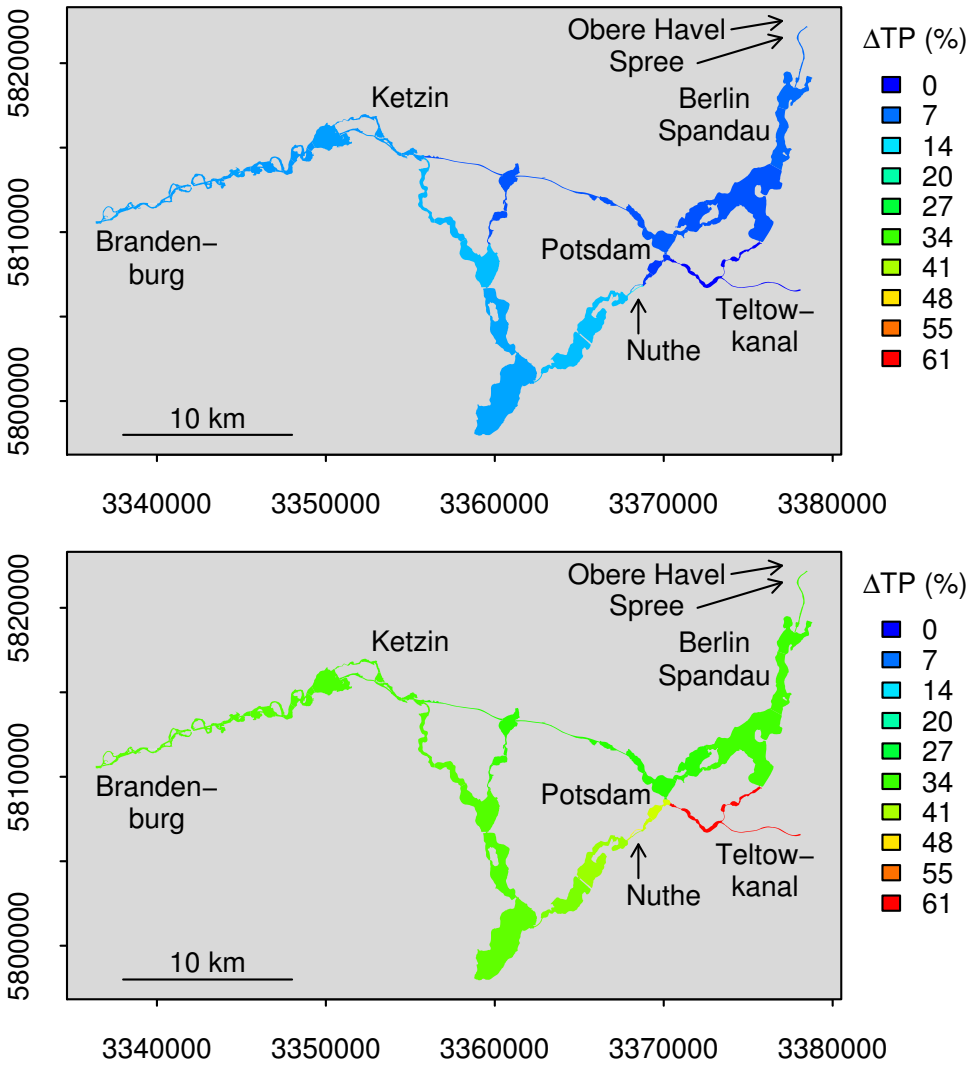

Figure 4.45: *Simulated proportional reduction of the TP level during the vegetation period (Mai–Sep; average over 2003–2015) for scenario S1 (upper panel) and S2 (lower panel) compared to the base scenario S0.*

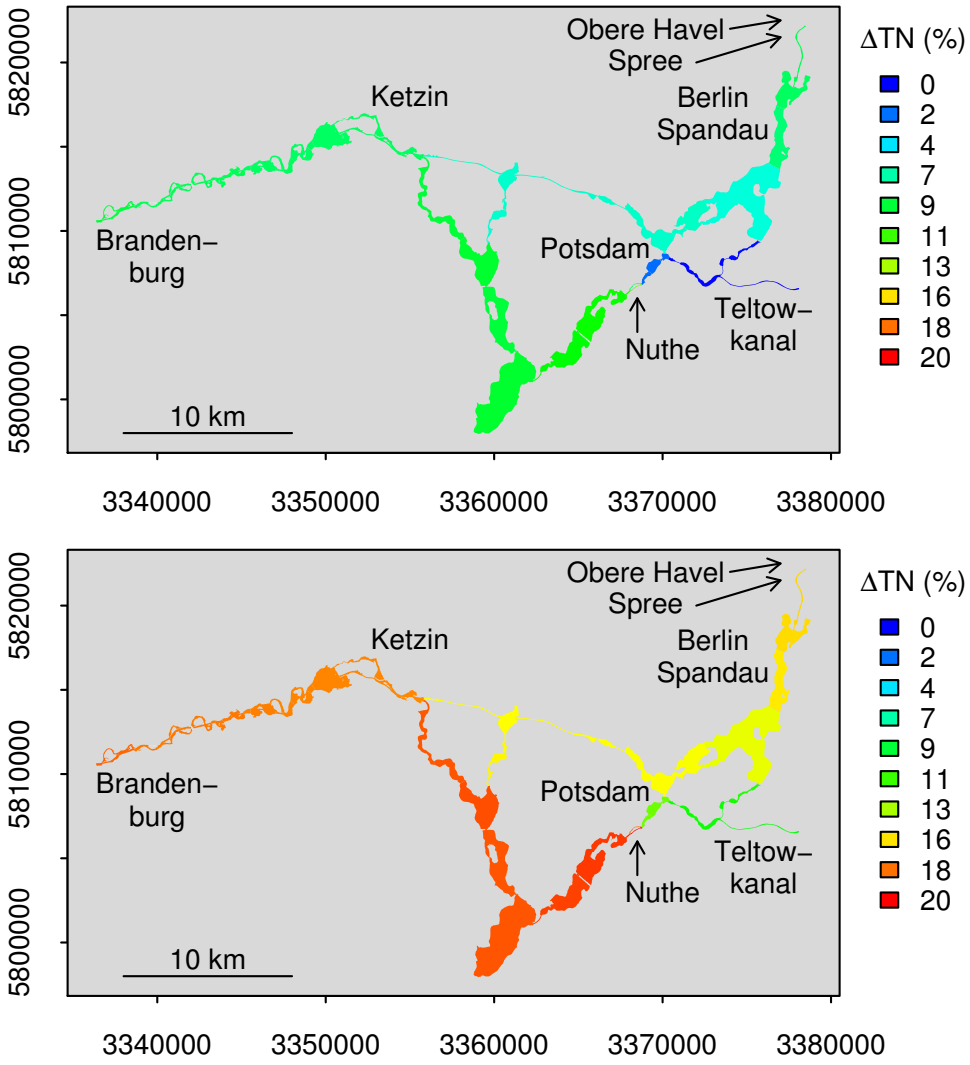

Figure 4.48: *Simulated proportional reduction of the TN level during the vegetation period (Mai–Sep; average over 2003–2015) for scenario S1 (upper panel) and S2 (lower panel) compared to the base scenario S0.*

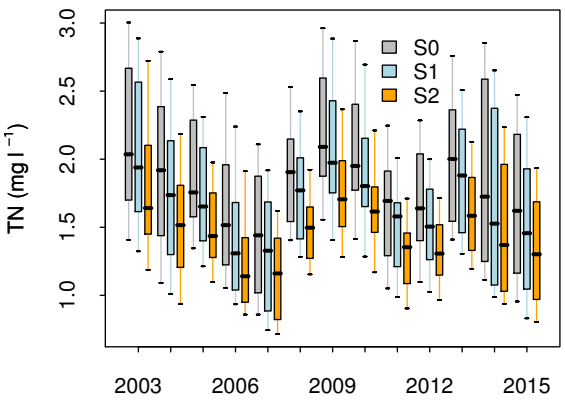

Figure 4.46: *Simulated TN concentrations at the Ketzin gage (see Fig. 4.5) for the management scenarios S0–S2 grouped by years. The box represents the interquartile range with the median as horizontal line. The full data range is shown by whiskers.*

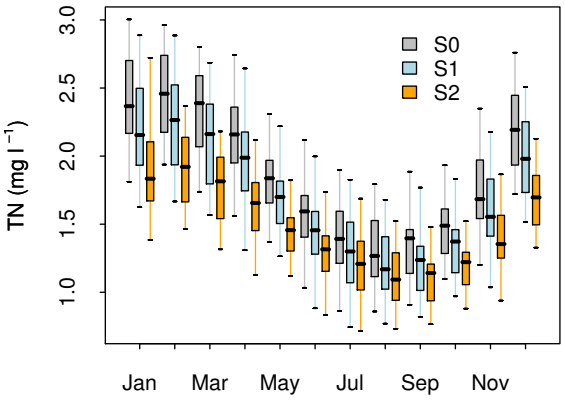

Figure 4.47: *Seasonality of the simulated TN concentration at the Ketzin gage for the three management scenarios S0–S2.*

assumed reduction of nitrogen emissions from the Spree catchment (Spree and Teltowkanal).

An assessment of the simulation results which is conformal with the requirements of the Water Framework Directive cannot be presented so far. As opposed to phosphorus, a well founded assessment scale for nitrogen concentrations in the Lower Havel River does not yet exist. The approach of deriving a scale for nitrogen from that for phosphorus (Table 4.2) using a critical N:P ratio (Kneis, 2005), was not adopted because the latter is merely a pragmatic and makeshift solution.

4.6.5 Uncertainty of predictions

If any inferences are to be drawn from the results of the scenario simulations presented in Sect. 4.6.4 one must keep at least two things in mind:

First, the scenarios are subject to certain *assumptions* with respect to the reduction in nutrient emissions from different sources and subcatchments (Sect. 4.6.3). The *scenarios* must therefore not be confused with actual *predictions* of the future.

Second, the results of model simulations are always associated with *uncertainties*. These uncertainties are the focus of the following sections.

4.6.5.1 Potential sources of errors

In the case of the model study presented, different sources of uncertainties can be distinguished. Some of them were already addressed in Sect. 4.4.4.2 and Sect. 4.4.4.3 but a more systematic overview shall be given hereafter.

Model structure

In any model, only a subset of the state variables and interactions existing in nature can be represented. Even those most relevant processes which the model takes into account are usually implemented in a greatly simplified, conceptual manner. The degree of simplification depends on many factors such as the understanding of interactions, the required accuracy, and the solvability of equations.

It also depends on the spatial and temporal scales which determine data availability and the computational effort.

In the application-oriented water quality model presented here, the structural simplification is far-reaching. It starts with the use of the reactor concept (Sect. 3.1.1) which circumvents the need for solving the full transport equations. The chosen water quality submodels presented in Sect. 4.4 imply even stronger abstractions of reality because the complexity of ecosystems is far beyond that of purely physical systems.

It is supposed that structural errors are the primary reason for uncertainties in water quality simulations. An analysis of structural uncertainties would require a number of alternative model formulations to be compared. With respect to the application presented here, this is impractical for two reasons: Firstly, the information content of observation data is limited insomuch (fortnightly surface water samples, sediment conditions at a single date) that the goodness of alternative and more complex model approaches cannot be assessed. Secondly, the effort for calibrating multiple nutrient turnover models of different structure was too high to be undertaken in this work. Consequently, any simulation results must not be viewed independently from the given model structure.

Initial values of state variables

TRAM requires initial concentrations of the simulated components to be specified and, in general, spatially interpolated observation data are used. In the case of mobile components, the errors resulting from improper measurement or interpolation fades during the simulation when the initial water is replaced or mixes with new incoming water. Measurement and interpolation errors may become severe in systems with long residence times or if, as was done here, sediment components are simulated. With respect to the phosphorus submodel described in Sect. 4.4.3.3, errors in the initial P and Fe contents assigned to the lakes' sediments influence the model results during the whole simulation period.

Observation data used in calibration

Apart from being used as initial conditions, observation data are required for model calibration.

During calibration, the model is driven by measured boundary conditions such as discharges and loads, with the latter being generated from observed concentrations interpolated in time. In rivers with large cross-section areas, flow measurements are not very accurate but the larger uncertainty usually results from interpolation of infrequently measured concentrations. In lowland rivers like the Havel, the problem is less severe because the short-scale variability in flow and concentrations is small.

Furthermore, observed concentrations at monitoring stations are used for assessing the goodness of the simulation. Errors in the data result in distorted optimum values for the calibration parameters. In the case of the applied nutrient models, measurement errors may, for example, result from spatial heterogeneity at the sampling site (surface blooms of algae, drift of organic sediment near the bottom) or incomplete pulping of samples. The latter is a common problem when analyzing *total* nutrient concentrations.

Simulated boundary conditions

During scenario simulations, TRAM's boundary conditions were adopted from hydrological catchment models rather than from observation data. Of course, the simulation results of SWIM and ArcEGMO-Urban are uncertain too, e.g. due to structural errors or inaccurate meteorological input. Finally, the hydrographs of stage and flow which drive the mass transport through TRAM's network of reactors are also subject to errors, depending on the quality of the hydrodynamic model simulations.

A comprehensive analysis of uncertainties would need all the errors in the connected models to be taken into account. At present, this is impossible since sufficient information on the uncer-

tainty of catchment modeling results is not available.

Parameter values
The water quality modeling approaches presented in Sect. 4.4.3 contain a number of parameters with different theoretical foundation. For example, the dimensionless temperature correction parameters θ_{TN} and θ_{prem} can only be determined by calibration since measurement in the field is impossible. Similarly, the nitrogen retention rate k_{TN} cannot be directly measured as it lumps the effects of different processes. How reliably an optimum value for a calibration parameter can be identified depends on many factors such as it's sensitivity as well as the amount and variance of observation data. It also depends on whether a shift in the parameter's value can be compensated by adjustment of another parameter. As exemplified in Fig. 4.34 even sensitive model parameters are not necessarily well identifiable and different parameter sets yield a similar goodness-of-fit.

As described in Sect. 4.4.4.3, other parameters of the phosphorus model such as the thickness of the active sediment layer z_s or the critical phosphorus to iron ratio $r_{P:Fe}$ were excluded from calibration and estimates were taken from the literature. Even though the adopted values were identified on similar waters, uncertainty remains whether a transfer from one system to another is actually permissible.

Numerical accuracy
Last but not least, the precision of simulation models is generally limited if numerical methods are involved. In TRAM, numerical imprecisions may appear in numerical integration (Sect. 3.5.2). Since the system of ODE resulting from the chosen nitrogen and phosphorus turnover models presented in Sect. 4.4.3.2 and Sect. 4.4.3.3 is simple and the processes do not act on very different time scales, even the Runge-Kutta solver yields a sufficient accuracy.

4.6.5.2 Objectives of the analysis

For a proper view on the results presented in Sect. 4.6.4 it is essential to know how reliable the quantitative model output actually is. Because it is not practically feasible to analyze all the above mentioned possible sources of errors, the following restrictions apply:

1. Only the uncertainty in parameter values and initial conditions is inspected. The focus is on those parameters which turned out to be particularly sensitive during model calibration.
2. The analysis is limited to the phosphorus submodel presented in Sect. 4.4.3.3.
3. The influence of uncertain parameters and initial conditions is analyzed for scenario S0 and S2 only (see Sect. 4.6.3).

The following Sect. 4.6.5.3 addresses the specification of reasonable ranges to be considered for each input parameter or variable.

Subsequently, Sect. 4.6.5.4 aims at figuring out how the simulation results for scenario S0 change if parameters and initial values are sampled from the outer bounds of the conceivable ranges. This is done by a classical *sensitivity analysis* with only a single parameter being altered at a time. The simulation results obtained with modified parameter values are compared to those being produced with the unmodified or 'standard' values.

Finally, Sect. 4.6.5.5 investigates how the simulation results for scenario S0 and S2 would change if the combined uncertainties in the model's input parameters were taken into account.

4.6.5.3 Considered parameters and ranges

Sediment phosphorus and iron content
While the iron content of the sediment is a constant model parameter, the sediment P concentration is a dynamically simulated variable for which initial values must be supplied. In Sect. 4.4.4.3 it

was described how the average Fe and P concentrations in the upper sediment of the Havel Lakes were derived from core samples. Because only 2–4 cores are available for each lake, the uncertainty in the computed averages is high. The impact on modeling results can be assessed if simulations are carried out with each lake's P and Fe concentration in the sediment being set to the upper or lower bounds of the 90% confidence intervals of the respective mean values.

The application of this straightforward approach is hindered by the small number of 2–4 cores per lake which does not permit a reliable estimation of confidence intervals. Fortunately, closely correlated sediment parameters such as the acid-soluble phosphorus and iron concentration (P_{as}, Fe_{as}) were measured at a greater number of locations (4–14 sites for each lake at 0–3 and 3–6 cm depth). For these data, lake mean values $(\overline{P_{as}}, \overline{Fe_{as}})$ and the associated lower and upper bounds of the 90% confidence interval were calculated, using a bootstrap technique (Crawley, 2002)[23]. Then, the width of the lower and upper confidence interval relative to the mean (D_L,D_U) was computed according to Eq. 4.45– Eq. 4.48.

$$D_L(\overline{P_{as}}) = \frac{\overline{P_{as}} - L(\overline{P_{as}})}{\overline{P_{as}}} \tag{4.45}$$

$$D_U(\overline{P_{as}}) = \frac{U(\overline{P_{as}}) - \overline{P_{as}}}{\overline{P_{as}}} \tag{4.46}$$

$$D_L(\overline{Fe_{as}}) = \frac{\overline{Fe_{as}} - L(\overline{Fe_{as}})}{\overline{Fe_{as}}} \tag{4.47}$$

$$D_U(\overline{Fe_{as}}) = \frac{U(\overline{Fe_{as}}) - \overline{Fe_{as}}}{\overline{Fe_{as}}} \tag{4.48}$$

where $L(\ )$ and $U(\ )$ represent the lower and upper limits of the 90% confidence intervals of its arguments. The obtained values are shown in Table 4.11.

[23] Non-parametric estimates of the confidence limits were determined as the empirical 0.05 and 0.95 quantiles of the distribution of mean values obtained from 10000 bootstrap replicates.

Table 4.11: *Width of the lower and upper 90% confidence interval for the mean value of P_{as} and Fe_{as} normalized by the corresponding means $\overline{P_{as}}$ and $\overline{Fe_{as}}$ (Eq. 4.45–Eq. 4.48). See Fig. 4.5 for lake labels.*

	$\overline{P_{as}}$		$\overline{Fe_{as}}$	
Lake label	D_L	D_U	D_L	D_U
E	0.17	0.18	0.10	0.11
F	0.13	0.14	0.08	0.09
G	0.22	0.22	0.15	0.20
H	0.10	0.10	0.10	0.14
Average	0.15	0.16	0.11	0.13

Under the assumption that the observed ratios D_L and D_U also hold for the data of interest, i.e. the total concentrations of P and Fe in the upper 20 cm of sediment, the range for the mean values $\overline{PS}$ and $\overline{Fe}$ at a probability level of 90% can be estimated from Eq. 4.49–Eq. 4.52.

$$L(\overline{PS}) \approx \overline{PS} - \overline{PS} \cdot D_L(\overline{P_{as}}) \tag{4.49}$$

$$U(\overline{PS}) \approx \overline{PS} + \overline{PS} \cdot D_U(\overline{P_{as}}) \tag{4.50}$$

$$L(\overline{Fe}) \approx \overline{Fe} - \overline{Fe} \cdot D_L(\overline{Fe_{as}}) \tag{4.51}$$

$$U(\overline{Fe}) \approx \overline{Fe} + \overline{Fe} \cdot D_U(\overline{Fe_{as}}) \tag{4.52}$$

The obtained values for $L(\overline{PS})$, $U(\overline{PS})$, $L(\overline{Fe})$, and $U(\overline{Fe})$ represent the lower and upper estimates of $\overline{PS}$ and $\overline{Fe}$ at p= 0.9 which can be used in the uncertainty analysis. Combining the upper estimate of $\overline{PS}$ with the lower estimate of $\overline{Fe}$ (or vice versa) assumes that the errors in both P and Fe data are independent. Since P and Fe are in fact correlated (see Fig. 4.49), the above mentioned combinations represent extreme cases with probabilities of about $1/4\%$.

Thickness of the 'active' sediment layer

The thickness of the active sediment layer contributing to P export cannot be estimated from available data on the investigated system and a vague literature value of 0.2 m had to be adopted. In order to figure out the sensitivity of simulation results, z_s was altered by ± 10 cm, i.e. values

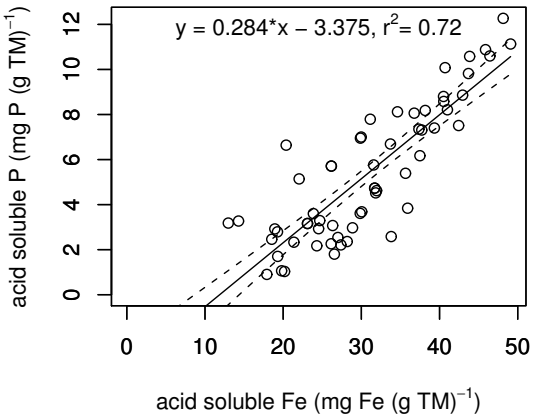

Figure 4.49: *Correlation of acid soluble iron (Fe_{as}) and phosphorus (P_{as}) in the Havel sediments. The 90% confidence interval of the regression is shown as dotted line.*

of 0.1 and 0.3 m were tested. The choice of a much larger value has little effect as the phosphorus excess in the sediment declines with increasing depth (Fig. 4.32). A much smaller value seems unlikely as numerical experiments with a 1D diffusion model[24] have shown.

Threshold P:Fe ratio

The threshold phosphorus to iron ratio is another highly uncertain parameter. The sensitivity of the model to altered values of $r_{p:fe}$ directly follows from its structure (Sect. 4.4.4.3). The assumed standard value of 0.025 (mass ratio) was varied by $\pm$0.015. The lower estimate of 0.01 is near to the value found by Maassen et al. (2005) and much higher values seem unlikely according to Fig. 4.31.

Effective settling velocity

For the scenario simulations, a standard value of u_{pset}= 0.04 m d^{-1} was used (Sect. 4.4.4.3). For assessing the impact of increased or lowered settling of phosphorus, simulations with u_{pset}= 0.02 and 0.1 m d^{-1} were carried out. Higher values were not tested because the model performance during the calibration period deteriorated significantly.

Phosphorus release parameters

As shown in Fig. 4.33, a number of parameter sets (k_{prem}, θ_{prem}) fitted the observed P concentrations in the calibration period equally well. The GLUE philosophy (Beven, 1993, 2000) suggests carrying out a simulation with each parameter set unless it is classified as 'unbehavioral'[25]. By interpreting the goodness-of-fit for each parameter set as a measure of its likelihood, a quasi-distribution function can be obtained from which – similar to confidence intervals – uncertainty estimates can be derived. Although the GLUE method does not yield probabilities in a strict sense, it provides a simple and transparent framework for (non-parametric) uncertainty estimation.

In order to make the uncertainty in the values of k_{prem} and θ_{prem} accessible with minimum computational effort, simulations were carried out with four selected parameter sets only. These sets were selected based on Fig. 4.50. The four combinations of k_{prem} and θ_{prem} represent the intersections of the border of 'zone 1' with the major axes of an imagined ellipse. That is, one set combines low values of k_{prem} and θ_{prem}, a second set assumes large values for both parameters and the two other sets combine small and large values. All four sets are equally likely with respect to their associated goodness-of-fit.

A summary of the test values for the parameters z_s, $r_{p:fe}$, and u_{pset} is given in Table 4.12.

4.6.5.4 Sensitivity of individual parameters

Fig. 4.51 displays the proportional change in the simulation results for scenario S0 that results from modifying the parameters u_{pset}, z_s, $r_{P:Fe}$ and the initial sediment concentrations of P and Fe individually. For each model configuration with altered

[24] A simple explicit finite-difference solution of Fick's second law was implemented in a spreadsheet program. Only molecular diffusion was considered.

[25] The term 'unbehavioral model' is used for parameter combinations that yield a low goodness-of-fit, e.g. efficiencies below zero or some positive threshold.

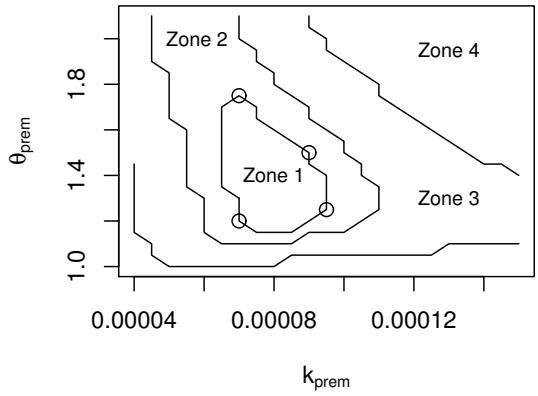

Figure 4.50: *Reclassified response surface of the phosphorus model with respect to the parameters k_{prem} and θ_{prem}. Zone 1: $E > 0.95 \cdot max(E)$ & $M < 1.05 \cdot min(M)$, Zone 2: $E > 0.9 \cdot max(E)$ & $M < 1.1 \cdot min(M)$, Zone 3: $E > 0.75 \cdot max(E)$ & $M < 1.25 \cdot min(M)$, Zone 4: remaining sets. In this definition, E is the Nash-Sutcliffe efficiency, M is the mean absolute percentage error, and min & max are the lowest & highest observed values for the two goodness-of-fit measures. The locations of the four selected parameter sets are marked by circles.*

parameters or initial values, the two main calibration parameters k_{prem} and θ_{prem} were fitted anew.

Since only a single parameter was altered at a time, the sensitivity of results with respect to that particular parameter can be assessed. By comparing the individual sensitivities, it can be figured out what additional information is required in order to reduce the uncertainties most effectively.

According to Fig. 4.51, the simulation results are most sensitive to an increase in the phosphorus settling velocity (u_{pset}, uppermost panel) and altered values of the sediment's phosphorus binding capacity related to iron ($r_{P:Fe}$, third panel from the top). In the case of modified values for u_{pset}, the 10% percentile is most affected (low concentrations in winter and spring). In contrast, changes in those parameters and variables which control the P remobilization from sediments primarily affect the 90% percentile (late summer concentrations).

As Fig. 4.51 shows, the sensitivity of results is not equal for all years of the simulation period because of the variability in flow dynamics. Furthermore, the deviation between the simulated concentrations obtained with standard and modified values for z_s, $r_{P:Fe}$, and the initial P and Fe levels increases with time. This is because these parameters basically control the quantity of the sediment phosphorus excess. If the P excess is assumed to be larger (high z_s, low $r_{P:Fe}$, high initial P:Fe ratio), its reduction takes more time and the rate of P remobilization declines more slowly. In contrast, if the sediment phosphorus excess is assumed to be lower, the simulated P concentrations decline faster. Therefore, the deviations in the statistics turn more and more negative for a lowered value of z_s, an increased $r_{P:Fe}$, or a low initial P:Fe ratio.

Fig. 4.52 illustrates how the predicted P concentrations under scenario S0 would change, if the simulations were carried out with near-optimum sets of k_{prem} and θ_{prem} (see Fig. 4.50) instead of the true best-fit parameter set. Like z_s and $r_{P:Fe}$ in Fig. 4.51, the parameters k_{prem} and θ_{prem} act on the magnitude of phosphorus release in summer. Hence, a modification of the values primarily causes a shift in the simulated 90% percentile while the 0.1 quantile is much less affected.

While the sensitivity of simulation results against altered values of z_s and $r_{P:Fe}$ or initial P and Fe concentrations increased over the simulation period (Fig. 4.51) an opposite trend is observed if k_{prem} or θ_{prem} are modified (Fig. 4.52). This can be explained by the significant decline in the sediment's P excess over time, causing the impact of P release on the concentrations to fade more and more. Consequently, the sensitivity of the controlling parameters k_{prem} and θ_{prem} must decrease too.

According to Fig. 4.52, the change in the simulation results is largest if the values for k_{prem} and θ_{prem} are both increased or lowered simultaneously. This is a result of parameter compensa-

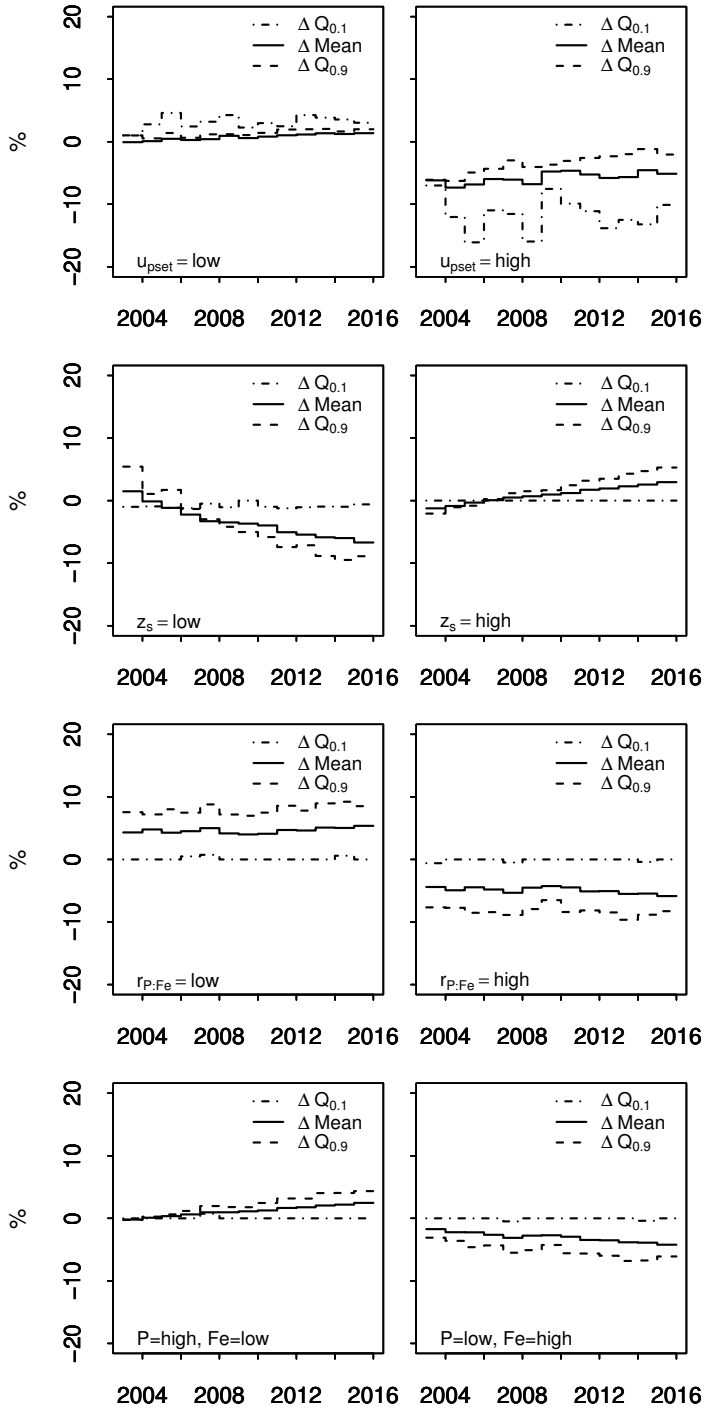

Figure 4.51: *Proportional change in the annual mean values and quantiles (α= 0.1 & 0.9) of the simulated P concentration at Ketzin under scenario S0 for upper and lower estimates of selected model input data. The change in the statistics is given as $100 \cdot (P^* - P)/P$ where P^* is the statistics of the model output produced with the upper/lower estimates and P is the statistics of the model output produced with standard values. u_{pset}: effective settling velocity of P (standard= 0.04, low= 0.02, high= 0.1 m d^{-1}), z_s: thickness of the active sediment layer (standard= 0.2, low= 0.1, high= 0.3 m), $r_{P:Fe}$: P binding capacity of the sediment depending on the iron content (standard= 0.025, low= 0.01, high= 0.04 g P (g Fe)$^{-1}$), P & Fe: Initial phosphorus and iron content of the individual lakes' sediments (standard= observed mean values, low/high= lower/upper limits of the 90% confidence interval of the mean).*

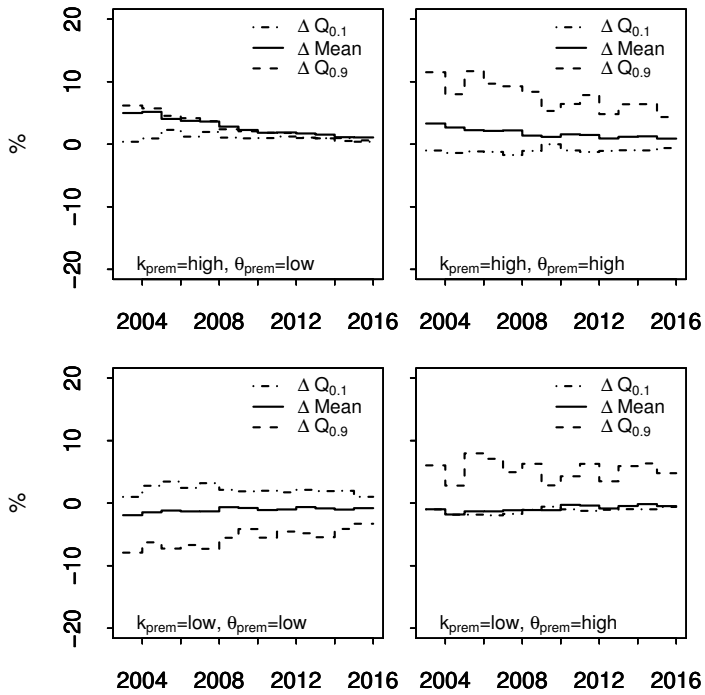

Figure 4.52: *Proportional change in the annual mean values and quantiles (α= 0.1 & 0.9) of the simulated P concentration at Ketzin under scenario S0 for different combinations of the calibration parameters k_{prem} and θ_{prem} (presentation like in Fig. 4.51).*

tion. For example, the effect of an increased value of k_{prem} can be compensated by a lower θ_{prem} as indicated by the upper left chart in Fig. 4.52. If both k_{prem} and θ_{prem} take high or low values at the same time, no compensation is possible.

4.6.5.5 Effects of multiple altered parameters

In the above Sect. 4.6.5.4, the sensitivity of simulation results with respect to a single parameter or variable was discussed. For actually assessing the reliability of the model predictions, it is necessary to consider the effect of combined uncertainties in the model's input data. There are two common options to do so:

One option would be 'best-case' and 'worst-case' simulations. For example, the parameters z_s and $r_{P:Fe}$ as well as the initial P:Fe ratio could be chosen in such a way as to produce a minimum (or maximum) initial sediment phosphorus excess. Herewith, the most extreme model results which are possible within the limits of the parameter ranges (see Sect. 4.6.5.3) could be obtained. While the method is attractive for it requires only two simulations, its benefit is limited because it does not provide information on how likely or unlikely the 'best' or the 'worst' case actually is.

The second option is to carry out a large number of simulations in order to cover many (or all) possible combinations of the parameter values. The extreme cases mentioned above are included then, but the majority of cases will be less 'extreme'. Using the GLUE approach mentioned in Sect. 4.6.5.3, a likelihood can be assigned to each of the simulation results. Though the method does not yield actual probabilities, the GLUE output permits a transparent identification of more likely and very unlikely results. Therefore, this second option was preferred.

Since no useful information on the distribution of the uncertain parameters is available, no random sampling was performed as in classical Monte Carlo simulations. Instead, three different values were tested for the parameters z_s, $r_{p:fe}$, and u_{pset}:

Table 4.12: *Distinct parameter values used in the uncertainty estimation. The units are g P m^{-2} surface area d^{-1} (g P excess)$^{-1}$ m^3 sediment for k_{prem}, m s^{-1} for u_{pset} and meters for z_s. The mass ratio $r_{P:Fe}$ and θ_{prem} are both dimensionless. The standard values are in the middle row.*

k_{prem}	θ_{prem}	u_{pset}	$r_{P:Fe}$	z_s
0.00007	1.2	0.02	0.01	0.1
0.00008	1.4	0.04	0.025	0.2
0.00009	1.75	0.10	0.04	0.3

the standard as well as the lower and upper estimate derived in Sect. 4.6.5.3 and used in Fig. 4.51. Similarly, three values where chosen for k_{prem} and θ_{prem} so that the range shown in Fig. 4.52 is covered. The values for all parameters are listed in Table 4.12. The initial P:Fe ratio in the sediment was left out of the analysis because of its small effect on results (Fig. 4.51) and for reducing the computational effort. All together, 243 (3^5) simulations had to be carried out for determining the model performance for each parameter set during the calibration period. Another 2×243 simulations were carried out for the period 2003–2015 with the boundary conditions of scenario S0 and S2, respectively[26].

Fig. 4.53 presents the outcome of the uncertainty estimation with respect to the annual average phosphorus concentrations at Ketzin for the scenarios S0 and S2. The figures were produced using the following algorithm:

1. For each of the 243 different parameter sets, the Nash-Sutcliffe efficiency (NSE; Eq. 4.34) was determined for the calibration period. For each run, NSE was rescaled to the interval [0,1] in order to yield the likelihood according to the GLUE approach. Rescaling simply meant dividing each model's efficiency by the sum of the 243 efficiencies. Before doing so, efficiencies below a certain positive threshold

[26] A single model run (88 reactors, 13 years) took about 200 seconds on a 2 GHz machine.

are usually set to zero ('unbehavioral' models). In this application, none of the models was classified unbehavioral. The computed values of NSE were generally >0.3.

2. In a second step, the annual average TP concentrations at Ketzin were determined for the scenario period 2003–2015, again using the 243 different parameter sets.
3. For all years in 2003–2015, the 243 simulated mean annual TP concentrations were sorted in ascending order and the associated likelihoods (determined in step 1) were accumulated, starting at the lowest mean value. From the obtained empirical quasi-distribution function[27], the 'GLUE confidence limits' shown in Fig. 4.53 were derived by interpolation.

The width of the confidence limits displayed in Fig. 4.53 illustrates the accuracy with which the annual average P concentrations at Ketzin can be predicted. The 50% GLUE confidence range has a span of about 20–30 μg l^{-1} and the spread of the 90% range is about 0.5 mg l^{-1}. However, the uncertainty about the exact mean values does not change the outcome of the scenario analysis presented in Sect. 4.6.4. According to Fig. 4.53, the quality status with respect to phosphorus is still classified as 'moderate' with a tendency to 'good' for scenario S0 and the good status is clearly achieved under scenario S2.

Retrospectively, the GLUE method appears to be a useful approach for assessing the reliability of the modeling results. One should, however, keep in mind that only parameter uncertainties were analyzed and that the model's structure was left untouched.

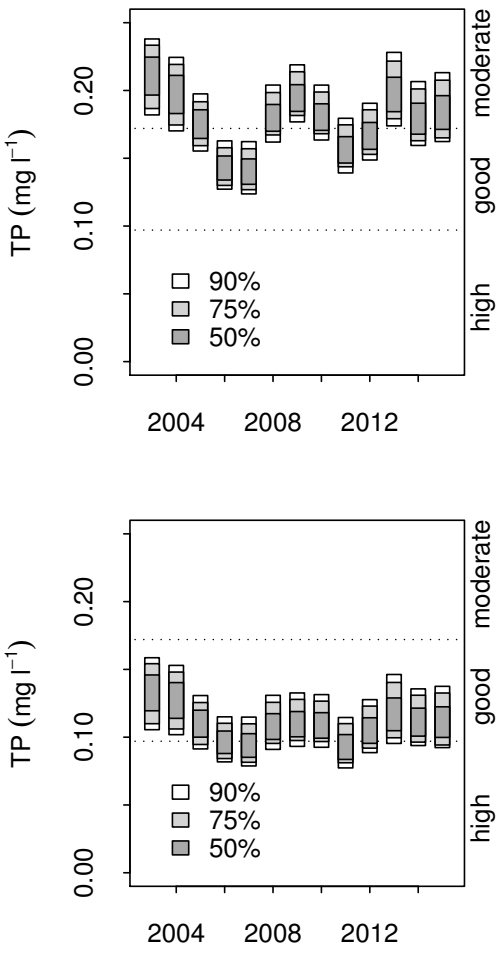

Figure 4.53: *Estimated uncertainty of the simulated P concentrations for scenario S0 (upper chart) and S2 (lower chart) at the Ketzin gage. The boxes indicate the 'GLUE confidence limits' for the annual mean values at likelihood levels of 50, 75, and 90%. It is important to realize that these are not confidence limits in a strict sense but just plausability ranges derived from the model performance. The water quality classes at the right margin refer to Table 4.2.*

[27] A true distribution function is built on non-exceedence probabilities while only likelihoods are available here.

Chapter 5

Summary and conclusions

In this chapter, the essential experiences and results of model development (Chapter 3) and application (Chapter 4) are summarized and conclusions are drawn. Apart from reviewing successfully applied concepts, the need for improved model approaches, process identification, and data collection is pointed out.

5.1 Model design

Representation of water bodies
The fundamental reason for developing TRAM was the need for a more detailed representation of individual water bodies in river basin modeling. In spite of the higher degree of detail, the new model had to be applicable to river networks of some ten to hundred kilometers of length.

By representing the actual river network as a series of coupled advective or dispersive reactors (Sect. 3.1), this fundamental target was achieved. The reactor approach proved to be a good compromise between accuracy and computational efficiency for simulations at larger spatial and temporal scales. In a future revision of TRAM, the introduction of a third type of reactor should be considered which allows for the simulation of stratification events in lakes (see Sect. 3.8).

In the presented study, TRAM was applied to a system which is not a typical river but a network of interlinked lakes and channels. In order to verify the model's applicability to a more typical river case, TRAM was also set up for a 4 km section of the Nuthe River (MQ = 2.5 m^3 s^{-1}, width $\approx$ 10 m, bed slope = 0.26‰). The study section was represented by 20 coupled plug-flow reactors using channel geometry data collected in 2003 (Hickisch & Kneis, 2004). The results of test simulations carried out with the classical Streeter-Phelps oxygen balance model were in agreement with analytical solutions and proved the transferability of the transport simulation approach (unpublished study by the author).

Open model structure
The creation of an efficient open-structure simulation environment was another major aim in the development of TRAM. With a division of the source code into a static kernel and a dynamic part, a satisfying solution to this objective was found (see Sect. 3.3.3.2). The generation of the dynamic part of the code from a user-contributed problem definition permits different turnover models to be set up and tested with little effort and without actual programing. In the development of the nitrogen and phosphorus turnover model for the Havel River, the approach taken proved to be reliable and convenient. The open-structure architecture facilitated the test of alternative model formulations with different complexity.

In the end, rather simple simulation approaches had to be selected due to a lack of data for model parametrization and validation (Sect. 4.4.3). However, even for the rejected, more complex turnover

models, the TRAM executable achieved a good performance.

The automatic verification of mass balances for each of the simulated components (Sect. 3.6.5.3) proved to be a valuable method for checking the consistency of the user-supplied turnover model.

Use of geographical information systems

The use of GIS facilities proved to be essential for efficient pre- and postprocessing of spatial data and the coupling of TRAM to the hydrodynamic model. The use of spatially referenced information also facilitated data analysis and visualization. The linkage between TRAM and open source GIS systems should be improved further in order to make model building and data analysis even more convenient.

5.2 Implications for water quality management of the Havel River

5.2.1 Significance of internal nutrient turnover

The results of mass balance analyses (Sect. 4.5) proved the large quantitative significance of internal nutrient turnover in the Havel River. The anticipated strong influence of P remobilization from lake sediments on the pelagic phosphorus concentrations was confirmed. Average daily net remobilization rates of about 20 mg P m^{-2} were identified during the seasonal climax in late summer.

Furthermore, the studied section of the Havel River was shown to be an important nitrogen sink. According to modeling results, nearly 30% of the external nitrogen input is retained in the river-lake system. Denitrification at the sediment-water interface is believed to explain most of the nitrogen losses.

In the development of strategies for eutrophication control, the observed turnover rates of N and P must be taken into account. Due to internal turnover, a reduction in external loading does not necessarily result in an immediate proportional decline in the water bodies' nutrient concentrations. Moreover, the effectiveness of management measures becomes seasonally variable.

For example, the possible reduction in the phosphorus level of the Havel River is severely limited by internal P loading. At present, even a drastic decline in the external input could not promote phosphorus limitation of primary production during summer.

In contrast to that, the self purification effect of nitrogen retention can be regarded as an ecosystem service which buffers the impact of high external N loads. Nitrogen retention was shown to be most effective during the summer period.

5.2.2 Implications of simulated medium-term scenarios

Three scenarios with different external nutrient loading were examined in Sect. 4.6. No further reduction in loading was assumed for the base scenario S0. The scenarios S1 and S2 considered different reductions in nitrogen and phosphorus emissions according to catchment modeling results and/or water quality targets. Whereas enhanced emission control in the Spree catchment was neglected in scenario S1, it was taken into account in scenario S2.

For drawing proper conclusions from the scenario simulations, the structure of the nutrient turnover model (Sect. 4.4.3) and possible uncertainties (Sect. 4.6.5) should be kept in mind. In addition, one should be informed about the underlying boundary conditions which were discussed in Sect. 4.6.2 & 4.6.3.

Nitrogen

According to simulation results, the reduction in the average nitrogen concentration during the vegetation period is 10% at maximum for scenario S1 and 20% for S2, compared to the base scenario S0. The highest reductions were predicted for the lakes of the Potsdamer Havel which receive significant N

loads from the polluted Teltowkanal. In absolute figures, the simulated decline in the summer concentration at Ketzin is only modest, with approximate values of 0.1 and 0.2 mg l^{-1} TN for scenario S1 and S2, respectively.

With respect to water quality management, even such modest reductions in nitrogen levels may be welcome, because temporary N limitation – if actually existent – would be intensified. Nevertheless, management actions focusing on nitrogen alone may not lead to *sustainable* success as long as phosphorus levels remain high. According to many studies (see e.g. Smith, 1983; Havens et al., 2003) intensified nitrogen shortage could favor the dominance of N fixing species of cyanobacteria which is certainly not desired. For two lakes in the lower course of the nearby Nieplitz River, which suffer from high internal P loading like the Havel River, significant nitrogen fixation is suspected (unpublished data analysis by the author). Furthermore, the release of phosphorus from sediments might be enhanced if the availability of nitrate as oxidizing agent is reduced (Benndorf, 2006; Schauser et al., 2006).

Nitrogen fixation as well as the 'nitrate effect' mentioned are not taken into account by the nutrient turnover model chosen for this study.

Phosphorus

On the one hand, the simulated phosphorus concentrations reflect the assumptions on external P loading associated with the scenarios S0, S1, and S2 (see Sect. 4.6.3). On the other hand, the model results are influenced by the decrease in the sediment phosphorus excess over the simulation period and the corresponding decline in internal loading.

As long as the options for emission control in the Spree catchment are neglected (scenario S1), only a minor reduction in the phosphorus concentration of the Havel River is predicted. At the monitoring station Ketzin, the decline in the annual average TP concentration amounts to 17 μg l^{-1} or 9% as compared to the base scenario S0. Under scenario S2, which assumes a drastic reduction in P export from the Spree catchment, the predicted change in the annual average TP level is ≈ 70 μg l^{-1} or 37%.

Based on the assessment scale developed by LUA (2005a), the quality status of the Havel River with respect to phosphorus is 'moderate' under the conditions of the base scenario S0. According to the model simulations, a quality status between 'moderate' and 'good' might be achieved by implementing the management actions considered in scenario S1. For scenario S2, the model predicts annual average TP concentrations which are generally below 172 μg l^{-1}. Hence, the conditions for the targeted 'good status' with respect to phosphorus are fulfilled in scenario S2.

As the analysis of the model sensitivity (Sect. 4.6.5) revealed, a medium-term prediction of phosphorus concentrations in the Havel River is associated with considerable uncertainties. However, even when parameter uncertainties are taken into account, the general conclusion remains the same: The state of the Havel River still classifies as 'moderate' for the base scenario S0 and as 'good' for scenario S2.

Synopsis

According to modeling results, the gain from reduced external phosphorus loading will be counteracted by internal loading until and beyond 2015, which is the deadline for achieving the 'good status' in the first cycle of the WFD. Although the impact of P release from sediments is likely to ease off noticeably within the next two decades, drastic measures of emission control in the whole river basin will be required in order to meet the targets of the Water Framework Directive.

In the short term, efforts to further reduce nitrogen loads are likely to be more effective for re-establishing nutrient limitation of primary production than a moderate decrease in the phosphorus input. The clearly preferred strategy, however, aims at simultaneously reducing the emissions of both nutrients.

5.3 Challenges for future research

Substantial further research is required if the quantitative results of this investigation are to become more precise and less uncertain. The following paragraphs present some focal points which should be addressed by future research.

5.3.1 Catchment modeling

For scenario simulations, the N and P loads at the system's upstream boundaries were taken from different sources (see Sect. 4.6.3). For a number of sub-basins, nitrogen and phosphorus export rates were simulated by the catchment models SWIM and ArcEGMO-Urban. For the large Spree catchment, however, load hydrographs for the scenario period had to be generated from observed data and quality targets, or extrapolation from other catchments (Sect. 4.6.2 & 4.6.3). A more consistent study would require catchment models to be applied to the total river basin, not only to selected sub-basins.

It is known that the output of eco-hydrological catchment models is still highly uncertain due to structural uncertainties and insufficient data for calibration and validation. With respect to phosphorus, this was demonstrated by Guse (2006). In the catchment model SWIM, the representation of runoff generation and nutrient transport mechanisms might need to be revised in order to improve its applicability to lowland river basins. According to the author's knowledge, leaching of P from saturated soil profiles and subsequent groundwater transport, nutrient release from degraded peat soils, artificial drainage, as well as retention effects are still under-represented.

Finally, the impact of climate change was left unconsidered in the present investigation. On the one hand, this is an advantage since it facilitates the interpretation of modeling results. On the other hand, changes in climatological boundary conditions could significantly affect nutrient emissions from the catchment (runoff processes) as well as nutrient turnover in the Havel River (change in residence times at altered flow rates). In future research, possible effects of climate change should be taken into account.

5.3.2 Classification of the ecological status

For a proper evaluation of management scenarios in the sense of the Water Framework Directive, a reliable assessment scale is required which accounts for the natural conditions of the river or lake. The scale developed for total phosphorus (LUA, 2005a) is certainly an important milestone. However, considering the pronounced seasonal dynamics of the phosphorus concentration in the Havel River, it seems questionable whether the annual average concentration is a suitable criterion for classification. The use of quantiles or alternative statistics with a focus on the vegetation period is proposed instead. A similar assessment scale for nitrogen (or N and P combined) still needs to be developed in order to allow for the evaluation of simulated nitrogen concentrations.

After all, the Water Framework Directive has its focus on the *ecological* status and nutrient levels are just surrogate parameters. An improved water quality assessment in the sense of the WFD requires both assessment scales *and* models to be enhanced in the future.

5.3.3 Simulation of nutrient turnover in rivers and lakes

Concerning the functionality of TRAM, a number of potential improvements were identified in Sect. 3.8. However, with respect to the application to the Lower Havel River, the greatest need for improvement is related to the chosen description of turnover processes, rather than to TRAM's basic features. The subsequent paragraphs point out which parameters need to be determined more precisely and which process descriptions should be refined most urgently. Suggestions of how this could be achieved in practice are provided.

Estimation of model parameters

If the present structure of the nutrient turnover model (Sect. 4.4.3) was maintained, it would be important to improve the identification of those parameter values which govern the retention and release of phosphorus in shallow lakes. As the analysis in Sect. 4.6.5.4 revealed, there is no single most sensitive parameter but better information on many items, such as the iron-specific P storage capacity $r_{P:Fe}$, the thickness of the active sediment layer z_s, or the magnitude of phosphorus settling and recycling is required. For a better identification of these parameters, field research, lab experiments, and modeling need to be combined.

An interesting attempt was made by Knösche (2006a) who conducted long-term phosphorus leaching experiments on sediment samples in a continuous flow system. If such experiments were carried out for a larger number of samples with different characteristics (e.g. contents of iron, calcite, and organic matter), the knowledge of the sediment's P storage capacity and the associated remobilization rates could be improved.

A promising method for getting better information on the thickness of the sediment layer contributing to P remobilization would be the continuous observation of vertical pore water profiles using dialysis samplers (e.g. Lewandowski et al., 2002). More reliable data on the magnitude of phosphorus settling and possibly resuspension could be obtained using state-of-the-art sediment traps (Kozerski & Leuschner, 1999). The installation of such equipment in the Havel Lakes is complicated by intensive recreational use, fishery, and navigation. Maintenance of the equipment and the analysis of samples is also costly. However, a broadened data base is indispensable for improving the reliability of simulation results!

Revision of the chosen turnover model

If the spatial transferability of the turnover model for N and P is to be improved or scenario simulations with more dramatically altered boundary conditions are required, better information on parameter values is not enough. Instead, a major revision of the structure of the nutrient turnover model would become necessary. The focus of such a revision must be on a more process-oriented description of the mass dynamics in the pelagic zone and in the bottom sediments. This includes a better representation of the coupling between the aquatic N and P cycle.

With respect to the turnover of nutrients in the pelagic zone, the implementation of a rather complex nutrient-algae model (NA-model) appears essential. Only NA-models allow the particulate organic N- and P-fractions to be simulated, which is a precondition for a reliable estimation of nutrient settling rates. Information on settling rates is required for quantifying N and P retention as well as for computing supply and degradation of fresh organic material at the sediment surface. Proper estimates of the degradation activity in the top sediment are again essential for simulating the exchange of nutrients between the benthic and the pelagic zone. The remobilization of both N and P as well as denitrification are linked to microbial activity directly (release of mineralized nutrients) and indirectly (pH, redox milieu).

Furthermore, NA-models are not limited to the simulation of nutrients. They offer the chance to directly compute those variables which are relevant for assessing water quality, e.g. chlorophyll concentrations. If different functional groups of phytoplankton were distinguished in the model, information on their proportions could be explicitly taken into account in the evaluation of the ecological status according to the WFD. Finally, a NA-model which considers different functional groups of algae is required for simulating nitrogen fixation by selected blue-green algae and the general pattern of the seasonal succession of the plankton.

The suitability of TRAM for implementing nutrient-algae models was proven by a test study on the Potsdamer Havel Lakes (lake E–H in Fig. 4.5). The basic equations were adopted from the WASP model (Ambrose et al., 2001). They were extended for taking into account a variable

stoichiometry of the phytoplankton with respect to N and P according to the Droop-model (Sommer, 1991). The complete model requires the specification of nearly 40 parameter values which were mostly taken from the literature (e.g. Bowie et al., 1985). Though test simulations were successful, a serious application to the Havel River turned out to be impossible as long as no specific field campaigns for data collection are carried out. Nevertheless, the simulation experiments confirmed TRAM's ability to cope with complex turnover models.

It is obvious that a nutrient-algae model also depends on a detailed description of turnover processes in the upper sediment (see subsequent paragraphs). Furthermore, the application of NA-models in the context of river basin management requires significant progress in the field of catchment modeling. Instead of computing the export of total nitrogen and phosphorus only, catchment models must be enabled to supply much more detailed boundary conditions including information on dissolved and particulate as well as organic and inorganic N and P fractions.

In order to achieve a more process-based description of nutrient turnover in the bottom sediments, the approach taken needs to be improved in several ways. First of all, it seems necessary to take into account vertical gradients in physical properties and concentrations instead of treating the sediment as a single homogeneous layer. With the current version of TRAM, multiple sediment layers can already be simulated for stirred tank reactors. However, for a convenient, numerically more exact description of stratified sediments, the use of a 1D finite difference advection-diffusion approach should be considered.

A proper representation of phosphorus retention and release mechanisms requires better information on the importance of different P fractions in the Havel sediments (see Sect. 4.4.2) and their stability under variable pH, redox, and temperature conditions. This is a precondition for modeling seasonal changes in the pore water concentrations. Information on pore water concentrations of dissolved nutrients again forms the basis of a process-based simulation of sediment phosphorus release and nitrogen recycling. In addition, a better understanding of the non-diffusive remobilization mechanisms discussed in Sect. 4.4.2.2 is believed to be essential for a more realistic modeling of the sediment nutrient dynamics.

Last but not least, special attention should be paid to the role of the oxidizing agent nitrate in the control of phosphorus release (Andrusch et al., 1992; Jensen & Andersen, 1992; Benndorf, 2005; Petzoldt & Uhlmann, 2006; Schauser et al., 2006). A better understanding of the advantages and possible drawbacks of high nitrate supply could be of great practical value for water quality management.

5.4 Final remarks

Well-founded predictions of an aquatic system's behavior under modified boundary conditions can only be achieved by the use of process-oriented simulation models. On the one hand, such models require huge amounts of data with high spatial and temporal resolution for parametrization and validation. On the other hand, the models themselves can be used for identifying which data need to be collected to further reduce the uncertainty of predictions.

However, in the absence of sufficient observation data, the use of very complex models may be counterproductive, as advantages of the sophisticated model structure are outweighed by parameter uncertainties. It is believed that water quality simulations for spatially large systems with scarce data should start with simple engineering models. Such models are transparent by nature, the residuals are easily interpretable, and their fast execution permits extensive uncertainty analyses to be carried out. As more information on processes and param-

eters becomes available, the modeling approaches can be gradually refined.

The simulation tool developed and used in this study allows for the creation of both simple engineering models as well as sophisticated ecosystem models with many variables and interactions. It offers the chance of adapting the model's complexity to the amount and quality of available data and knowledge. This is necessary when preliminary answers to urgent questions of management are required. Due to the open-structure approach, simulation models built with TRAM are, by design, open for continuous improvement.

List of Figures

List of Tables

Bibliography

Ambrose, R. B. J., Wool, T. A., Martin, J. L., Shanahan, P. & Alam, M. M. (2001): WASP - Water quality analysis simulation program, Version 5.2-MDEP, Model documentation, Environmental Research Laboratory & AScI Corporation, Athens, Georgia.

Andrusch, T., Hupfer, M. & Luther, D. (1992): Chemical and microbial binding forms of phosphorus considering the availability of nitrate in sediment-water systems, *Int. Revue. ges. Hydrobiol.*, 77 (1): 109–120.

Becker, A. (2006): pers. comm., German Federal Water Institute.

Begon, M., Harper, J. & Townsend, C. (1996): Ecology: Individuals, populations and communities, Blackwell scientific publications.

Behrendt, H. & Mischke, U. (2002): Entwicklung und Erprobung eines Konzeptes für ein Bewertungssystem zum Merkmalskomplex Phytoplankton in Berliner und Brandenburger Fließgewässern - Überarbeiteter Endbericht, Report, Institut für Geässerökologie und Binnenfischerei (IGB), im Auftrag des Senats Berlin, als pdf vorhanden.

Behrendt, H. & Opitz, D. (1996): Güteklassenbezogene Zielvorgaben zur Nährstoffreduzierung im Berliner Gewässersystem, *IGB-Mitteilungen*, 1: 27–92.

Behrendt, H. & Opitz, D. (2000): Retention of nutrients in river systems: Dependence on specific runoff and hydraulic load, *Hydrobiologia*, 410: 111–122.

Benndorf, J. (2005): Ecotechnology: basis of a new immission concept in water pollution control, *Water science and technology*, 52 (5): 17–24.

Benndorf, J. (2006): pers. comm., Head of limnology section at Dresden Technical University.

Beven, K. (1993): Prophecy, reality and uncertainty in distributed hydrological modelling, *Advances in Water Resources*, 16: 41–51.

Beven, K. (2000): Rainfall-runoff modelling, The primer, Wiley & Sons.

BfG (Ed.) (2002): Mathematisch-numerische Modelle in der Wasserwirtschaft, Handlungsempfehlung für Forschungs- und Entwicklungsarbeiten, *BfG Mitteilungen*, vol. 24, Bundesanstalt für Gewässerkunde.

BfG (2003): GLOWA Elbe I, Schlussbericht zur Teilaufgabe 2.3 "Ballungsraum Berlin/Untere Havel", BfG-Bericht Nr. 1398, Report, Bundesanstalt für Gewässerkunde.

Biegel, M. (2005): Hydrologische Modellierung urbaner Nährstoffeinträge in Gewässer auf Flussgebietsebene, Ph.D. thesis, Technische Universität Dresden.

Biegel, M., Schanze, J. & Krebs, P. (2005): ArcEGMO-URBAN - Hydrological model for point sources in river basins, *Water Science and Technology*, 52 (5): 249–256.

Borchardt, D. (1998): Gewässergütemodellierung – Stand und Perspektiven, in: Mathematische

Modelle in der Gewässerkunde – Stand und Perspektiven, *BfG Mitteilungen*, vol. 19, pages 95–103, Bundesanstalt für Gewässerkunde.

Borchardt, D. & Reichert, P. (2001): River Water Quality Model no. 1 (RWQM1): Case study I. Compartmentalisation approach applied to oxygen balances in the River Lahn (Germany), *Water science and technology*, 43 (5): 41–49.

Bowie, G. L., Mills, W. B., Porcella, D. B., Campbell, C. L., Pagenkopf, J. R., Rupp, G. L., Johnson, K. M., Chan, P. W. H., Gherini, S. A. & Chamberlin, C. E. (1985): Rates, constants and kinetics formulations in surface water quality modeling (2nd ed.), Report EPA/600/3-85/040, U.S. Environmental protection agency.

Bronstert, A., Biegel, M., Habeck, A., Itzerott, S., Jacobs, J., Kneis, D., Krause, S., Lahmer, W., Schanze, J., Pfützner, B. & Schönfelder, I. (2005): Bewirtschaftungsmöglichkeiten im Einzugsgebiet der Havel, in: Typologie, Bewertung, Management von Oberflächengewässern, *Limnologie aktuell*, vol. 11, pages 204–220, Schweizerbart.

Bronstert, A. & Itzerott, S. (Eds.) (2006): Bewirtschaftungsmöglichkeiten im Einzugsgebiet der Havel - Abschlussbericht zum BMBF-Projekt (FKZ 0330227), *Brandenburgische Umweltberichte*, vol. 18, Mathematisch-Naturwissenschaftliche Fakultät der Universität Potsdam.

Brown, L. & Barnwell, T. (1987): The enhanced stream water quality models QUAL2E and QUAL2E-UNCAS: Documentation and user manual, EPA/600/3-87/007, U.S. Environmental protection agency.

Carignan, R. & Lean, D. R. S. (1991): Regeneration of dissolved substances in a seasonally anoxic lake: The relative importance of processes occuring in the water column and in the sediments, *Limnol. Ocenaogr.*, 36 (43): 683–707.

Carlson, R. E. (1977): A trophic state index for lakes, *Limnol. Ocenaogr.*, 22: 361–369.

Chapra, S., Pelletier, G. & Tao, H. (2006): QUAL2K: A Modeling Framework for Simulating River and Stream Water Quality, Version 2.04, Documentation and Users Manual, Civil and Environmental Engineering Dept., Tufts University, Medford, MA.

Chapra, S. C. (1997): Surface water quality modeling, McGraw-Hill.

Cole, T. & Wells, S. (2006): CE-QUAL-W2: A Two-Dimensional, Laterally Averaged, Hydrodynamic and Water Quality Model, Version 3.5, User Manual (Draft for USACE), Department of Civil and Environmental Engineering, Portland State University.

Crawley, M. (2002): Statistical computing, An introduction to data analysis using S-Plus, Wiley & Sons.

Dekissa, T., Meirlaen, J., Ashton, P. J. & Vanrolleghem, P. A. (2004): Simplifying dynamic river water quality modelling: A case study of inorganic nitrogen dynamics in the crocodile river (South Africa), *Water, Air and Soil Pollution*, 155: 303–319.

DHI (2006): ECO Lab – a numerical laboratory for ecological modeling, Danish hydraulic institute (DHI), URL: http://www.dhisoftware.com/ecolab/ News/ Downloads/ final-brochure.pdf.

Doherty, J. (2004): PEST – Model-independent parameter estimation, User manual, Watermark Numerical Computing, 5 edn.

DVWK (1996): Ermittlung der Verdunstung von Land- und Wasserflächen, *DVWK-Merkblätter*, vol. 238, Deutscher Verband für Wasserwirtschaft und Kulturbau.

European Commission (2000): Directive 2000/60/EC (Water Framework Directive).

Gervais, F., Opitz, D. & Behrendt, H. (1997): Influence of small-scale turbulence and large-scale mixing on phytoplankton primary production, *Hydrobiologia*, 342: 95–105.

Golterman, H. (1988): The calcium- and iron bound phosphate phase diagram, *Hydrobiologia*, 159: 149–151.

Golterman, H. (1995a): The role of the ironhydroxide-phosphate-sulfide system in the phosphate exchange between sediments and overlying water, *Hydrobiologia*, 297 (1): 43–54.

Golterman, H. L. (1995b): The labyrinth of nutrient cycles and buffers in wetlands: Results based on research in the Camargue (southern France), *Hydrobiologia*, 315 (1): 39–58.

Golterman, H. L. & Meyer, M. L. (1985): The geochemistry of 2 hard water rivers, the Rhine and the Rhone .4. The determination of the solubility product of hydroxy-apatite, *Hydrobiologia*, 126 (1): 25–29.

Granéli, W. (1999): Internal phosphorus loading in lake Ringsjön, *Hydrobiologia*, 404: 19–26.

Granger Morgan, M., Henrion, M. & Small, M. (2003): Uncertainty - A guide to dealing with uncertainty in quantitative risk and policy analysis, Cambridge university press.

Guse, B. (2006): Anwendung und Vergleich von zwei hydrologischen Modellen unterschiedlicher Komplexität zur Quantifizierung des Wasserhaushaltes und Phosphateintrags im Einzugsgebiet der Weißen Elster, Master's thesis, Universität Potsdam, Institut für Geoökologie.

Habeck, A. (2006): Ergebnisse der Wasserhaushaltsmodellierung mit SWIM und simulierte Stoffausträge aus Teileinzugsgebieten der Havel, in: Bronstert, A. & Itzerott, S. (Eds.) Bewirtschaftungsmöglichkeiten im Einzugsgebiet der Havel - Abschlussbericht zum BMBF-Projekt (FKZ 0330227), *Brandenburgische Umweltberichte*, vol. 18, Universität Potsdam.

Havens, K., James, R., East, T. & Smith, V. (2003): N:P ratios, light limitation, and cyanobacterial dominance in a subtropical lake impacted by non-point source nutrient pollution, *Environmental pollution*, 122: 379–390.

Hellmann, H. (1999): Qualitative Hydrologie – Wasserbeschaffenheit und Stoff-Flüsse, *Lehrbuch der Hydrologie*, vol. 2, Gebrüder Borntträger.

Hellstrøm, T. (1991): The effect of resuspension on algal production in a shallow lake, *Hydrobiologia*, 213 (3): 183–190.

Hickisch, A. & Kneis, D. (2004): Bewirtschaftungsmöglichkeiten im Einzugsgebiet der Havel - Teilprojekt 3: Renaturierung der Flussmorphologie zur Verbesserung des ökologischen Zustands; Leitbild und Wirkung ausgewählter Maßnahmen am Beispiel der Mittleren Nuthe (unpublished), Report, Universität Potsdam, Institut für Geoökologie.

Hieltjes, A. & Lijklema, L. (1980): Fractionation of inorganic phosphates in calcareous sediments, *Journal of Environmental Quality*, 9 (3): 405–407.

Hoffmann, A. (1999): Mathematical modeling of phosphorus dynamics in rivers with special regard to phosphorus remobilization from sediment, Master's thesis, BTU Cottbus.

ISO/IEC (2003): Fortran 2003 standard draft (Information technology - Programming languages - Fortran - Part 1: Base Language), Working document: ISO/IEC JTC1/SC22/WG5 N1578.

Jacobs, J. & Jessel, B. (2003): Design of landuse scenarios for river basin management (in German), pages 117–121, UVP-Report 3+4, UVP-Gesellschaft e.V.

Jacobsen, O. (1978): Sorption, adsorption and chemosorption of phosphate by Danish lake sediments, *Vatten*, 4: 230–243.

James, A. (Ed.) (1993): An introduction to water quality modelling, Wiley & Sons.

James, R. T., Martin, J., Wool, T. & Wang, P. F. (1997): A sediment resuspension and water quality model of Lake Okeechobee, *Journal of the American water resources association*, 33 (3): 661–680.

Jensen, H. S. & Andersen, F. (1992): Importance of temperature, nitrate and pH for phosphate release from aerobic sediments of four shallow, eutrophic lakes, *Limnol. Ocenaogr.*, 37: 577–589.

Jensen, H. S., Kristensen, P., Jeppesen, E. & Skythe, A. (1992a): Iron:phosphorus ratio in surface sediment as an indicator of phosphate release from aerobic sediments in shallow lakes, *Hydrobiologia*, 235/236: 731–743.

Jensen, J. P., Jeppesen, E., Kristensen, P., Christensen, P. B. & Søndergaard, M. (1992b): Nitrogen loss and denitrification as studied in relation to reductions in nitrogen loading in a shallow hypertrophic lake, *Int. Revue ges. Hydrobiol.*, 77: 29–42.

Jeppesen, E., Kristensen, P., Jensen, J. P., Søndergaard, M., Mortensen, E. & Lauridsen, T. (1991): Recovery resilience following a reduction in external phosphorus loading of shallow eutrophic Danish lakes: Duration, regulating factors and methods for overcoming resilience, *Mem. Ist. ital. Idrobiol.*, 48: 127–148.

Jokiel, C. (1995): Gewässergütesimulation natürlicher Fließgewässer, RWTH Aachen, Institut für Wasserbau und Wasserwirtschaft.

Keizer, P. & Sinke, A. J. C. (1992): Phosphorus in the sediment of the loosdrecht lakes and its implications for lake restoration perspectives, *Hydrobiologia*, 233 (1-3): 39–50.

Kirchesch, V. & Schöl, A. (1999): Das Gewässergütemodell QSIM - Ein Instrument zur Simulation und Prognose des Stoffhaushalts und der Planktondynamik von Fließgewässern, *Hydrologie und Wasserbewirtschaftung*, 43: 302–308.

Klausmeier, C., Litchman, E., Daufresne, T. & Levin, S. (2004): Optimal nitrogen-to-phosphorus stoichiometry of phytoplankton, *Nature*, 421: 171–174.

Kleeberg, A. (1995): Die Sanierung/Restaurierung des Großen Müggelsees - mit oder ohne eine Baggerung der phosphorreichen Sedimentschichten?, in: Jaeger, D. & Koschel, R. (Eds.) Verfahren zur Sanierung und Restaurierung stehender Gewässer, *Limnologie aktuell*, vol. 8, pages 281–293, Gustav Fischer Verlag.

Kleeberg, A. & Kozerski, H. P. (1997): Phosphorus release in lake Grosser Müggelsee and its implications for lake restoration, *Hydrobiologia*, 342: 9–26.

Kneis, D. (2002): Verkürzung der Verweilzeit des Wassers - Eine Option zur Verbesserung der Gewässergüte eines See-Fluss-Systems?, Master's thesis, Universität Potsdam, Institut für Geoökologie.

Kneis, D. (2005): Bewirtschaftungsmöglichkeiten im Einzugsgebiet der Havel - Teilprojekt 3: Bericht zum Arbeitspaket Nährstofftransport im Gewässersystem., Report, Universität Potsdam, Institut für Geoökologie.

Kneis, D., Knösche, R. & Bronstert, A. (2006): Analysis and simulation of nutrient retention and management for a lowland river-lake system, *Hydrology and Earth System Sciences*, 10: 575–588.

Knösche, R. (2006a): Nährstoffaushagerung von Flusssee-Sedimenten, in: Bronstert, A. & Itzerott, S. (Eds.) Bewirtschaftungsmöglichkeiten im Einzugsgebiet der Havel - Abschlussbericht zum BMBF-Projekt (FKZ 0330227), *Brandenburgische Umweltberichte*, vol. 18, Universität Potsdam.

Knösche, R. (2006b): Organic sediment nutrient concentrations and their relationship with the hydrological connectivity of floodplain waters (River Havel, NE Germany), *Hydrobiologia*, 560: 63–76.

Kozerski, H. & Leuschner, K. (1999): Plate sediment traps for slowly moving waters, *Water Research*, 33 (13): 2913–2922.

Kozerski, H. P. (1977): Ein einfaches mathematisches Modell für den Phosphoraustausch zwischen Sediment und Freiwasser, *Acta hydrochim. hydrobiol.*, 5: 53–65.

Kozerski, H. P., Behrendt, H. & Köhler, J. (1999): The N and P budget of the shallow, flushed lake Müggelsee: retention, external and internal load, *Hydrobiologia*, 409: 159–166.

Kozerski, H. P. & Kleeberg, A. (1998): The sediments and benthic-pelagic exchange in the shallow lake Müggelsee (Berlin, Germany), *International Review of Hydrobiology*, 83 (1): 77–112.

Krause, S. (2005): Untersuchung und Modellierung von Wasserhaushalt und Stofftransportprozessen in grundwassergeprägten Landschaften am Beispiel der Unteren Havel, Ph.D. thesis, Universität Potsdam, Institut für Geoökologie.

Kronvang, B., Hezlar, J., Boers, P., Jensen, J., Behrendt, H., Anderson, T., Arheimer, B., Venohr, M., Hoffmann, C. & Nielsen, C. (2005): Nutrient Retention Handbook – Software Manual for EUROHARP-NUTRET & Scientific Review on Nutrient Retention (EUROHARP 9-2004), Report, Norwegian Institute for Water Research (NIVA), Norway.

Kronvang, B., Svendsen, L. M., Jensen, J. P. & Dorge, J. (1999): Scenario analysis of nutrient management at the river basin scale, *Hydrobiologia*, 410: 207–212.

Krysanova, V., Wechsung, F., Arnold, J., Srinivasan, R. & Williams, J. (2000): SWIM (Soil and Water Integrated Model), User manual, PIK Report No. 69, Potsdam Institute for Climate Impact Research, URL: http://www.pik-potsdam.de/ pik_web/ publications/ pik_reports/ reports/ reports/ pr.69/ pr69.pdf.

Lampert, W. & Sommer, U. (1993): Limnoökologie, Thieme.

Lavery, P. S., Oldham, C. E. & Ghisalbert, M. (2001): The use of Fick's First Law for predicting porewater nutrient fluxes under diffusive conditions, *Hydological processes*, 15: 2435–2451.

LAWA (2002): Methode zur Klassifizierung der Trophie planktonführender Fließgewässer - Ergebnisse der Erprobungsphase, Report, Länderarbeitsgemeinschaft Wasser.

LAWA (2003): Musterverordnung zur Umsetzung der Anhänge II und V der Richtlinie 2000/60/EG des Europäischen Parlaments und des Rates vom 23. Oktober 2000 zur Schaffung eines Ordnungsrahmens für Maßnahmen der Gemeinschaft im Bereich der Wasserpolitik (Entwurf), Report, Länderarbeitsgemeinschaft Wasser.

Legates, D. R. & McCabe Jr., G. J. (1999): Evaluating the use of "goodness-of-fit"measures in

hydrologic and hydroclimatic model validation, *Water Ressources Research*, 35: 233–241.

Lewandowski, J., Rüter, K. & Hupfer, M. (2002): Two-dimensional small-scale variability of pore water phosphate in freshwater lakes: Results from a novel dialysis sampler, *Environ. Sci. Technol.*, 36: 2039–2047.

Li, Y. & Gregory, S. (1974): Diffusion of ions in sea water and in deep-sea sediments, *Geochimica et cosmochimica acta*, 38(5): 703–714.

LUA (2002): Fachbeiträge des Landesumweltamtes, Heft 68: Stoffeinträge in die Gewässer des Landes Brandenburg, Report, Landesumweltamt Brandenburg.

LUA (2005a): Fachbeiträge des Landesumweltamtes, Heft 93: Paläolimnologische Leitbildkonstruktion und biozönotisch basierte Bewertungsansätze für Flussseen am Beispiel der Diatomeen, Report, Landesumweltamt Brandenburg.

LUA (2005b): Umsetzung der Wasserrahmenrichtlinie - Bericht zur Bestandsaufnahme für das Land Brandenburg (C-Bericht), Report, Landesumweltamt Brandenburg.

Maassen, S., Uhlmann, D. & Röske, I. (2005): Sediment and pore water composition as a basis for the trophic evaluation of standing waters, *Hydrobiologia*, 543: 55–70.

Maerki, M., Wehrli, B., Dinkel, C. & Müller, B. (2004): The influence of tortuosity on molecular diffusion in freshwater sediments of high porosity, *Geochimica et Cosmochimica Acta*, 68(7): 1519–1528.

McCutcheon, S. C. (1989): Water quality modeling, Vol. 1 - Transport and surface exchange in rivers, CRC press.

Mermillod-Blondin, F., Gaudet, J. P., Gerino, M., Desrosiers, G. & des Chatelliers, M. C. (2003): Influence of macroinvertebrates on physico-chemical and microbial processes in hyporheic sediments, *Hydological processes*, 17 (4): 779–794.

Mietz, O. & Vietinghoff, H. (1994): Die Gewässergütesituation von 62 Seen des Potsdamer Seengebietes, *Naturschutz und Landschaftspflege in Brandenburg*, 2: 29–34.

Molins, S., Carrera, J., Ayora, C. & Saaltink, M. W. (2004): A formulation for decoupling components in reactive transport problems, *Water Ressources Research*, 40: W10301, doi:10.1029/2003WR002970.

Müller, S. (2002): ATV Gewässergütemodell – Beschreibung der Modellbausteine (Stand 07.02.2002), Report, München.

Nash, J. E. & Sutcliffe, J. V. (1970): River flow forecasting through conceptual models part I - A discussion of principles, *Journal of Hydrology*, 10 (3): 282–290.

Naumann, A. (1995): Hydrographische und hydrologische Charakteristik (der Havel), in: Die Havel, *Studien und Tagungsberichte*, vol. 8, pages 11–14, Landesumweltamt Brandenburg.

Noges, T., Kisand, V., Noges, P., Pollumae, A., Tuvikene, L. & Zingel, P. (1998): Plankton seasonal dynamics and its controlling factors in shallow polymictic eutrophic lake Vortsjarv, Estonia, *International review of hydrobiology*, 83 (4): 279–296.

Petzoldt, T., Rolinski, S., Rinke, K., König, M., Baumert, H. Z. & Benndorf, J. (2005): SALMO: Die ökologische Komponente des gekoppelten Modells, *Wasserwirtschaft*, 95(5): 28–33.

Petzoldt, T. & Uhlmann, D. (2006): Nitrogen emissions into freshwater ecosystems: Is there a need for nitrate elimination in all wastewater treatment plants?, *Acta hydrochimica et hydrobiologica*, 34 (4): 305–324.

Preissler & Bollrich (1985): Technische Hydromechanik 1, VEB Verlag für Bauwesen Berlin.

Press, W. H., Teukolsky, S. A., Vetterling, W. T. & Flannery, B. P. (2002): Numerical recipes in Fortran 90 - The art of parallel scientific computing, Cambridge university press, 2 edn.

Psenner, R., Pucsko, R. & Sager, M. (1984): Die Fraktionierung organischer und anorganischer Phosphorverbindungen von Sedimenten, *Arch. Hydrobiol. Suppl.*, 70: 111–155.

Rachimow, C. (2004): pers. comm., German Federal Water Institute.

Ramm, K. & Scheps, V. (1997): Phosphorus balance of a polytrophic shallow lake with the consideration of phosphorus release, *Hydrobiologia*, 342/343: 43–53.

Regnier, P., Vanderborght, J. P., Steefel, C. I. & O'Kane, J. P. (2002): Modeling complex multicomponent reactive-transport systems: Towards a simulation environment based on the concept of a Knowledge Base, *Applied Mathematical Modelling*, 26: 913–927.

Reichert, P. (1998): AQUASIM 2.0 - Computer program for the identification and simulation of aquatic systems, User manual, EAWAG, URL: www.aquasim.eawag.ch.

Reichert, P., Borchardt, D., Henze, M., Rauch, W., Shanahan, P., Somlyody, L. & Vanrolleghem, P. A. (2001): River water quality model No. 1, IWA Publishing.

Rohde, E. (1995): On the problem of phosphorus release from sediments of the Havel Lakes (in German), in: Die Havel, *Studien und Tagungsberichte*, vol. 8, pages 57–60, Landesumweltamt Brandenburg.

Saaltink, M., Ayora, C. & Carrera, J. (1998): A mathematical formulation for reactive transport that eliminates mineral concentrations, *Water Ressources Research*, 34 (7): 1649–1656.

Saaltink, M., Battle, F., Ayora, C., Carrera, J. & Olivella, S. (2004): RETRASO, a code for modeling reactive transport in saturated and unsaturated porous media, *Geologica acta*, 2 (3): 235–251.

Sas, H. (Ed.) (1989): Lake restoration by reduction of nutrient loading: Expectations, experiences, extrapolations, Academia Verlag.

Schauser, I., Chorus, I. & Lewandowski, J. (2006): Effects of nitrate on phosphorus release: comparison of two Berlin lakes, *Acta Hydrochimica et Hydrobiologica*, 34 (4): 325–332.

Scheffer, M. (1998): Ecology of shallow lakes, Chapman & Hall, 1 edn.

Scheffer, M., Rinaldi, S., Gragnani, A., Mur, L. R. & Van Nes, E. H. (1997): On the dominance of filamentous cyanobacteria in shallow, turbid lakes, *Ecology*, 78 (1): 272–282.

Schellenberger, G., Behrendt, H., Kozerski, H.-P. & Mohaupt, V. (1983): Ein mathematisches Ökosystemmodell für eutrophe Flachgewässer, *Acta hydrophysica*, 28: 109–127.

Schettler, G. (1995): The sediments of the Havel Lakes and their seasonal dynamics (in German), in: Die Havel, *Studien und Tagungsberichte*, vol. 8, pages 46–57, Landesumweltamt Brandenburg.

Schlaeger, F. (2003): Die Gewässergütesimulation von Fließgewässern als Grundlage der langfristigen Flussgebietsbewirtschaftung, Ph.D. thesis, Technische Hochschule Aachen, Lehrstuhl und Institut für Wasserbau und Wasserwirtschaft.

Schreiber, H., Behrendt, H., Constantinescu, L. T., Cvitanic, I., Drumea, D., Jabucar, D., Juran, S., Pataki, B., Snishko, S. & Zessner, M. (2005): Nutrient emissions from diffuse and

point sources into the River Danube and its main tributaries for the period of 1998-2000: Results and problems, *Water Science and Technology*, 51 (3-4): 283–290.

Schulz, M. (2004): Measuring and modelling phosphorus retention in lowland rivers, in: Tagungsbericht der Deutschen Gesellschaft für Limnologie, Jahrestagung 2004 in Potsdam, Weißensee Verlag.

Seitzinger, S. P. (1988): Denitrification in freshwater and coastal marine ecosystems: Ecological and geochemical significance, *Limnol. Oceanogr.*, 33: 702–724.

Senat (2001): Abwasserbeseitigungsplan Berlin (Wastewater management plan for the city of Berlin, in German), Report, Senatsverwaltung für Stadtentwicklung Berlin.

Smith, V. (1983): Low nitrogen to phosphorus ratios favor dominance by blue-green algae in lake phytoplankton, *Science*, 221: 669–671.

Smits, J. G. C. & Van der Molen, D. T. (1993): Application of SWITCH, a model for sediment water exchange of nutrients, to Lake Veluwe in the Netherlands, *Hydrobiologia*, 253 (1-3): 281–300.

Sommer, U. (1991): The application of the Droop-model of nutrient limitation to natural phytoplankton, *Verh. Internat. Verein. Limnol.*, 24: 791–794.

Sommer, U., Gliwicz, Z., Lampert, W. & Duncan, A. (1986): The PEG-model of seasonal succession of planktonic events in fresh waters, *Arch. Hydrobiol.*, 106(4): 433–471.

Søndergaard, M., Jensen, J. P. & Jeppesen, E. (2003): Role of sediment and internal loading of phosphorus in shallow lakes, *Hydrobiologia*, 506 (1-3): 135–145.

Søndergaard, M., Jensen, J. P., Jeppesen, E. & Møller, P. H. (2002): Seasonal dynamics in the concentrations and retention of phosphorus in shallow danish lakes after reduced loading, *Aquatic Ecosystem Health and Management*, 5: 19–29.

Stumm, W. & Morgan, J. (1996): Aquatic chemistry, Wiley interscience.

Svendsen, L. M., Kronvang, B. K., Laubel, A. R., Larsen, S. E. & Andersen, B. (1998): Phosphorus retention in a Danish lowland river system, *Verh. Internat. Verein. Limnol.*, 26: 956–962.

Thullner, M., Van Cappelen, P. & Regnier, P. (2005): Modeling the impact of microbial activity on redox dynamics in porous media, *Geochimica et Cosmochimica Acta*, 69: 5005–5019.

USACE, H. E. C. (2002): HEC-RAS River Analysis System User's manual, Version 3.1, URL: www.hec.usace.army.mil/software/hec-ras/hecras-hecras.html.

Van der Molen, D. (1991): A simple, dynamic model for the simulation of the release of phosphorus from sediments in shallow eutrophic systems, *Water Research*, 25 (6): 737–744.

Van Griensven, A. & Bauwens, W. (2003): Concepts for river water quality processes for an integrated river basin modelling, *Water Science and Technology*, 48 (3): 1–8.

Van Puijenbroek, P. J. T. M., Janse, J. H. & Knoop, J. M. (2004): Integrated modelling for nutrient loading and ecology of lakes in The Netherlands, *Ecological Modelling*, 174 (1-2): 127–141.

Venohr, M., Donohue, I., Fogelberg, S., Arheimer, B., Irvine, K. & Behrendt, H. (2003): Nitrogen retention in a river system under consideration of the river morphology and occurence of lakes, in: Proceedings of the International Conference

on Water Ressources Management (Diffuse pollution conference, Dublin 2003).

Vollenweider, R. A. (1979): Das Nährstoffbelastungskonzept als Grundlage für den externen Eingriff in den Eutrophierungsprozess stehender Gewässer und Talsperren, *Zeitschrift für Wasser- und Abwasser-Forschung*, 2: 46–56.

Vollenweider, R. A. & Kerekes, J. (1982): Eutrophication of waters. Monitoring, assessment and control. OECD Cooperative programme on monitoring of inland waters (Eutrophication control), OECD environmental directorate, Paris.

Von Keitz, S. & Schmalholz, M. (Eds.) (2002): Handbuch der Wasserrahmenrichtlinie, Erich Schmidt Verlag.

Weithoff, G. & Walz, N. (1999): Problems in estimating phytoplankton nitrogen limitation in shallow eutrophic lakes, *Hydrobiologia*, 409: 367–373.

Welch, E. B. & Cooke, G. D. (2005): Internal phosphorus loading in shallow lakes: Importance and control, *Lake and Reservoir Management*, 21 (2): 209–217.

Witter, R. (2002): Auswirkungen einer künstlichen Destratifikation auf die thermischen und hydrodynamischen Verhältnisse in der Bleilochtalsperre, Ph.D. thesis, Bauhaus-Universität Weimar.

WSA (2003): Bericht zur Staubeiratssitzung 2003, Report, Wasser und Schifffahrtsamt Brandenburg.

www.g95.org (2006): g95 open source Fortran compiler and runtime libraries, URL: www.g95.org.

Acknowledgments

First of all, I should like to thank my supervisor Axel Bronstert from the Institute of Geoecology at Potsdam University. It was Axel who invited me to participate in the 'Havel Project' and he taught me thinking the engineer's way. Dietrich Borchardt from Kassel University and Jesús Carrera from CSIC Barcelona contributed a large number of helpful comments on this work. Jesús also gave me a spontaneous lecture on water quality modeling and pointed me to some details of mathematics I was not aware of before.

I want to express my special thank to Rüdiger Knösche from Potsdam University who taught me the fundamentals of limnology and sediment chemistry. Without his engagement in collecting and analyzing sediment samples from the Havel and the Nieplitz Lakes, reasonable phosphorus modeling would have been impossible. I like to thank him for long and helpful discussions and wise comments on many over-ambitious ideas.

Celia Kirby proofread the final version of the manuscript. Thanks a lot!

I greatly acknowledge the cooperativeness of the state and federal authorities for hydrology, navigation, and environmental issues (Bundesanstalt für Gewässerkunde, Wasser- und Schifffahrtsamt Brandenburg, Landesumweltamt Brandenburg, Senat für Stadtentwicklung und Umwelt Berlin). These organizations provided most of the hydrological and water quality data used in this study.

I'm grateful for having found good friends at the Institute of Geoecology. I will certainly miss Theresa's face behind my monitors and the debates about statistics, politics, hydrology, canteen food, English terms, and life in general. Theresa supplied me with an uncounted number of chocolate cookies and 'Quarkies' getting only a handful of Excel macros back. She helped me to recover from many crisis during the preparation of this thesis.

Furthermore, I appreciate the unlimited help of Andi who always had the required cable or recovery software at hand. I should also like to say thanks to Saskia. Together we struggled through the 'Polder Project' and finally produced our first scientific paper.

Among the many others who helped me during the preparation of this thesis are Dominik, the expert for any computer language, Thomas, who dug deep into SWIM's phosphorus module and Sibylle, our project's manager, as well as Anja, Markus, and Stephan. I also appreciate the work of all the people who push science forward by making useful software such as 'g95' or 'R' freely available.

I'm especially grateful to my friends and my family who were less interested in my dissertation but the more relevant things in life. Thank you Basti, Bernd, Christoph, Franz, Heike, Jenny, Jonna, Katja, Matze, Peter, Stefan, Stephan, Suse, Susi, Till & Wiebke.

Author's declaration

I prepared this dissertation without illegal assistance. The work is original except where indicated by special reference in the text and no part of the dissertation has been submitted for any other degree.

This dissertation has not been presented to any other University for examination, neither in Germany nor in another country.

David Kneis
Potsdam, April 2007